UNIVERSITÀ
DEGLI STUDI
FIRENZE

PhD in
Biomedical Sciences

CYCLE XXXVIII

COORDINATOR Prof. Fabrizio Chiti

ESR1 activating mutations confer metabolic vulnerabilities in ER+ breast cancer

Academic Discipline (SSD): BIOS-07A

Doctoral Candidate
Dr. (Bonechi Francesca)

Supervisor
Prof. (Morandi Andrea)

Coordinator
Prof. (Chiti Fabrizio)

INDEX

Abbreviations

2-DG, 2-deoxy-D-glucose
4-OH-TAM, 4-hydroxytamoxifen
AAT, amino acid transporter
ACAT, acyl-coenzyme A cholesterol acyltransferase
ACC, acetyl-CoA carboxylases
ACLY, ATP citrate lyase
ACSL, long-chain fatty acyl-CoA synthetase
ACSS2, acetyl-CoA synthetase 2
ACSS2, acetyl-CoA synthetase 2
AF-1, activation function domain 1
AGPAT3, 1-acylglycerol-3-phosphate O-acyltransferase 3
AIs, aromatase inhibitors
Akt, protein kinase B
AP1, activator protein 1
ATGL, adipose triglyceride lipase
ATP, adenosine triphosphate
BAP1, BRCA1-associated protein 1
BH4, tetrahydrobiopterin
BRCA, breast cancer gene
cAMP, cyclic adenosine monophosphate
CCND1, cyclin D1
CCNE1, cyclin E
CDK, cyclin-dependent kinases
CE, cholesteryl ester
cfDNA, cell-free DNA
CNS, central nervous system
CoQH2, ubiquinol
COX, cyclooxygenase
CPT1, carnitine palmitoyltransferase-1
ctDNA, circulating tumor DNA
CYP, cytochrome p450
DBD, DNA-binding domain
ddPCR, digital droplet polymerase chain reaction
DDR2, discoidin domain–containing receptor 2
DFOM, deferoxamine
DGAT, diacylglycerol acyltransferase
DHFR, dihydrofolate reductase
DHODH, dihydroorotate dehydrogenase
E1, estrone
E2, 17-β-estradiol
E3, estriol
EGFR, epidermal growth factor receptor
ELOVL, fatty acid elongase
ELOVL, fatty acid elongases
EMT, epithelial-to-mesenchymal transition
ENO1, enolase 1
ER, estrogen receptor
ERE, estrogen response elements
ERK, extracellular signal-regulated kinase
ET, endocrine therapy
ETC, electron transport chain
F6P, fructose-6-phosphate
FA, fatty acid
FABP, fatty acid binding protein
FADS, fatty acid desaturase
FADS, fatty acid desaturases
FAO, fatty acid oxidation
FASN, fatty acid synthase
FAT, fatty acid translocase

FATP, fatty acid transport protein
FDA, Food and Drug Administration
Fer-1, ferrostatin-1
FGFR, fibroblast growth factor receptor
FINs, ferroptosis inducers
FIT, fat storage-inducing transmembrane
FOXA1, forkhead Box A1
FSP1, ferroptosis suppressor protein 1
GCH1, guanosine triphosphate cyclohydrolase 1
GLS1, glutaminase 1
GPER, G protein-coupled estrogen receptor
GPX4, glutathione peroxidase 4
GREB1, growth regulating estrogen receptor binding 1
GSH, glutathione
H2O2, hydrogen peroxide
HDI, Human Development Index
HER2, human epidermal growth factor receptor 2
HK, hexokinase
HMGCR, 3-hydroxy-3-methylglutaryl-coenzyme A reductase
HO•, hydroxyl radical
HSL, hormone sensitive lipase
Hsp, heat shock protein
IGF1-R, insulin growth factor 1 receptor
IKE, imidazole ketone erastin
iPLA2 β, calcium-independent phospholipase A2 β KEAP1,
Kelch-like ECH-associated protein 1
LBD, ligand-binding domain
LD, lipid droplet
LDH, lactate dehydrogenase
LDL, low-density lipoprotein
LDLR, low-density lipoprotein receptor
LOO•, lipid peroxyl radical
LOOH, lipid hydroperoxide
LOX, lipoxygenase
LPCAT, lysophosphatidylcholine acyltransferase
LPCAT3, lysophosphatidylcholine acyltransferase 3
MAGL, monoacylglycerol lipase
MAPK, mitogen-activated protein kinase
MBOAT, membrane-bound glycerophospholipid O-Acyltransferase
MEK, mitogen-activated protein kinase kinase
MLKL, mixed lineage kinase domain-like pseudokinase
MLL4, myeloid/lymphoid or mixed-lineage leukemia 4
mTOR, mechanistic target of rapamycin
MUFA, monounsaturated fatty acid
MVK, mevalonate kinase
NCOA4, nuclear receptor coactivator 4
NF1, neurofibromin 1
NF-κB, nuclear factor kappa-light-chain-enhancer of activated B cells
NLS, nuclear localization signal
OS, overall survival
PC, phosphatidylcholine
PDE, ex vivo tumor explants
PDX. patient-derived xenograft
PDXO, PDX-derived organoid
PE, phosphatidylethanolamine
PFK1, phosphofructokinase-1
PFKFB, phosphofructokinase-2/fructose-2,6-bisphosphatase
PFS, progression-free survival
PG, phosphatidyl glycerol
PHGDH, phosphoglycerate dehydrogenase
PHGDH, phosphoglycerate dehydrogenase

PI, phosphatidylinositol
PI3K, phosphatidylinositol 3-kinase
PIM2, proviral insertion in murine lymphomas
PK, pyruvate kinase
PKA, protein kinase A
PKC, protein kinase C
PLC, phospholipase C
PLIN, perilipin
POR, oxidoreductases cytochrome p450
PR, progesterone receptor
PS, phosphatidylserine
RAF, rapidly accelerated fibrosarcoma
RAS, rat sarcoma
Rb, retinoblastoma
Rb, retinoblastoma
SCD, stearoyl-CoA desaturase
SCD, stearoyl-CoA desaturase
SCD, stearoyl-CoA desaturases
SERCA, selective estrogen receptor covalent antagonists
SERDs, selective ER downregulators
SERMs, selective ER modulators
SLC, solute carrier
SOC, standard of care
SP1, specific protein 1
SQS, squalene synthase
SREBP, sterol regulatory element-binding protein
TAG, triacylglycerol
TAZ, transcriptional coactivator with PDZ-binding motif
TCA, tricarboxylic acid
TFR1, transferrin receptor 1
TNBC, triple-negative breast cancer
TRP, transient receptor potential
WT, wild type
YAP, yes-associated protein
ZEB1, zinc finger E-box binding homeobox 1

Abstract

Endocrine therapy (ET) is the standard of care for estrogen receptor-positive (ER+) breast cancer. Point mutations in the ligand-binding domain of the gene encoding the estrogen receptor (*ESR1*) are rare in naïve ER^+ breast cancer while becoming common in the ET-resistant setting. Here, we found that *ESR1* mutations expose breast cancers to critical vulnerabilities related to lipid metabolism. Particularly, *ESR1* mutations that induce constitutive ER activation drove aberrant lipid biogenesis and lipid upload in parallel with increased expression of the acyl-CoA synthetase long-chain family member 4 (ACSL4), which has a crucial role in fatty acid activation and has been shown to correlate with increased ferroptosis susceptibility. While ER+ breast cancer cells displayed ferroptosis resistance, the presence of *ESR1* mutations rendered tumor cells sensitive to ferroptosis induction. Importantly, ferroptosis inducers potentiated the effects of the selective estrogen receptor degraders fulvestrant and elacestrant, which are the standard of care for breast cancers carrying *ESR1* mutations. These findings, validated both in preclinical models and in patient-derived material, identify a combinatory therapeutic approach in the setting of ET resistance and establish ACSL4 as an important biomarker to recognize ER^+ breast cancers susceptible to ferroptosis induction.

Chapter I. Introduction

1. Breast cancer

Based on Global Cancer Observatory data, in 2022, there were 2.3 million new cases and 670,000 deaths from breast cancer, corresponding to 25% of new cases and 15.5% of cancer-related deaths among females. Globally, one in 20 women will be diagnosed with breast cancer, and one in 70 will die from the disease in their lifetime; however, this varies across countries and continents (1). Indeed, the burden of breast cancer is not equally distributed worldwide but depends on the extent of human development. Specifically, in countries with high Human Development Index (HDI), one in 12 women will be diagnosed with breast cancer during their lifetime, and one in 71 will die from it, in contrast to countries with low HDI, where only one in 27 women is diagnosed with breast cancer in their lifetime, and one in 48 will die from it. Consequently, there is a marked pattern of increasing mortality-to-incidence ratio with decreasing HDI, due to the greater accessibility of diagnostic technologies and care in developed regions, which allows for improved survival rates and better prognosis for breast cancer patients (1, 2). Breast cancer susceptibility is related to genetic predisposition or family history, with the most common factors being germline mutations in the *BRCA1* and *BRCA2* genes (BReast CAncer gene 1 and 2), associated with a lifetime risk of about 70%. Additionally, a significant percentage of breast cancer cases can be attributed to factors related to pregnancy, hormone therapy, lifestyle (e.g., obesity, physical inactivity, alcohol intake, low-fibre diet, and smoking), and other risk factors (3). Most breast cancers arise in the terminal duct-lobular units, which are the functional units of the breast and consist of a terminal duct and multiple lobules. Both ductal carcinoma and lobular carcinoma, the most frequent histological subtypes of breast cancer, originate in the lobular unit, in the breast ducts and lobules, respectively, and correspond to the invasive lesions; while their respective preinvasive counterparts are ductal carcinoma in situ and lobular carcinoma in situ (or lobular neoplasia) (**Figure 1**) (4). The histological and molecular features of breast cancer have important implications for therapy, which is why several classifications based on these characteristics have been developed. Following diagnosis and staging of the tumor based on size and lymph node involvement, breast cancer patients undergo specific treatment. When possible, patients have surgery, followed by radiotherapy, chemotherapy (e.g., anthracyclines, taxanes), biological therapy (e.g., antibody against human epidermal growth factor receptor 2, HER2,

trastuzumab), endocrine therapy (ET), or a combination of treatments, depending on the genetic and molecular profile of the cancer.

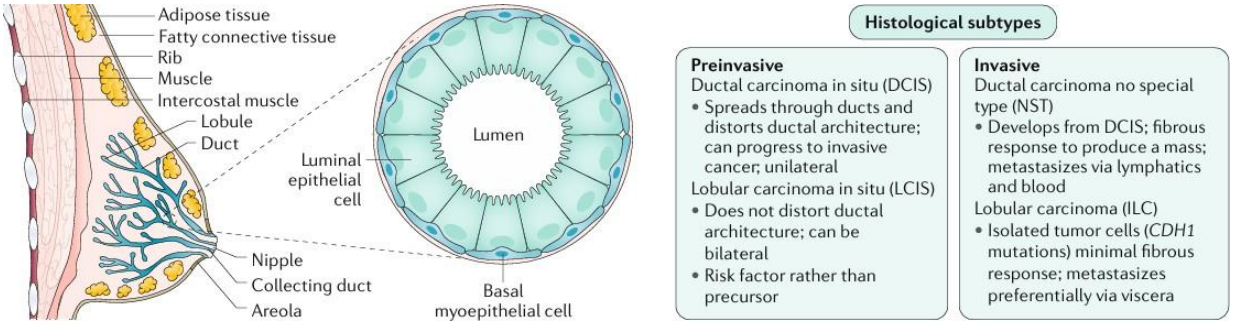

Figure 1. Breast anatomy and histological subtypes of breast cancer [taken from (1)]

1.1 Molecular subtypes of breast cancer

Breast cancer is a complex disease that displays a large degree of heterogeneity, and its histological and molecular characteristics largely influence treatment decisions. Therefore, several classifications have been widely adopted through high-throughput and microarray-based gene-expression methods to determine the molecular features of breast cancer and identify signatures associated with prognosis and response to therapy. The intrinsic classification of Perou, Sorlie and colleagues (5), distinguished four subtypes of breast cancer: luminal A and luminal B, expressing the estrogen receptor (ER), basal-like, and HER2-enriched (without ER expression). This classification has made it possible to change the clinical management of breast cancer from a tumour burden approach to a biology-centred approach. Currently, clinical practice typically uses a surrogate classification of five subtypes based on histology and immunohistochemistry expression of key proteins: ER, progesterone receptor (PR), HER2, and the proliferation marker Ki67 (**Figure 2**) (4). Luminal A tumors are characterized by the presence of ER and/or PR, as well as the absence of HER2, and have low expression of the cell proliferation marker Ki67. Clinically, they are low-grade, slow-growing, and have the best prognosis, with a lower incidence of relapse and higher survival rates. Luminal B tumors are of higher grade and worse prognosis compared to Luminal A. They are ER+ and/or PR+, can express HER2 and HER2-related genes, have high expression of Ki67, and express a consistent set of genes related to proliferation and cell cycle. Generally, they are of intermediate to high histologic grade. The elevated Ki67 causes them to grow

faster than Luminal A tumors, resulting in a worse prognosis (6). The HER2-enriched group represents 10-15% of breast cancer and is characterized by the amplification of the HER2 gene and/or overexpression of its related kinase receptor protein, without ER and PR expression. These tumors grow faster than Luminal tumors and have a worse prognosis, but due to the introduction of HER2-targeted therapies (including trastuzumab, trastuzumab combined with emtansin, pertuzumab, and tyrosine kinase inhibitors such as lapatinib and neratinib), they show a significantly higher therapeutic response compared to HER2 negative cancers (7). The Basal-like subtype includes tumors that are negative for ER, PR and HER2. It is characterized by a high proliferation rate, alteration in DNA repair genes and increased genomic instability. These tumors are typically high-grade and have a greater tendency to be diagnosed in advanced stages (8). In summary, classifying breast cancer as ER+, HER2+, or triple-negative (TNBC) (ER-, PR-, HER2-) is clinically important, as treatment strategies are tailored accordingly with ET, HER2-targeted agents, or chemotherapy.

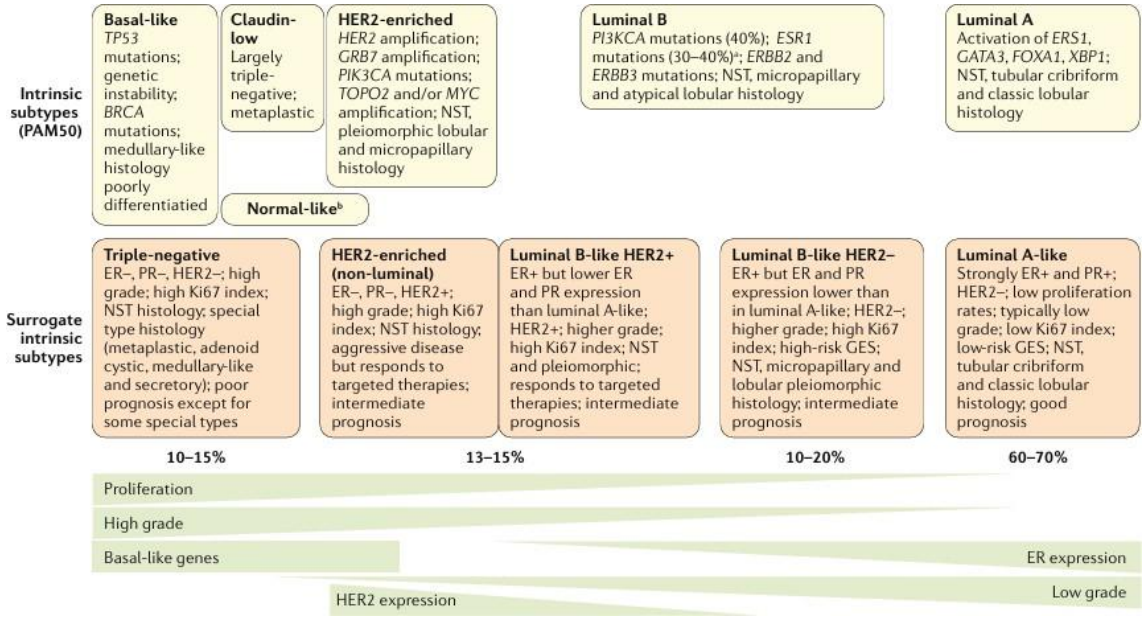

Figure 2. Intrinsic subtypes of breast cancer [taken from (1)]

1.2 Estrogen receptor positive breast cancer

ER+ breast cancer is characterized by ER expression and includes both luminal A and B subtype tumors, making it the most common type of breast cancer among women, with 70% of related diagnoses (9). In the normal human breast, 10-15% of mammary luminal epithelial cells express ER at detectable levels but do not proliferate, even though they are in proximity to proliferating cells. Interestingly, estrogen stimulation of ER+ breast cells induces the release of paracrine factors, promoting the proliferation of the surrounding ER- epithelial cells (10). In contrast, ER+ human breast cancer cells promptly proliferate and, because they are dependent on estrogens for their growth and survival, inhibiting this dependency with the ET that targets the ER pathway is the standard of care (SOC) for this subset of tumors (11).

1.2.1 Estrogen and breast cancer risk

Estrogens belong to the steroid hormone class synthesized from cholesterol and mainly secreted by the ovaries. The three main forms of estrogens are: estrone (E1), estradiol (E2, or 17β-estradiol), and estriol (E3). E2 is the major product derived from the biosynthetic process and the most potent estrogen in premenopausal women. Estrogens play key role in the development and maintenance of female sexual and reproductive function and regulate physiological processes in the cardiovascular, skeletal, immune and central nervous system (CNS) (12). In premenopausal women, under the control of pituitary gonadotropins, the ovaries are the main source of serum estrogen, and only a small amount comes from peripheral organs. In contrast, the estrogen produced in postmenopausal women mainly results from the aromatization of androgens in extragonadal tissues such as the liver, muscle, and fat tissues (13). Differences in exercise and dietary intake of certain nutrients may also influence estrogen levels; however, studies on the relationship between breast cancer risk and intakes of alcohol, fat, antioxidant vitamins, and fiber have yielded conflicting results (14). The association between exogenous sex steroids and breast cancer risk has also been extensively studied. Initial epidemiological studies suggested little, if any, increase in breast cancer risk with oral contraceptive use. However, other studies have found an association in women currently taking an oral contraceptive, women who have used it for an extended period, and women who began using an oral contraceptive at a young age. Still, there is no evidence of an increased risk 10 or more years after cessation of oral contraceptive (15). Estrogen-replacement therapy has been implicated as a risk factor for breast

cancer in postmenopausal women. The increase in risk relates to the duration of estrogen-replacement therapy and is observed only during therapy and short after its cessation (13). Estrogens play a significant role in promoting the proliferation of both normal and neoplastic breast epithelium. Evidence of this includes the increased risk of breast cancer associated with early menarche, late first full-term pregnancy, and late menopause, along with the reduced risk associated with early menopause. Although the exact mechanisms remain to be fully elucidated, the stimulation of cellular proliferation through receptor-mediated hormonal activity, the generation of active radicals that can damage DNA, and the potential genotoxic effects have been implicated (16).

1.2.2 Estrogen receptor and mechanism of action

The cellular effects of estrogens are mediated by two estrogen receptors, ERα and ERβ. ERα is primarily expressed in reproductive tissues (such as the uterus and ovary), as well as in the breast, kidney, bone, white adipose tissue, and liver, while ERβ expression is found in the ovary, CNS, cardiovascular system, lung, male reproductive organs, prostate, colon, kidney, and immune system (17). After binding to the ligand, the ER can dimerize, translocate to the nucleus, bind to specific DNA promoter sequences known as estrogen response elements (EREs), and regulate transcription through interactions with coactivators and corepressors (18). The two receptors are structurally related, evolutionarily conserved, and contain several structural domains with unique functional characteristics (**Figure 3**). Domains A and B, located in the N-terminal domain, contain the activation function domain 1 (AF-1), which activates the transcription of target genes. Domain C corresponds to the DNA-binding domain (DBD), featuring a zinc-finger motif that facilitates receptor dimerization and binding to the EREs. The D domain is marked by the presence of a nuclear localization signal (NLS), which becomes exposed after the conformational change of the ER induced by binding the ligand and is essential for translocation to the nucleus. The E domain serves as the ligand-binding domain (LBD), it contains 12 α-helices (named h1–h12) linked together by loop regions. Without ligand, the LBD is bound by heat shock proteins (Hsp) such as Hsp90 and therefore kept in an inactive conformation. In the presence of estrogen, the LBD dimerizes and the α-helix h12 forms a hydrophobic groove that binds to co-activator proteins to promote the expression of ER target genes. The F domain, found at the C-terminus, includes the additional regulator of ER transcriptional activity, AF-2, and plays a role in interaction with coactivators (12, 19). ERα and ERβ display high homology in the LBD and DBDs, yet

they differ in the transcription-activating domain, which explains the different responses of the two receptors (20).

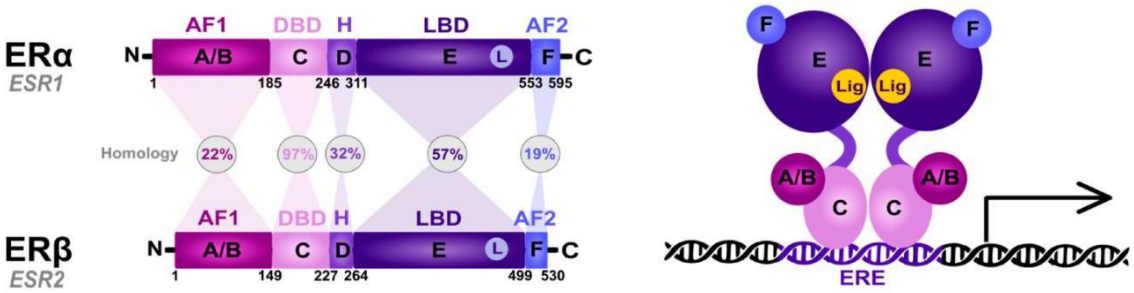

Figure 3. Schematic representation of the structural and functional domains of human ERα and Erβ [taken from (12)]

Although most estrogen-mediated signaling pathways are ER-dependent, ER-independent signaling mechanisms have been described (**Figure 4**). Two different ER-dependent mechanisms exist, classified as either “genomic” or “nongenomic,” based on whether the result of ER signaling involves transcription regulation (21). Unlike ER-dependent pathways, estrogen initiates ER-independent signaling mechanisms not by binding to estrogen receptors, but by regulating enzymatic activities or interacting with non-sex steroid hormone nuclear receptors. Each of these regulatory mechanisms has been observed in the context of specific estrogen activities in cells or tissues(22).

The genomic effects involve the classic mechanism of estrogen signaling. In this process, estradiol binds to ERα or ERβ in the cytoplasm, causing a conformational change that triggers receptor dimerization. The estrogen-ER complex then moves into the nucleus, where it attaches to chromatin at ERE sequences, thus promoting the transcription of ER-dependent genes (19, 23). Although EREs have been identified in numerous promoters and regulatory regions of genes, reports indicate that over one-third of human ER-regulated genes lack ERE sequence elements (24). These genes can be regulated by indirect genomic signaling, providing interaction between estrogen-activated ER and transcription factors such as AP1 (activator protein 1), SP1 (specific protein 1), and NF-κB (nuclear factor kappa-light-chain-enhancer of activated B cells), thus influencing gene transcription without direct DNA binding (24-26). Given that certain estrogen-induced responses occur too rapidly to be explained by genomic signaling, it has been proposed that estrogen may act through mechanisms that do not involve direct target gene transcription, resulting in the discovery of the G protein-coupled estrogen

receptor (GPER), another type of estrogen-dependent receptor that belongs to the family of transmembrane metabotropic receptors (27). It is a seven-transmembrane-domain receptor that mediates non-genomic estrogen-dependent signaling. In response to extracellular signals from estrogens, GPER initiates multiple downstream pathways that exert various biological effects on cell growth regulation, migration, and programmed cell death across a range of tissues (28). In particular, non-genomic actions of estrogen involve the activation of signal transduction mechanisms, leading to the production of intracellular second messengers, regulation of cyclic adenosine monophosphate (cAMP), and activation of protein kinases. This includes the phospholipase C (PLC)/protein kinase C (PKC) pathway, the rat sarcoma /rapidly accelerated fibrosarcoma/mitogen-activated protein kinase (RAS/RAF/MAPK) cascade, the phosphatidylinositol 3-kinase/protein kinase B (PI3K/Akt) cascade, and the cAMP/protein kinase A (PKA) signaling pathway (29-32). Following this, the phosphorylation of transcription factors by protein kinases can modify their function and capacity to bind to genomic sequences, thereby affecting gene expression. Both ERα and ERβ are also targets for phosphorylation by protein kinases, including MAPKs, suggesting that non-genomic actions of estrogen may also involve self-regulation of receptor expression (33). Finally, by proximity, ERα and ERβ interact with G proteins and various membrane receptors, such as tyrosine kinase, insulin growth factor 1 receptor (IGF-1R), and epidermal growth factor receptors (EGFR). This interaction promotes the intracellular activation of MAPK and Akt signaling pathways, influencing transcriptional regulation (34). Many ER-dependent genes regulate key processes in tumor biology, including cell proliferation, apoptosis, angiogenesis, invasion, and metastasis. Among these, the nuclear transcription factor c-Myc promotes cell cycle progression and plays a central role in protein biogenesis, cell adhesion, metabolism, and signal transduction, thereby acting as a critical oncogenic driver and an attractive therapeutic target. Accordingly, c-Myc is frequently deregulated in cancer and is overexpressed in approximately 20–30% of breast cancers (35). Another important ER target gene is cyclin D1 (CCND1). CCND1 activates cyclin-dependent kinases (CDK) 4 and 6, driving cell cycle progression through phosphorylation—and consequent inactivation—of cell cycle inhibitory proteins such as the retinoblastoma (Rb) protein (36).

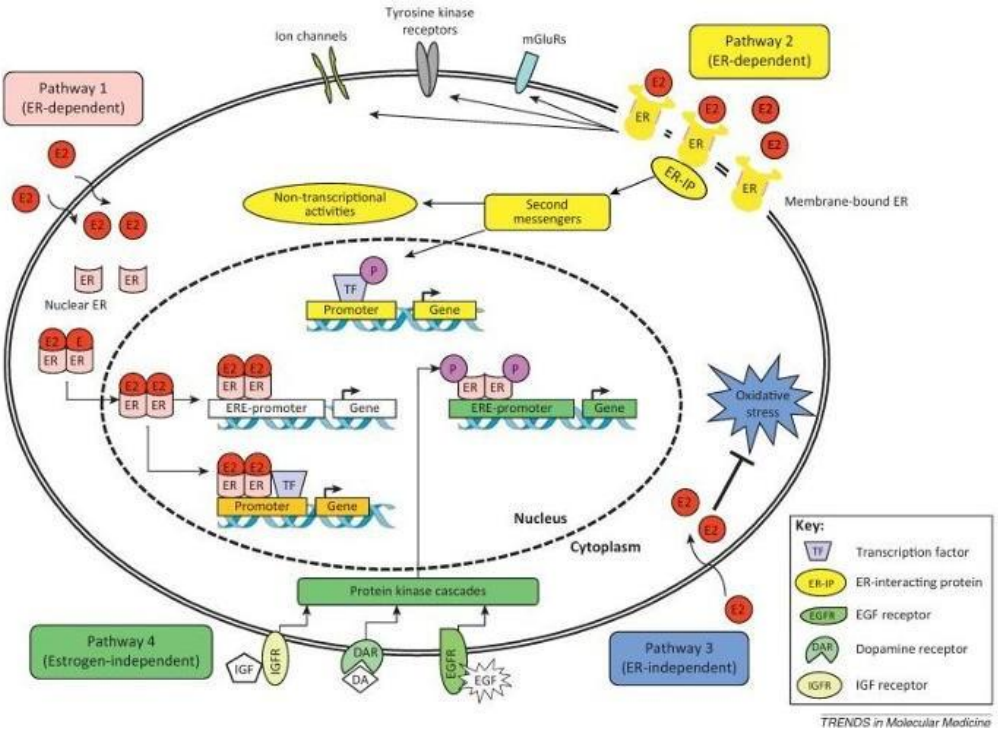

Figure 4. Schematic illustration of the key ER signaling pathways. [taken from (22)]

2. Endocrine therapy

ER-positive and HER2-negative breast cancer is the most common subtype of mammary tumors. Estrogen binding to ER stimulates receptor-regulated transcription, which in turn promotes tumor cell growth and proliferation, making the tumors dependent on estrogen. ET, the SOC for this type of tumors, acts by depleting estrogen production, interrupting ER signaling, or degrading ER, thus resulting in tumor growth inhibition (37). Adjuvant ET for 5 to 10 years is recommended for nearly all patients with ER+ breast cancer to prevent metastatic disease, local–regional recurrence, and contralateral tumors (38). ET includes selective ER modulators (SERMs), selective ER degraders (SERDs), and aromatase inhibitors (AIs). AIs (e.g., letrozole, anastrazole, exemestane) deplete systemic estrogen levels in postmenopausal patients by blocking the conversion of androgens to estrogens. SERMs (e.g., tamoxifen) competing with estrogen for binding to ER, have mixed agonist/antagonist capacities and are primarily used in pre-menopausal patients. SERDs (e.g., fulvestrant) are thought to act primarily by inducing ER protein degradation or blocking ER transcriptional activity (**Figure 5**). In recent years, as the prognostic stratification of early breast cancer has become more precise, it has become a clinical consensus to tailor the intensity and duration of ET according to risk stratification (39).

2.1 SERMs

SERMs are a class of structurally diverse molecules that produce tissue-specific responses by binding to both ER isoforms, acting as a partial agonist for ERα while functioning as a pure antagonist for ERβ receptors (40). The mechanism of action of SERMs involves three processes: (i) SERMs bind to the LBD of both ER isoforms and competitively block E2 binding. (ii) When a SERM binds to the LBD site, its side chain prevents H12 from forming an active conformation of AF-2. (iii) The H12 helix anchors in the AF-2 hydrophobic groove restraining co-activator binding (41). Currently, several SERMs such as tamoxifen, raloxifene, and toremifene are Food and Drug Administration (FDA)-approved for treating breast carcinoma in both premenopausal and postmenopausal women, and many others with tissue-selective antagonistic effects on breast tissue are in clinical trials (42). The journey of SERMs began with the first pilot study in 1985, which investigated the prevention of breast cancer using tamoxifen on a small group of high-risk women. Since then, tamoxifen has become the gold standard for adjuvant breast cancer treatment and a pioneer in reducing breast tumors. Tamoxifen is a prodrug and after oral administration, it is metabolized by cytochrome P450, which results in the formation of hydroxylated tamoxifen metabolites, 4-hydroxy-N-desmethyl-tamoxifen (endoxifen) and 4-hydroxytamoxifen (4-OH-TAM). In comparison to tamoxifen, 4-OH-TAM binds more effectively to its target protein ER but has a shorter biological half-life, while endoxifen has a lower binding affinity for the ER but a longer biological half-life (43). Tamoxifen exhibits tissue-specific effects, functioning as both an estrogenic agonist and antagonist. It competes with estrogen for binding sites in the breast, exerting antiestrogenic and antitumor effects. In bone, it stimulates ER rather than blocking the receptors, producing an estrogenic agonist effect that may help prevent osteoporosis in postmenopausal women. Tamoxifen also has an agonistic effect in other areas, such as the vascular system and endometrium, leading to side effects like thromboembolic events and uterine cancer (44, 45). Five years of treatment with tamoxifen has been the traditional SOC, regardless of menopausal status, reducing both distant and local–regional recurrence by 10 to 30% when ER expression is moderate and by 40 to 50% when ER expression is high, with carryover effects lasting 15 or more years (46). However, long-term tamoxifen treatment can lead to acquired resistance. Indeed, approximately 40% of breast cancer patients receiving tamoxifen become resistant to this therapy and the disease recurs (47). Promising results have been observed with lasofoxifene, a new-generation non-steroidal SERM. In phase 2 studies of ELAINE-1 and ELAINE-2, lasofoxifene demonstrated significant antitumor activity in patients with mutation in the ER gene (encoded by *ESR1*), endocrine-resistant metastatic breast

cancer. The ongoing phase 3 study ELAINE-3 (NCT05696626) aims to evaluate the effects of abemaciclib combined with either lasofoxifene or fulvestrant in patients with *ESR1*-mutated, locally advanced or metastatic ER+/HER2− breast cancer (48, 49).

2.2 SERDs

SERDs are a newer class of ET that bind to the ER and induce its degradation, thereby reducing the overall activity of the receptor. Unlike SERMs, which can act as either agonists or antagonists, SERDs act exclusively as antagonists of the ER. SERDs can block the effects of estrogen on breast cancer cells by binding to the ER and promoting its degradation, leading to a decrease in the expression and activity of ER target genes (50). This class of drugs includes fulvestrant, the first and, until January 2023, the only FDA-approved SERD. Fulvestrant has been shown to induce the proteasomal degradation of the ER in a dose-dependent manner. In fact, fulvestrant promotes the dissociation of chaperone proteins such as Hsp90 and p23 from the ER, exposing a hydrophobic surface on the receptor that is recognized by the E3 ubiquitin ligase complex, which promotes its degradation by the proteasome. Additionally, fulvestrant has been shown to have a longer duration of action than other ER antagonists due to its ability to induce downregulation and degradation of the receptor, rather than just blocking its activity (51, 52). Compared to AIs, fulvestrant seems to be more effective in treating ER+ metastatic breast cancer with *ESR1* mutations, which play a key role in the development of ET resistance in breast cancer. However, the efficacy of fulvestrant against *ESR1* mutant metastatic breast cancer in the second line is modest, with median progression-free survival (PFS) ranging from 3 to 4 months (53, 54). Still, fulvestrant has several limitations. Due to its low oral bioavailability, it is administered monthly via intramuscular injection, which limits its clinical efficacy. To address these issues, several oral SERDs have been developed and are currently undergoing clinical trials. Elacestrant is a nonsteroidal oral SERD that, in January 2023, received FDA approval for treating ER+ HER2− metastatic breast cancer. The EMERALD trial, a phase III trial comparing the efficacy and safety of elacestrant with the SOC therapy (fulvestrant or exemestane) in patients with breast cancer who have previously received a CDK4/6 inhibitor, showed an increase in PFS with elacestrant versus SOC therapy, demonstrating also more benefit among the patients with *ESR1* mutations (55).

2.3 Aromatase inhibitors

AIs act by inhibiting aromatase, which converts androgens to estrogen through the process called aromatization (56). Estrogens are crucial in promoting the proliferation of neoplastic breast epithelium; therefore, decreasing estrogen production helps control breast cancer (57). In reproductive females, the ovaries are the primary source of estrogen, while the adrenal glands and adipose tissues produce smaller amounts. During menopause and post-menopause, estrogen levels decline as the ovaries become nonfunctional; however, this is partially compensated by increased androgen production driven by hypothalamic-pituitary signaling (22, 58). These androgens are aromatized in organs like the adipose tissue and the brain to form estrogen. AIs, by binding to aromatase, inhibit estrogen production, thereby blocking cell proliferation and breast cancer growth (59). AIs are classified as either steroidal or nonsteroidal based on their structure. Steroidal AIs, such as formestane and exemestane, bind covalently and irreversibly, while nonsteroidal AIs like aminoglutethimide, anastrozole, and letrozole bind non-covalently and irreversibly to aromatase (60). According to clinical study timelines, efficacy, and specificity, AIs are categorized into first, second, and third generations. First- (e.g., aminoglutethimide) and second-generation AIs (e.g., fadrozole and formestane) were discontinued due to excessive toxicity, lack of selectivity, and adverse effects (61). Third-generation AIs are highly selective for aromatase and well tolerated, with only minor side effects (62). Among these, exemestane is approved for treating advanced breast cancer in postmenopausal women whose disease has progressed after antiestrogen therapy (63).

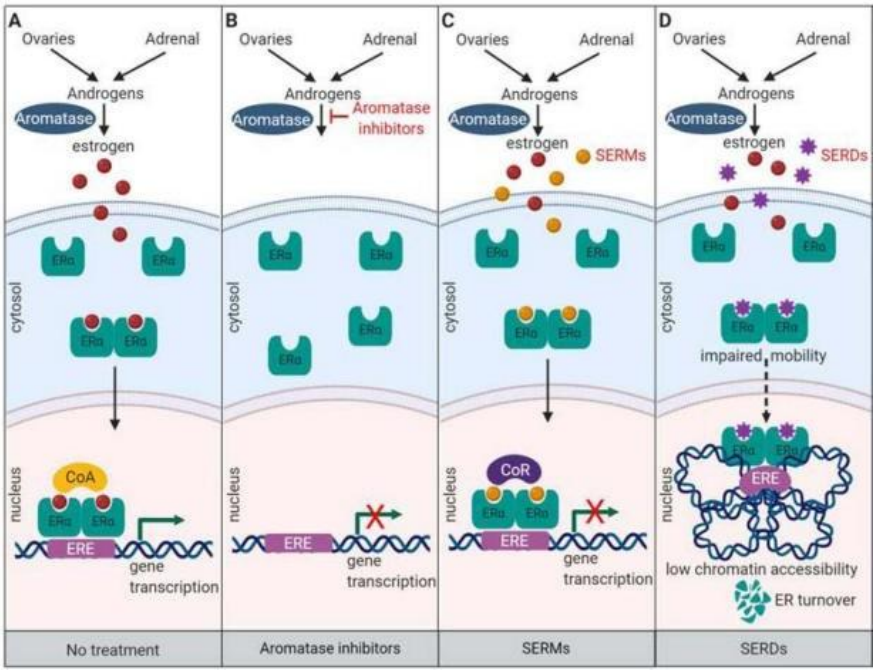

Figure 5. Mechanism of action of endocrine therapy. [taken from (74)]

3. Endocrine therapy resistance

Although ET significantly improves the prognosis of ER+ breast cancer patients, recurrences still occur and can ultimately lead to death. Importantly, up to 20% of patients diagnosed with operable ER+ tumors experience recurrence with metastatic disease, with more than half of all recurrences happening more than 5 years after the initial breast cancer diagnosis (64, 65). Endocrine resistance is inevitable in ER+ metastatic breast cancer and can result from various mechanisms as show in **Figure 6**. Loss of ER expression occurs in about 10% of endocrine-resistant breast cancers (66). More frequently, endocrine resistance is caused by ligand-independent ER reactivation, which can occur through gain-of-function mutations in *ESR1*, altered interactions of ER with coactivators or corepressors, or the upregulation of growth factor receptor pathways—including the ERBB family of receptors, fibroblast growth factor receptor (FGFR), IGF-1R, and their downstream signaling involving MAPK and PI3K–AKT–mechanistic target of rapamycin (mTOR), as well as deregulation of apoptosis and cell cycle machinery (67).

3.1 Crosstalk between estrogen receptor and growth factor receptors

Upon adaptation or resistance to antiestrogens, growth factor-driven mitogenic and survival pathways [i.e., PI3K/mTOR, RAS/RAF/mitogen-activated protein kinase kinase (MEK)/extracellular signal-regulated kinase (ERK)] can drive reactivation of ER transcription in the absence of estradiol. Overexpression of HER2, detected in approximately 10% of ER+ breast cancer cases, promotes ligand-independent activation of ER through various mechanisms, including phosphorylation and modulation of ER and transcriptional coregulators (68). Breast tumors expressing both receptors show reduced sensitivity to ET compared to HER2-negative tumors and are linked to worse outcomes and a higher risk of relapse (69). Additionally, HER2 overexpression causes hyperactivation of downstream PI3K and MAPK pathways, which contribute to ET failure (70). Patients with both HER2 and ER expression benefit more from simultaneous inhibition of these pathways than from ET alone (71). Phase III trials, such as EGF30008 and TAnDEM, have shown improved PFS when adding lapatinib to letrozole and trastuzumab to anastrozole in patients with ER+/HER2+ advanced breast cancer (72, 73). EGFR activation can stimulate breast cancer cell proliferation in response to various environmental factors and pro-inflammatory cytokines (74). The administration of gefitinib, a potent EGFR inhibitor, was associated with a significant increase in overall survival (OS) in ER+ tamoxifen-resistant breast cancer patients in a Phase II study. Notably, higher EGFR expression in breast cancer patients treated with tamoxifen correlates with poor prognosis and lower disease-free survival rates (75). Moreover, IGF-1R activation is linked to the development of tamoxifen resistance, primarily through the PI3K/Akt and MAPK signaling pathways (76). Although the role of IGF-1R is recognized, no clinical trials have yet shown a meaningful improvement in outcomes with IGF-1R targeting. Several Phase II studies combining monoclonal antibodies targeting IGF-1R (such as cixutumumab, ganitumab, figitumumab) with antiestrogens have failed to demonstrate clinical benefit (77, 78). About 10% of breast cancers, mainly ER+, exhibit FGFR1 amplification, which is associated with a poor prognosis (79, 80). The effectiveness of combining FGFR inhibitors with ET is currently under investigation. The RADICAL Phase IIa trial suggests that adding an FGFR inhibitor provides clinical benefits for ER+ breast cancer patients who have progressed after AIs (81). Ongoing trials are also exploring the combination of the FGFR inhibitor erdafitinib, palbociclib, and fulvestrant for advanced ER+ breast cancer with *FGFR1* amplification.

3.2 PI3K and MAPK pathway alterations

Gain-of-function mutations in *PIK3CA* and *AKT1*, and inactivating mutations in *PTEN*, are common in ER+ breast cancer. Aberrant activation of the pathway promotes acquired resistance to estrogen depletion in preclinical models (8, 82). Indeed, targeting the PI3K/Akt/mTOR pathway aims to overcome ET resistance by suppressing proliferation driven by both ligand-dependent and ligand-independent ER activation. Overall clinical data suggest that *PIK3CA* mutations in ER+ tumors may be a favorable prognostic marker (83, 84). Indeed, the addition of PI3K pathway antagonists has improved the outcome of ER+ breast cancer patients. For example, alpelisib, a selective PI3Kα inhibitor, showed antitumor activity in *PIK3CA*-mutant ER+ breast cancer in early-phase studies when combined with ET (85), and this benefit was confirmed in the phase III SOLAR-1 trial, leading to its approval with fulvestrant for patients following progression on ET (86). In human samples, 60% of ductal carcinoma *in situ* demonstrated Akt overexpression and its constitutive activation was found to confer resistance to both SERM and SERD therapy by causing estrogen-independent activation of ER (87-89). In the clinic, the most studied Akt inhibitors are capivasertib and ipatasertib, selective pan-Akt inhibitors with activity against Akt 1, 2, and 3. In particular, capivasertib, in combination with fulvestrant, has shown preliminary efficacy in endocrine-resistant ER+ breast cancers (90, 91). mTOR inhibition, which blocks a critical signaling node downstream of PI3K, has been extensively studied in combination with ET in the metastatic breast cancer setting. Indeed, the mTORC1 inhibitor everolimus is approved in combination with AIs for metastatic breast cancers that have progressed on ET, regardless of *PIK3CA* mutational status (92, 93). Additionally, components of the MAPK pathway are frequently mutated across many cancer types. Notably, neurofibromin 1 (NF1) mutations are common in metastatic breast cancer (94). Since NF1 functions as a negative regulator of RAS GTPase activity, loss of NF1 leads to constitutive activation of RAS signaling. Consistent with this mechanism, loss-of-function alterations of NF1 are associated with both intrinsic and acquired resistance to ET (95). In ER+ breast cancer cells, NF1 loss drives ER-independent CCND1 expression, and *in vitro* studies demonstrate that combining antiestrogens with CDK4/6 inhibitors can overcome NF1-mediated endocrine resistance (94). Additionally, acquired hotspot alterations in KRAS, BRAF, and MAP2K1 have been reported in post treatment biopsies compared to matched pre-treatment tumors (82). Collectively, these findings suggest that targeting the MAPK pathway with BRAF, MEK, or ERK inhibitors may represent a therapeutic strategy to overcome endocrine resistance driven by alterations in this pathway (96, 97).

3.3 Cell cycle checkpoint alterations

Estrogen can induce cell cycle progression from G1 to S phase via transcriptional upregulation of cell cycle regulators, including CCND1 and cyclin E (CCNE1), or activation of CDKs, which further phosphorylate downstream substrates, such as Rb (98). Accordingly, endocrine-resistant tumors frequently harbor alterations in these cell cycle regulators that enable them to bypass the inhibitory effects of ET on the G1–S transition (99). Amplification of *CCND1*, the activator of CDK4/6, correlates with ER positivity and is associated with worse prognosis and resistance to ET in ER+ breast cancer patients (100). c-Myc was shown to induce the activation of CCNE1/CDK2 through the transcriptional repression of p21, promoting endocrine resistance (101). Accordingly, the addition of CDK4/6 inhibitors to antiestrogens has markedly prolonged PFS compared to antiestrogens alone in patients with ER+ metastatic breast cancer. There are currently three CDK4/6 inhibitors (palbociclib, ribociclib, and abemaciclib) approved by the FDA in combination with ET to treat ER+HER2− breast cancer patients at the first line and advanced settings (102, 103). Mechanistically, CDK4/6 inhibitors prevent Rb hyperphosphorylation, thereby arresting cell cycle progression at the G1 phase. Given the deregulation of cell cycle progression in the endocrine resistance setting, CDK4/6 inhibitors were shown to greatly synergize with ET (104, 105). The efficacy of CDK4/6 inhibition can further be improved by targeting receptor tyrosine kinases, given the extensive crosstalk between CDK4/6 and the mitogenic signaling pathways. For instance, the combination of palbociclib with an FGFR inhibitor caused a synergistic growth inhibition in the estrogen-deprived ER+ breast cancer cells harboring *FGFR1*/*CCND1* co-amplification (106). Triple combinations involving ET, CDK4/6 inhibitors and PI3K/mTOR inhibitors have been tested in clinical trials and showed manageable toxicity and encouraging signs of clinical benefit (107, 108).

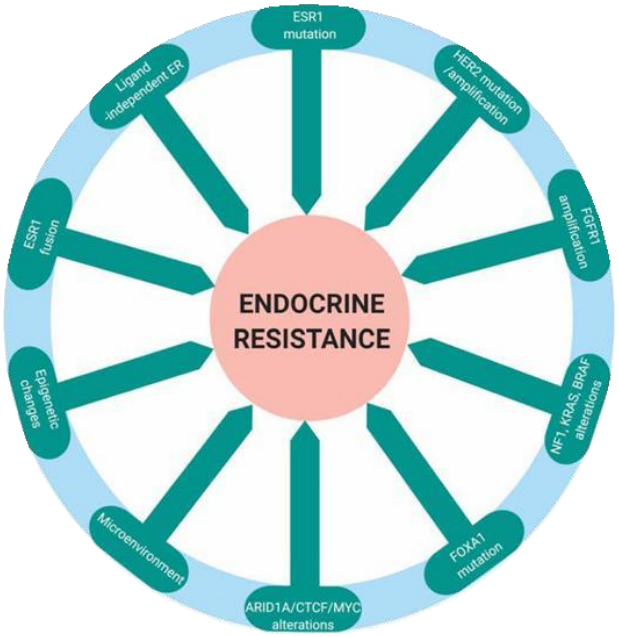

Figure 6. Mechanisms of endocrine resistance. [adapted from (74)]

3.4 *ESR1* mutations

The most common genomic mechanisms of acquired resistance to ET are activating mutations of *ESR1*, which are found in up to 60% of metastatic tumors that have progressed on ET (109-111). To date, over 50 point mutations in *ESR1* have been identified in clinical breast cancer samples. However, most pathogenic mutations believed to lead to ET resistance occur in codons 536–538 of the LBD, mainly at residues E380, L536, Y537, and D538, as shown in **Figure 7**. Structural and biochemical studies show that *ESR1* mutations stabilize ER in an agonist conformation, even in the absence of estrogen. Mutant ER recruits co-activators like estrogen-activated ER, enabling estrogen-independent transcription of ER target genes and conferring a growth advantage to *ESR1*-mutant cells, particularly under estrogen-deprived conditions (112-114). The distinct activity of ER in *ESR1*-mutant breast cancer results in a variety of phenotypes, including enhanced mitogenic signalling from growth factor receptors, stem cell biology, epithelial-to-mesenchymal transition (EMT), and ultimately metastasis (115). *In vitro* works on cell line models of *ESR1* Y537N, Y537S, and D538G mutations showed an increased IGF-1 signalling sustained by enhanced binding of IGF-1R with ER and conferring resistance to tamoxifen (116). Overexpression of Y537S or D538G mutations in MCF-7 cells induces the activation of the PI3K–AKT–mTOR pathway, which regulates cell metabolism, inducing increased mitochondrial activity and promoting

cellular migration (117). Studies have also linked *ESR1* mutations with enhanced stem cell and EMT phenotypes, both of which are associated with metastasis. Cell lines overexpressing *ESR1* mutations exhibited enrichment in $CD44^{+}/CD24^{-}$ cells compared to wild type (WT) cells, indicating an increase in the breast cancer stem-cell phenotype (118). A recent study showed that the transcriptomic profile of Y537S MCF-7 cells correlates with EMT and PAM50 basal-like signatures, which have been associated with stem-cell phenotypes, shorter recurrence-free survival, and poor response to neoadjuvant chemotherapy in breast cancer patients (8, 119). Though these mutations are common in metastatic and ET-resistant cases, they are rarely detected in primary tumors (<1%) (120). The prevalence of *ESR1* mutations rises after exposure to AIs in the metastatic setting, indicating that these mutations evolve by clonal selection under the pressure of endocrine treatment in metastatic disease (82). Since mutant ER exhibits estrogen-independent activity, strategies like AIs are less effective. Notably, the mutated ER conformation decreases the binding affinity of ER antagonists (121): SERMs such as tamoxifen, raloxifene, bazedoxifene, as well as the SERD fulvestrant, show reduced binding affinity to mutant ER compared to the WT one, requiring higher drug concentrations to inhibit the mutant receptor (112, 120). Besides its constitutive ligand-independent activity, mutant ER also gains neomorphic and hypermorphic functions, leading to the activation of novel gene expression patterns not observed in WT ER cells. This may result from new interactions with co-regulators and increased associations with factors like forkhead box A1 (FOXA1) and growth regulating estrogen receptor binding 1 (GREB1), among others yet to be identified. Genes regulated by mutant ER are enriched for roles in inflammation, cell migration, and metastasis (122, 123). Additionally, even in the presence of estrogen, *ESR1* mutations can exhibit significantly higher transactivation ability than *ESR1*-WT (124). As previously reviewed, *ESR1* mutations are a strong predictor of poor response to single-agent AI therapy (125). For example, retrospective analyses of the SoFEA and EFECT trials compared fulvestrant and exemestane in metastatic breast cancer patients with prior progression on AIs, focusing on preexisting *ESR1* mutations in circulating cell-free DNA (cfDNA) (54). These mutations predicted a significantly shorter PFS compared to cases with WT *ESR1*. Currently, the field is shifting away from AI monotherapy as the first-line treatment for HR+ metastatic breast cancers, focusing instead on combination therapies and ER-targeted agents. New SERMs and selective estrogen receptor covalent antagonists (SERCAs) have been developed and tested specifically against *ESR1* mutations. Lasofoxifene is in Phase II trials for patients with *ESR1* mutations and for those after progression on ET and CDK4/6 inhibitors (126). H3B-6545, an optimized SERCA that covalently inactivates ER by targeting S530, showed promising efficacy against *ESR1*-mutant metastatic breast cancer in a Phase I

trial (127). Among the new oral endocrine treatments, elacestrant received FDA approval in January 2023 for treating ER+ HER2− metastatic breast cancer, based on the EMERALD trial, which compared single-agent elacestrant to standard ET in patients who progressed following prior treatment with CDK4/6 inhibitors and ET. For patients with *ESR1* mutations, the median PFS was 3.78 months with elacestrant versus 1.87 months with standard ET (p = 0.005). Despite a modest increase in median PFS, there was a notable rise in the proportion of patients without disease progression at 12 months when treated with elacestrant compared to standard ET (55, 128). *ESR1* mutations may also serve as biomarkers for monitoring treatment response and guiding therapy decisions. The use of plasma circulating tumor DNA (ctDNA) to detect *ESR1* mutations for treatment optimization was pioneered in two phase III trials: PADA-1, where patients with newly diagnosed ER+ metastatic breast cancer received first-line letrozole and palbociclib, monitored every two cycles via digital droplet polymerase chain reaction (ddPCR) for *ESR1* mutations (129); and SERENA-6, which studied the role of *ESR1* mutation monitoring for selecting patients who would benefit from a next-generation SERD combined with a CDK4/6 inhibitor (130).

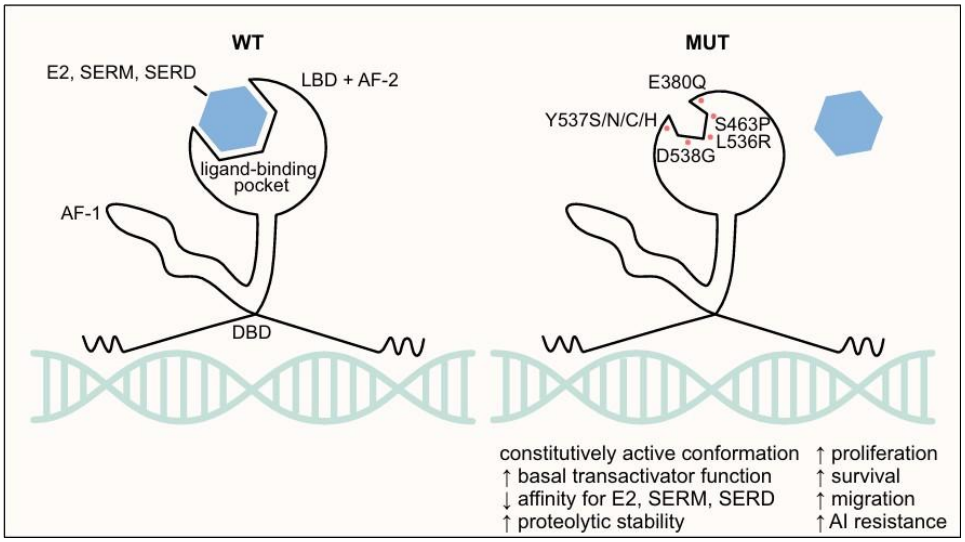

Figure 7. *ESR1* point mutations. [taken from (115)]

4. Tumor metabolism

During the progression of normal cells to a neoplastic state, they acquire a series of distinct biological capabilities, known as hallmarks of cancer, that allow them to develop tumorigenic traits and features (**Figure 8**). Among these, altered cellular metabolism and energetics are well-established hallmarks of cancer cells. In fact, uncontrolled cell proliferation, which is central to neoplastic disease, involves not only uncontrolled growth but also the deregulation of energy metabolism to support cell growth and division (131). The reprogramming of metabolism in cancer cells enables them to obtain necessary nutrients from a nutrient-poor environment and use these nutrients to maintain viability and produce new biomass. Changes in intracellular and extracellular metabolites in cancer cell metabolism have significant effects on gene expression, cellular differentiation, and the tumor microenvironment (132). The field of cancer metabolism began when Otto Warburg first observed abnormal characteristics of cancer cell energy metabolism. Under aerobic conditions, normal cells convert glucose into pyruvate via glycolysis, and then pyruvate is transported into mitochondria to enter the citric acid cycle, a key metabolic pathway crucial for adenosine triphosphate (ATP) production; under anaerobic conditions, glycolysis is favored, and pyruvate transport into oxygen-consuming mitochondria is reduced. Otto Warburg demonstrated that even in the presence of oxygen, cancer cells can reprogram their glucose metabolism—and thus their energy production—by largely relying on glycolysis, leading to a state known as “aerobic glycolysis” (133, 134). In subsequent years, many different metabolic reprogramming events have been identified, and importantly, since metabolic rewiring can make cancer cells dependent on specific pathways, this offers a potential therapeutic opportunity (135).

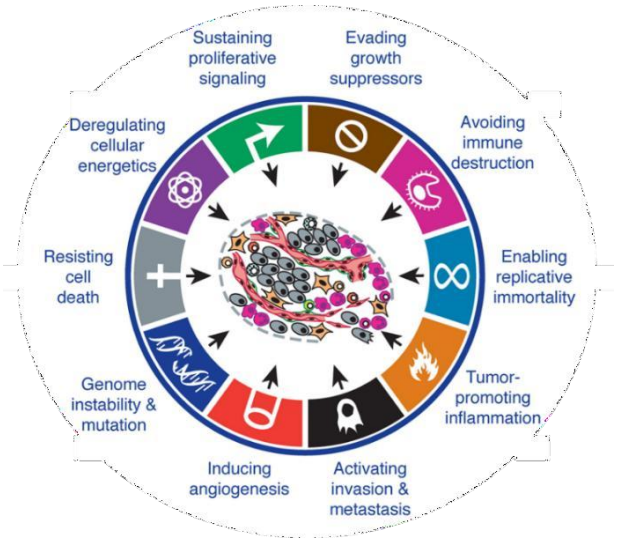

Figure 8. Hallmarks of cancer. [taken from (131)]

4.1 Lipid metabolism

In addition to increased demand for glucose, glutamine, and certain amino acids, cancer cells undergo lipid metabolic reprogramming. This involves upregulating *de novo* lipogenesis, fatty acid (FA) uptake, and fatty acid oxidation (FAO), enabling cancer cells to store energy and produce membranes necessary for rapid proliferation (**Figure 9**). Lipids also play many other roles, and understanding how cancer cells utilize lipid metabolic reprogramming to support their malignant phenotype may help identify novel therapeutic targets for cancer treatment (136, 137). FAs, phospholipids, and cholesterol are the three main classes of lipids dysregulated in tumors. FAs, which have a terminal carboxyl group and a hydrocarbon chain that varies in length and saturation, are the building blocks for lipid synthesis (138). Phospholipids and cholesterol are primary components of cell membranes, crucial for maintaining the cancer phenotype by promoting multidrug resistance and driving distant metastasis (139). Normal mammalian cells mainly acquire FAs through external uptake, whereas cancer cells primarily produce FAs *de novo*. The substrate for *de novo* lipogenesis is citrate or acetate-derived cytoplasmic acetyl-CoA, produced by ATP citrate lyase (ACLY) and acetyl-CoA synthetase 2 (ACSS2), respectively. Acetyl-CoA is then activated by irreversible carboxylation into malonyl-CoA, a reaction catalyzed by acetyl-CoA carboxylases (ACC)—the rate-limiting enzyme in this process. Subsequently, fatty acid synthase (FASN) mediates the condensation of seven malonyl-CoA with one acetyl-CoA molecule, ultimately producing palmitate, a saturated 16-carbon FA (140). Palmitate could be then elongated by fatty acid elongases (ELOVL) and desaturated by stearoyl-CoA desaturases (SCD) or fatty acid desaturases (FADS) to form the cellular pool of more complex non-essential FAs (141). The upregulation of various lipogenic enzymes primarily drives *de novo* lipogenesis in cancer cells. A key regulator of cellular lipid metabolism is the sterol regulatory element-binding protein (SREBP), a family of helix-loop-helix leucine zipper transcription factors that regulate genes involved in FA synthesis and cholesterol biosynthesis pathways. Several studies have shown that SREBPs are activated downstream of oncogenic signaling pathways, mainly the PI3K/Akt/mTORC1 axis. Indeed, mTORC1 promotes SREBP1 nuclear accumulation, thereby driving lipid synthesis during cell growth (142). Increased ACLY expression has been observed in lung, prostate, bladder, breast, liver, stomach, and colon tumors (143). ACLY can be phosphorylated at different sites by kinases, such as Akt, which promotes its activation and stabilization. In human lung adenocarcinoma, ACLY phosphorylation correlates with stage, differentiation grade, and poor prognosis (144). ACSS2 is also dysregulated in cancer (145). Indeed, high levels of ACSS2 are commonly found in

invasive ductal carcinomas of the breast, TNBC, glioblastoma, ovarian cancer, and lung cancer, often correlating with higher tumor grades and poorer survival compared to tumors with low ACSS2 expression (146, 147). ACC consists of two enzyme subtypes: ACC1 and ACC2. ACC1, expressed mainly in lipogenic tissues, facilitates FA synthesis in the cytosol. In contrast, ACC2, which is highly expressed in oxidative tissues like the heart and muscles, is anchored to the outer mitochondrial membrane, where malonyl-CoA production inhibits carnitine palmitoyltransferase-1 (CPT1), preventing FAs from entering mitochondria for FAO (148). ACC1 is regulated at the transcriptional level by SREBP1 and post-translationally through phosphorylation, allosteric regulators, and protein interactions. It is highly expressed in various human cancers, including breast, prostate, liver, and gastric carcinomas (148, 149). Overexpression and hyperactivity of FASN are common in many cancers and correlate with higher risks of recurrence and mortality. FASN is often a poor prognostic marker, with overexpression associated with decreased patient survival (150). Over the years, numerous studies have highlighted FASN's involvement in key cancer hallmarks, including cell metabolism, proliferation, migration, invasion, resistance to cell death, immune escape, and angiogenesis (151). A fraction of *de novo* synthesized FAs undergo desaturation to form monounsaturated FAs (MUFA), and this process is also critical for cancer cell survival (152). SCD1, the enzyme responsible for the introduction of a double bond at the cis-delta-9 position of saturated FAs, is overexpressed in many tumors, including breast cancer, bladder cancer, and hepatocellular carcinoma (153-155). SCD1 is involved in cancer cell proliferation, migration, metastasis, and tumor growth, and is a critical enzyme that helps protect cancer cells from saturated lipid toxicity-induced ER stress and apoptosis (156-158). Another common lipogenic pathway stimulated in cancer is the mevalonate pathway, which leads to the production of cholesterol, a key molecule for cell membrane function, as well as other important molecules that can support tumor growth and progression (159). Indeed, cholesterol deficiency in cell membranes has been shown to inhibit cancer progression (160), while cholesterol metabolic reprogramming enhances the malignant phenotype of cancer cells, such as increased drug resistance, proliferation, immune escape, metastasis, and stemness properties (161). Moreover, the cholesterol synthesis enzymes 3-hydroxy-3-methylglutaryl-coenzyme A reductase (HMGCR), mevalonate kinase (MVK), and squalene synthase (SQS) are increased in human hepatocellular carcinoma and are associated with poorer clinical outcomes. Furthermore, overexpression of the catalytic domain of HMGCR has been shown to increase transformation in human breast and liver tumor cells *in vitro* (162). Phospholipid content has been shown to regulate various carcinogenic processes such as tumor growth, migration, and metastasis (139). Phosphoglycerides and sphingolipids are two major

phospholipid structures. Phosphoglyceride, also called glycerophospholipids, is the most abundant phospholipid and the major constituent of membrane bilayers. In phosphoglycerides, two FAs are esterified to a glycerol backbone. They include various head groups, and they can be further divided into phosphatidylcholine (PC), phosphatidylserine (PS), phosphatidylethanolamine (PE), phosphatidyl glycerol (PG), phosphatidylinositol (PI), and cardiolipin(152). Tumors also absorb FA from the tumor environment through multiple routes, including the endocytosis of low-density lipoprotein (LDL) particles via the LDL receptor (LDLR), the fatty acid translocase (FAT/CD36), fatty acid transport proteins (FATPs/SLC27A), and fatty acid binding proteins (FABPs)(152). FA uptake can be essential for cancer, as uptake of extracellular FA was shown to promote migration and metastasis in squamous cell carcinoma(163). Similarly, inhibition of FA uptake via CD36 blockade has been shown to provide therapeutic benefit in preclinical models of prostate cancer. Moreover, high expression of lipid-uptake-associated proteins (such as CD36 in lung, bladder, breast, and ovarian cancer and the LDLR in pancreatic cancer) are connected to worse patient prognosis (164, 165).

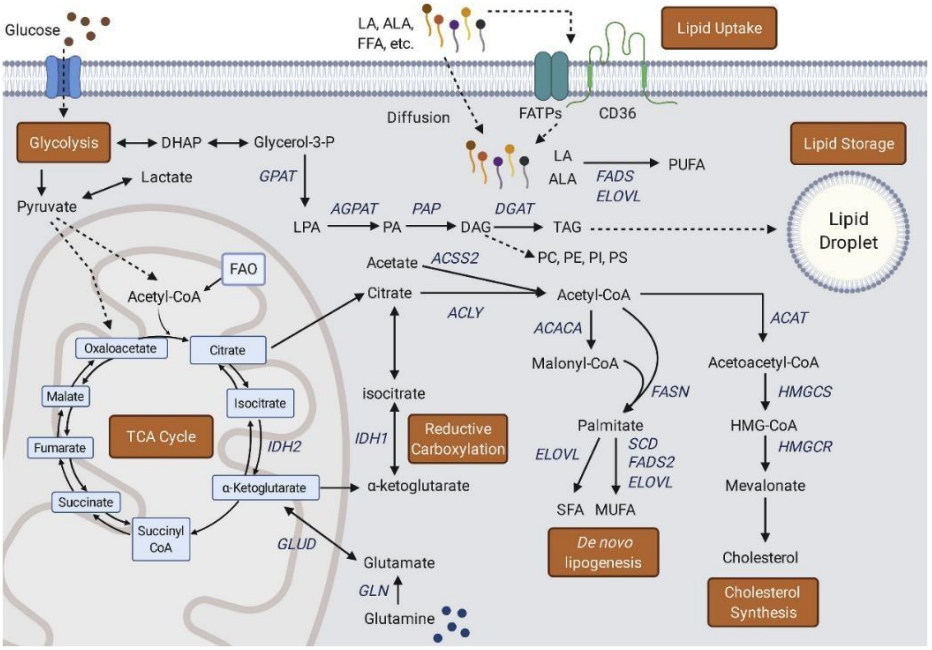

Figure 9. Lipid metabolism in cancer. [taken from (136)]

4.2 Lipid droplets

Lipid droplets (LDs) are cellular organelles with a unique structure, consisting of a hydrophobic core composed of neutral lipids, mainly triacylglycerols (TAGs), cholesterol, and other sterols in the form of sterol esters, surrounded by a single layer of phospholipids and various proteins involved in regulating LD structure and function (166-168). Perilipins (PLINs) are the major cytosolic LD-associated proteins and include five genes (PLIN 1–5). PLINs show differential patterns of gene expression, with PLIN-1 limited to adipose tissues, PLIN-2 and PLIN-3 in the rest of cell types (including preadipocytes), PLIN-4 to adipocytes but also brain, heart, and skeletal muscle, and PLIN-5 restricted to FA-oxidizing tissues such as heart, brown adipose tissue, and skeletal muscle(169). The first step in LD biogenesis is the synthesis of neutral lipids, which involves different enzymes located in the endoplasmic reticulum: acyl-coenzyme A cholesterol acyltransferase (ACAT1 and ACAT2), important for producing sterol esters, and diacylglycerol acyltransferases (DGAT), responsible for generating TAGs (170). The newly synthesized neutral lipids accumulate in lipid “lenses” within the intercalated layers of the endoplasmic reticulum and eventually give rise to nascent LDs that bud from the membrane and are released into the cytosol (171). The budding process is facilitated by proteins recruited to the nascent droplet, such as the membrane protein seipin, which is essential for the stabilization and growth of the droplet, as well as fat storage-inducing transmembrane (FIT) proteins, requiring a particular rearrangement of membrane lipids that drives asymmetrical budding into the cytosol (172). The composition, size, and mobility of LDs change in response to nutrient availability and cellular states. Cancer cells are metabolically active, characterized by increased lipid uptake and *de novo* lipid synthesis. These large amounts of FAs can rapidly activate TAG synthesis and culminate in the accumulation of newly formed LDs (173). Indeed, LDs are a key metabolic organelle in cancer cells, controlling both lipid acquisition and utilization for various purposes depending on specific cellular needs (174) (**Figure 10**). LDs can supply phospholipid membranes for the synthesis of organelles needed during rapid cancer cell growth; they store various lipid precursors, including vitamin E, vitamin A, retinyl esters, and retinol, which are essential for antioxidant responses; and contain many lipid signaling molecules, including steroid hormones, that play crucial roles in cellular signaling (175).

TAGs are the major neutral lipids in LDs and are formed by a glycerol esterified to three FAs, yielding diacylglycerol, which DGAT then esterifies to TAG. Thanks to DGAT, cancer cells convert free FAs into harmless neutral lipids and store them in LDs, preventing lipid oxidation, thus protecting tumor cells from lipotoxicity. DGAT1 is upregulated in

glioblastoma and melanoma, where it facilitates cell proliferation by preventing oxidative stress. Inhibition of DGAT1 blocked the incorporation of FAs into TGs and effectively suppressed tumor growth by increasing reactive oxygen species (ROS) production (176, 177). Furthermore, DGAT1 is overexpressed in prostate cancer cells, and its inhibition decreases LD density, microtubule organizing center numbers, and microtubule stability, which affects cell migration and growth(178). TAGs are sequentially hydrolyzed into a glycerol backbone and free FAs by three different lipases: adipose triglyceride lipase (ATGL), hormone sensitive lipase (HSL), and monoacylglycerol lipase (MAGL). Data available on the deregulation of ATGL in cancer are controversial. *In vitro* studies have proposed pro-neoplastic features of ATGL, as depletion of the enzyme in colorectal cancer cells and non-small-cell lung carcinoma cell lines induced a reduction of proliferation and invasiveness (179, 180). Furthermore, ATGL upregulation in breast and pancreatic ductal adenocarcinoma induced an accumulation of adipocytes in the tumour microenvironment, contributing to the aggressiveness of the tumor (181, 182). Conversely, *in vivo* findings evidenced anti-neoplastic effects of ATGL in mouse models and human cancer. Indeed, mice lacking ATGL displayed spontaneous development of pulmonary neoplasia, and the gene encoding ATGL is deleted in 38% of lung cancer and in other cancer types, including ovarian serous cystadenocarcinoma, glioblastoma, oesophageal and stomach carcinomas (183). While the role of ATGL in cancer is still debated, the oncogenic role of MAGL in cancer is well established. MAGL is highly expressed in many aggressive human cancers where it orchestrates lipid signalling-mediated tumorigenesis, migration and invasion, acting as a critical regulator of metastasis (184-186). Another important component of LDs is cholesteryl ester (CE), the storage form of cholesterol synthesized by ACAT. Tumor cells are characterized by an aberrant accumulation of CE in LDs, representing a potential target of tumor metabolism remodelling. Indeed, CE accumulation in LDs is a metabolic feature of breast, prostate, and pancreatic cancer (187-189) and is positively correlated with advanced clinical staging, metastasis, and poor survival. Importantly, ACAT inhibition suppresses cancer proliferation, migration, invasion, and tumor growth *in vitro* and *in vivo* (187, 190). Increased LDs in cancer cells play an important role in maintaining cell survival during cancer therapy (191). In colorectal cancer, lysophosphatidylcholine acyltransferase 2 (LPCAT2)-mediated LD accumulation is involved in anti-apoptotic response to endoplasmic reticulum stress, leading to resistance to chemotherapy (192). In progesterone-dependent breast cancer, increased intracellular accumulation of LDs has been associated with resistance to docetaxel, which is readily sequestered within LDs (193). In ER+ breast cancer cells, increased intracellular lipid storage in LDs driven by

ACC1 supports metabolic adaptability and contributes to resistance to AI treatment (149).

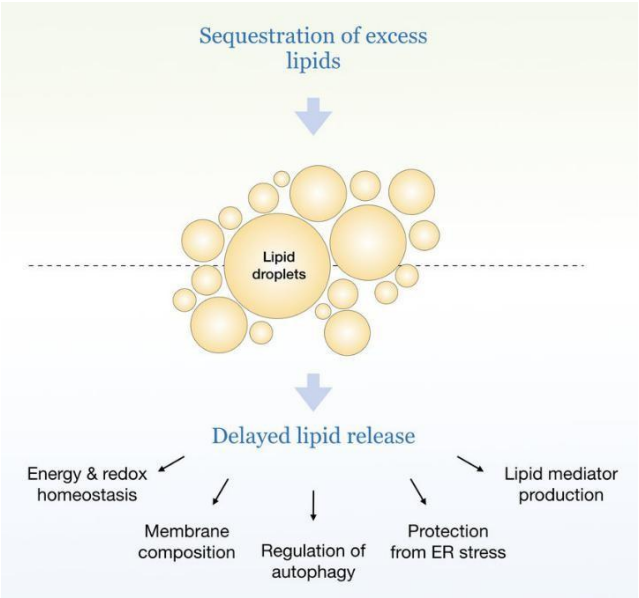

Figure 10. Lipid droplets. [taken from (174)]

5. Tumor metabolic reprogramming

As previously mentioned and illustrated in **Figure 8**, normal cells acquire a set of distinct biological traits, defined as the hallmarks of cancer, as they progress to a neoplastic state. Among these, altered cellular metabolism and energetics represent key features of cancer development (131). Specifically, metabolic reprogramming refers to the adaptive alterations in cellular metabolic pathways in response to specific physiological or pathological conditions, enabling cells to adapt to environmental changes and support growth and survival. Metabolic reprogramming in cancer cells allows them to adapt to environments with limited nutritional resources, altering various metabolic pathways as shown in **Figure 11**, supporting survival, growth, and proliferation. Alterations in cellular metabolism also influence signaling pathways, epigenetic regulation, and interactions with the surrounding tumor microenvironment, shaping both cancer progression and response to therapy (132). In these years, numerous metabolic reprogramming events have been identified. Indeed, metabolic alterations involve different processes that influence various aspects of cellular metabolism. These include not only glucose metabolism, which plays a crucial role in fueling cancer cell growth, but also amino acid metabolism, important for protein synthesis and cellular functions, as well as lipid

metabolism, involved in membrane synthesis and signaling pathways (194, 195). All these alterations result in rapid growth of cancer cells and contribute to treatment resistance. Importantly, since metabolic rewiring can render cancer cells dependent on specific pathways, this offers a potential therapeutic opportunity (135).

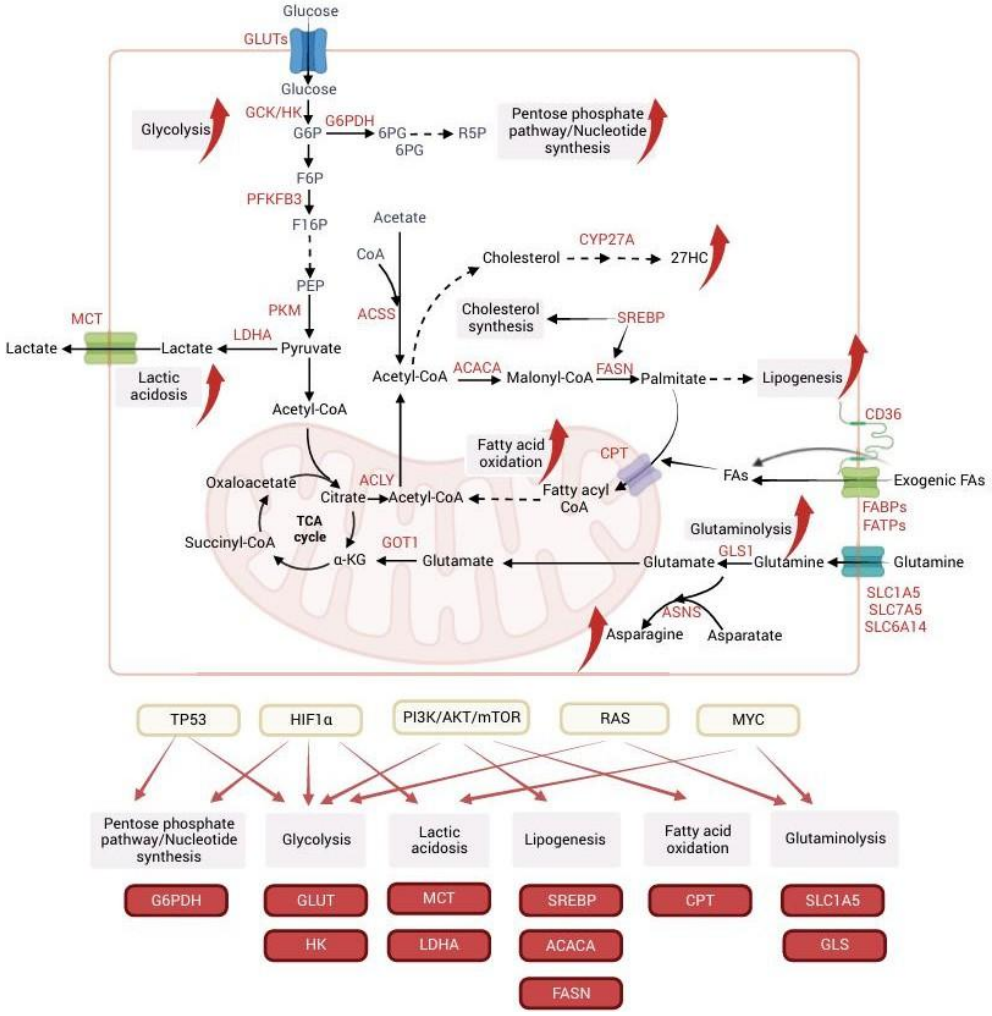

Figure 11. Metabolic reprogramming. [taken from (194)]

5.1 Deregulated metabolism and therapy resistance in breast cancer

Accumulating evidence has shown that metabolic reprogramming is closely associated with tumor development, progression, and drug resistance. Indeed, by altering metabolic pathways, cancer cells not only enhance their plasticity and resilience but also alter the microenvironment, reducing drug accumulation or accelerating its degradation, ultimately leading to treatment failure (196). In the context of metabolic reprogramming

and therapy resistance, when referring to breast cancer, it's important to highlight that there is considerable heterogeneity among different subtypes of breast cancers (197). For this reason, investigating this aspect is crucial for identifying metabolic vulnerabilities that can improve anticancer therapies or reverse drug resistance in breast cancer cells, such as resistance to chemotherapy, ET, and HER-2 targeted treatment (**Figure 12**).

The expression of specific isoforms of key enzymes in glucose catabolism, such as hexokinase (HK), phosphofructokinase-1 (PFK1), and pyruvate kinase (PK), are linked to drug-resistant tumor cells. HK, the first enzyme in glycolysis, converts glucose into glucose 6-phosphate. The HK family includes three members: HK1, HK2, and HK3. HK2 is highly expressed in many tumors, with breast cancer cells showing elevated HK2 levels (198). Our laboratory demonstrated that AI-resistant breast cancer cells depend more on glycolysis, but due to their enhanced metabolic plasticity, they can switch to oxidative phosphorylation when glycolysis is impaired. Specifically, the miR-155/HK2 axis plays a key role in this reprogramming, and reducing miR-155 levels subsequently lowers HK2 expression, making AI-resistant cells more sensitive to metformin (199), a biguanide known to target complex I and therefore used as oxidative phosphorylation inhibitor. HK2 also contributes to tamoxifen resistance. In ER+ breast cancer cells, increased HK2 promotes autophagy by inhibiting the mTOR pathway, leading to tamoxifen resistance. This suggests HK2 as a potential target for overcoming endocrine resistance (200). Additionally, the serine/threonine kinase and proto-oncogene proviral insertion in murine lymphomas (PIM2) binds to and activates HK2, boosting glycolysis and cell growth, which has been linked to paclitaxel resistance (201). PFK1, the second key glycolytic enzyme, converts fructose-6-phosphate (F6P) into fructose-1,6-bisphosphate. Its activity is regulated by phosphofructokinase-2/fructose-2,6-bisphosphatase (PFKFB), which produces fructose 2,6-bisphosphate from F6P, serving as a critical regulator of glycolysis and a potential tumor therapy target (202). Upregulation of PFKFB3 is seen in ET resistant breast cancer cells and correlates with poor recurrence-free survival in patients (203). Breast cancer cells resistant to lapatinib, a dual inhibitor of EGFR and HER2, restore PFKFB2 phosphorylation levels, which increases glycolytic flux and supports cell survival (204). Lactate, the final product of aerobic glycolysis, plays a vital role in breast cancer drug resistance. Accumulation of lactate via lactate dehydrogenase (LDH) acts as an important resistance mechanism to PI3Kα inhibitors in ER+ breast cancer (205). Moreover, our laboratory demonstrated that ER+/HER2+ breast cancer cells resistant to the CDK4/6 inhibitor palbociclib show significant changes in glucose metabolism, and the inhibition of glycolysis or key metabolic enzymes could sensitize resistant cells to CDK4/6 inhibitors (206).

Importantly, also dysregulated lipid metabolism contributes to tumor cell plasticity and is associated with anti-cancer therapy resistance. Alterations in lipid metabolism, such as abnormal accumulation of FAs, can interfere with breast cancer treatment by supplying additional energy to tumor cells, promoting triglyceride synthesis that contributes to LDs formation, altering cell-membrane composition, and functioning as signaling molecules that activate pro-survival pathways (137). ACLY, the first rate-limiting enzyme in lipid synthesis, has been related to therapeutic resistance (207). In breast cancer, ACLY is involved in the development of acquired resistance to tamoxifen and palbociclib. Importantly, ACLY inhibition could help improve the efficacy of the therapy (208, 209). FASN, promoting the synthesis of FAs to provide raw materials for cell membrane synthesis, as well as signaling molecules, may play a role in the acquisition of endocrine resistance in ER+ breast cancer. Indeed, FASN inhibition impairs the growth of tamoxifen-resistant breast tumors by altering ER expression and localization (210). Our laboratory has previously identified ACC1 as playing an important role in the response and adaptation to estrogen deprivation in ER+ breast cancer. We found that ACC1 controls a metabolic reprogramming that involves LDs and peroxisomes, promoting therapy resistance. ACC1 targeting reduced tumor growth of resistant patient-derived xenografts, identifying a targetable hub to combat the acquisition of estrogen independence in ER+ breast cancers (211). However, the role of ACC in breast cancer remains a topic of debate. Indeed, Rios Garcia et al. demonstrated that ACC1 inhibition promotes the accumulation of cellular acetyl-CoA, the subsequent acetylation and activation of the transcription factor Smad2, which promotes metastasis formation (211). Among the traits that correlate with metabolic alterations and therapy resistance, uptake of FAs from the environment represents an important metabolic biomarker in cancer. Feng et al. observed an increase in CD36 expression in lapatinib-resistant breast cancer cells that promoted FAs uptake to compensate for reduced FAs synthesis caused by HER2 inhibition. Inhibition of CD36 suppresses the growth of lapatinib-resistant cells both *in vitro* and *in vivo* (212). Another critical metabolic pathway that contributes to therapy resistance is FAO, a mitochondrial metabolic process that converts long-chain FAs into acetyl-CoA, which subsequently enters the tricarboxylic acid (TCA) cycle and drives the electron transport chain (ETC) to produce ATP (213). ER+ endocrine-resistant breast cancer cells display increased reliance on FAO compared with primary tumor cells, and both FAO flux and ATP generation are elevated in tamoxifen-resistant ER+ breast cancer models (214). Similarly, chemoresistant MDA-MB-231 cells exhibit enhanced mitochondrial FAO activity, implicating FAO in the development of chemotherapy resistance in TNBC (215). Increasing evidence suggests that also LD dysfunction contributes to the development and progression of breast cancer. Our

laboratory has shown that LDs are enriched and metabolically active in estrogen-deprived ER+ cells, where they are essential for maintaining redox balance and supporting metabolic adaptability in resistant tumors (149). Consistent with this, doxorubicin-resistant TNBC cells contain abundant LDs (216), and tamoxifen-resistant T-47D cells exhibit a rapid accumulation of neutral lipids within LDs along with increased free cholesterol in lysosomes (217). Overall, LDs play a crucial role in breast cancer progression by regulating redox homeostasis, mediating signaling pathways, and supporting the energetic demands that promote tumor growth and dissemination.

Amino acids are essential molecules for protein synthesis and play a key role in various cellular functions, including energy production, nucleoside synthesis, and cellular redox balance maintenance. Tumor cells, which undergo rapid proliferation, have an increased demand for amino acids, which demands metabolic reprogramming to meet these nutritional requirements for accelerated growth (218). Breast cancer cells exhibit increased uptake and utilization of specific amino acids (e.g., glutamine, serine, and arginine), which are not only substrates for protein synthesis, but also play key roles in cellular signaling, energy production, and maintenance of redox balance (219). Amino acid transporters (AATs) are membrane-bound solute carrier (SLC) transporter proteins that facilitate the exchange of amino acids across biological membranes. Some SLCs have been demonstrated to exhibit significantly elevated expression levels in breast cancer cells (220). In addition to controlling glutamine uptake, SLC1A5 can also transport other amino acids, such as alanine, serine, cysteine, threonine, and asparagine. SLC1A5 has been implicated in ET failure in some luminal breast cancers. Chen et al. reported that SLC1A5 is upregulated in ET-resistant breast cancer cells, and that inhibition of SLC1A5 suppresses the proliferation of cells resistant to AIs (221). SLC3A2 forms a complex with SLC7A5, an interaction required for the membrane localization of the AAT. This interaction increases the cellular uptake of leucine, promotes tumor growth, and confers tumor cell resistance to tamoxifen treatment (222, 223). In our laboratory, we demonstrated that endocrine-resistant ER+ breast cancer increased intracellular aspartate and glutamate levels, sustaining the aggressive phenotype associated with therapeutic resistance. This metabolic shift is driven by increased expression of miR-23b-3p, which induced a decrease in the neutral AAT SLC6A14 and ET resistance. This dysregulation disrupts amino acid homeostasis, initiating autophagy and increasing reliance on SLC1A2-driven uptake of aspartate and glutamate. Together, these changes maintain the anabolic and catabolic activities that facilitate metabolic reprogramming and foster ET resistance (224). Beyond changes in aspartate and glutamate metabolism, breast cancer cells exploit the transporter SLC7A11 to sustain redox balance. Indeed, the upregulation of SLC7A11 expression leads to an increase in glutathione (GSH)

synthesis, by enhancing cysteine uptake, thus enabling the adaptation to oxidative stress conditions, maintenance of cell proliferation and resistance to chemotherapy- and radiotherapy-induced ROS production. It has been shown that SLC7A11 is associated with chemoresistance and metastasis of breast cancer. Mechanistically, chemotherapy induces the expression of SLC7A11 in a HIF-1-dependent manner, resulting in elevated intracellular GSH levels. Similarly, serine synthesis through phosphoglycerate dehydrogenase (PHGDH) is involved in maintaining redox homeostasis, promoting cancer cell proliferation and drug resistance (225). Doxorubicin exposure in TNBC cells activates PHGDH-driven serine synthesis, increasing GSH levels to buffer chemotherapy-induced ROS. Targeting PHGDH could therefore enhance doxorubicin's antitumor activity in TNBC.

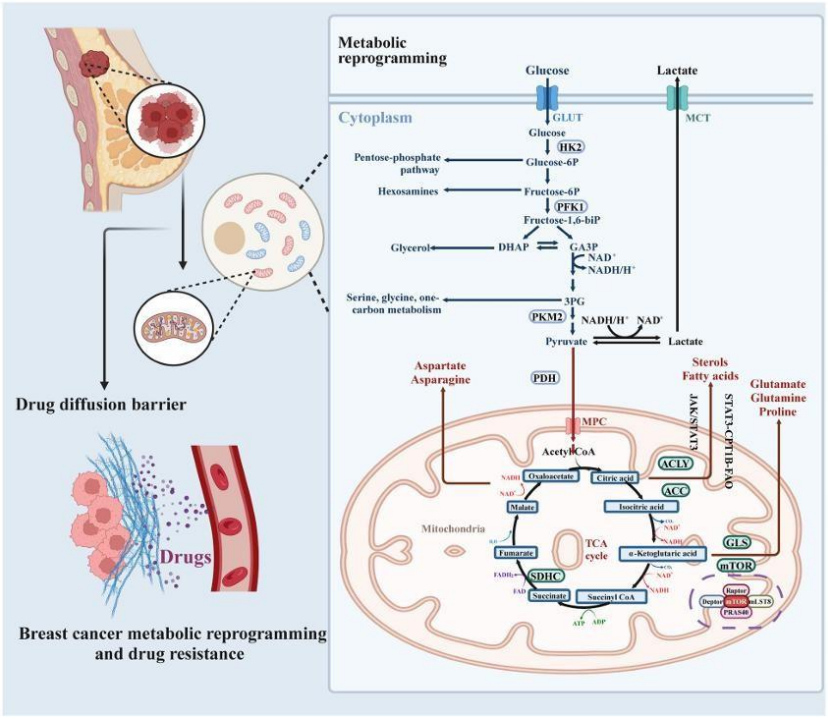

Figure 12. Metabolic reprogramming and drug resistance in breast cancer. [taken from (200)]

5.2 Metabolic targeting in breast cancer

As discussed above, the aberrant metabolic reprogramming in breast cancer cells underlies their remarkable ability to adapt to anti-tumor therapies. Consequently, targeting the metabolic pathways offers a promising strategy to enhance the effectiveness of standard treatments and to overcome resistance to chemotherapy, ET, and HER2-targeted therapies (226) (**Figure 13**).

Inhibition of glucose uptake is a therapeutic opportunity and has been investigated in several studies. BAY-897, an inhibitor of the glucose transporter GLUT1, was reported to impair tumour growth in a TNBC patient-derived xenograft model (227). However, whether the compound has the desired pharmacokinetic properties to advance to the clinic remains to be established. HK catalyzes the first step in glycolysis, and HK2, in particular, shows increased expression in cancer. Moreover, loss of HK2 diminishes tumorigenesis *in vivo*, highlighting its potential role as a therapeutic target (198). HK2 targeting synergizes with trastuzumab in breast cancer cells and reverts resistance in models insensitive to the treatment, both *in vitro* and *in vivo* (228). Clinical studies have used 2-deoxy-D-glucose (2-DG), which competes with glucose for HK binding, inhibiting glycolysis, as an adjunctive therapy in breast cancer, demonstrating that 2-DG has chemosensitizing effects (229, 230). Although blocking glycolysis is theoretically appealing, current glycolysis inhibitors have largely failed in clinical trials. So far, these inhibitors are non-selective and alter metabolism in both cancerous and normal cells. LDH, catalyzing the final step of glycolysis, converts pyruvate to lactate, playing a crucial role in tumor cell metabolism. Inhibiting LDH-A selectively suppresses the growth of HER2-overexpressing cells and increases the responsiveness of trastuzumab-resistant breast cancers to trastuzumab therapy (228).

Recent progress in understanding FA synthesis, desaturation, and lipid uptake in cancer cells has revealed promising opportunities for developing clinically effective treatments that target lipid metabolism. However, no FDA-approved cancer therapies currently target lipid-related pathways. FASN, the key enzyme in the synthesis of FA palmitate, is certainly the most studied therapeutic target. A phase I clinical trial with TVB-2640, an orally available inhibitor of FASN, has been recently completed, proving the safety and efficacy of the drug in patients with advanced solid malignancies (NCT02223247). Combined with paclitaxel, TVB-2640 proved to be beneficial in pretreated breast cancer patients. Moreover, FASN has been implicated in HER2+ breast cancer based on a positive feedback loop between the two proteins (231), and a Phase 2 clinical trial (NCT03179904) testing TVB-2640 with Herceptin in metastatic HER2+ breast cancer is ongoing. Studies have also shown that FAO contributes to tumor chemotherapy

resistance, and that blocking FAO not only resensitizes cancer cells to chemotherapy but also suppresses the proliferation of cancer stem cells in mouse breast tumor models (232).

Targeting amino acid metabolism has emerged as a promising strategy in breast cancer therapy, as tumor cells may rely on specific amino acids for growth and survival. For example, inhibiting extracellular glutamine uptake and metabolism through SLC1A5 targeting represents a promising strategy for breast cancer therapy. Benzylserine was the first molecule discovered to inhibit SLC1A5; however, it was found to have additional targets, making it nonspecific (233). More recently, MEDI7247, a novel pyrrolobenzodiazepine (PBD) antibody-drug conjugate targeting SLC1A5, was in Phase I clinical trials for relapsed/refractory hematologic malignancies. However, due to adverse events related to repeated dosing and response durability, the study was prematurely terminated (234). Despite SLC1A5 inhibition shows promise in cell and murine studies, safe and specific drugs targeting this transporter have yet to be developed. SLC6A14 expression is upregulated in ER+ breast cancer tissues and cell lines, supporting increased demand for amino acids, such as leucine, glutamine, and arginine, and making it a good candidate for anti-tumor effect. Since SLC6A14 must leave the endoplasmic reticulum through Hsp70 and Hsp90beta, ganetespib (an HSP90 inhibitor) has been used in combination with various chemotherapeutic drugs in phase II clinical trials for treating ER+ and HER2+ metastatic breast cancer patients (NCT01560416, NCT02060253), showing encouraging results (235). CB-839 (telaglenastat) is a selective and orally bioavailable glutaminase inhibitor that inhibits the proliferation of TNBC cells by blocking glutaminase 1 (GLS1) activity, the key enzyme of glutaminolysis, thus interfering with glutamine utilization, glutamate synthesis, oxygen consumption, and GSH levels (236). Currently, CB-839 is undergoing phase I/II clinical trials, with patients showing good tolerability and no significant side effects observed in preclinical trials (237). Approaches limiting amino acids through modulating their availability have been tested in preclinical models and clinical trials (238). A phase II clinical trial evaluated a fasting-mimicking (FMD), plant-based, low–amino acid substitution diet as an adjunct to neoadjuvant chemotherapy in women with HER2-negative stage II/III breast cancer, demonstrating both safety and efficacy (NCT02126449) (239). Moreover, the BREAKFAST trial, a phase II clinical investigation in early-stage TNBC, evaluates metabolic therapy approaches in combination with the standard neoadjuvant chemotherapy. The trial explores whether cyclic FMD — with or without metformin — can enhance the antitumor effects of chemotherapy by disrupting cancer metabolism. The results showed that patients receiving FMD alongside anthracycline and taxane-based neoadjuvant chemotherapy

showed promising responses characterized by substantial modulation of metabolic pathways in tumor cells (240). Building on these findings, the BREAKFAST-2 trial is a larger, randomized phase II study designed to test whether combining fasting-like approach with the SOC, preoperative, anthracycline-taxane-carboplatin chemotherapy plus the immunotherapic pembrolizumab improves the pathological response in a population of patients with stage II-III TNBC (NCT05763992). Combining personalized diets with therapies such as chemotherapy or immunotherapy may yield synergistic benefits that enhance metabolic and immune outcomes. However, to apply dietary interventions effectively in cancer treatment, patients must be stratified according to both the tumor's metabolic vulnerabilities and the host's overall metabolic state.

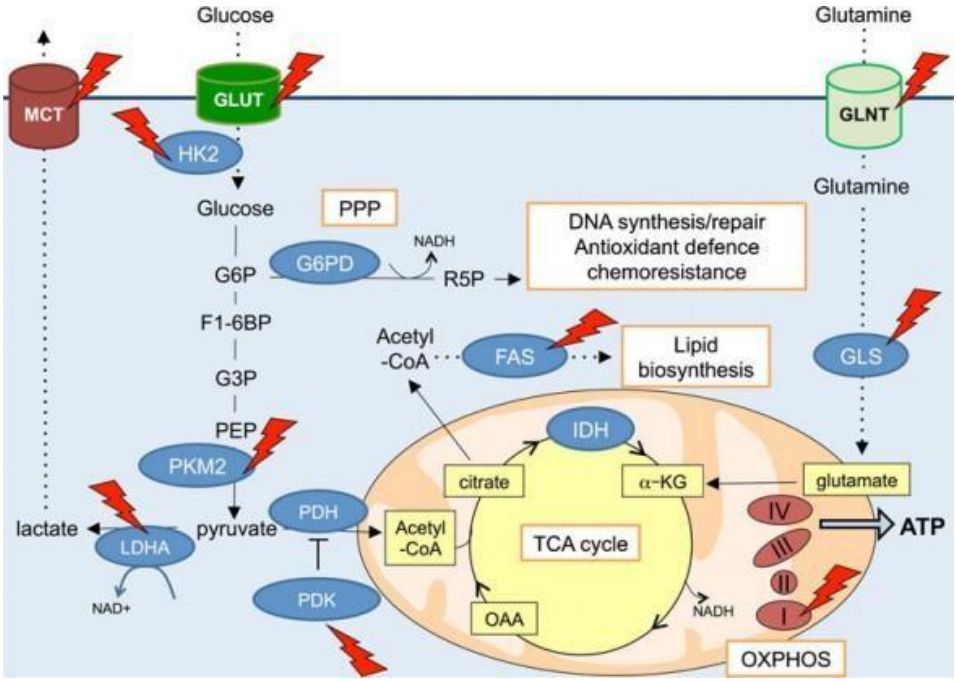

Figure 13. Metabolic targeting in breast cancer. [taken from (226)]

6. Ferroptosis

Ferroptosis is a unique form of non-apoptotic cell death that requires the redox-active metal iron (241, 242) (**Figure 14**). Free intracellular iron reacts with oxygen and PUFA-containing lipids to generate high levels of membrane lipid peroxides — the distinct feature of ferroptosis — which leads to altered ion fluxes and ultimately to the alteration of plasma membrane integrity (243). These membrane lipid peroxides can be lethal to the cell when they accumulate at high levels. Therefore, cells have evolved several

mechanisms to defend against oxidative membrane damage, and ferroptosis ultimately occurs when ferroptosis-promoting events significantly override the antioxidant-buffering capabilities provided by ferroptosis defence systems (244, 245). This type of cell death is markedly different from other forms of non-apoptotic cell death, such as necroptosis and pyroptosis, regulated by pore-forming proteins such as mixed lineage kinase domain-like pseudokinase (MLKL), gasdermin D and ninjurin 1 (246, 247). Ferroptosis execution involves a distinct set of lipid-centric mechanisms, inducing a phospholipid profiles that differ from those of cells undergoing other forms of cell death (248). We can distinguish the execution of ferroptosis from mechanisms that regulate ferroptosis sensitivity. The execution of ferroptosis involves membrane lipid peroxidation, the aberrant movement of ions across the plasma membrane and plasma membrane rupture (249). Cellular sensitivity to ferroptosis is regulated positively and negatively by molecules and pathways that control lipid metabolism, iron homeostasis, redox regulation and related processes (250).

Ferroptosis has been linked to cancer, and its targeting might provide new therapeutic opportunities, in particular in the context of therapy resistance (251). Indeed, ferroptosis has been recognized as a critical cell death response triggered by a variety of cancer therapies, including radiotherapy, immunotherapy, chemotherapy and targeted therapies (252, 253). Thus, ferroptosis inducers (FINs) hold great potential in cancer therapy, especially in combination with conventional therapies.

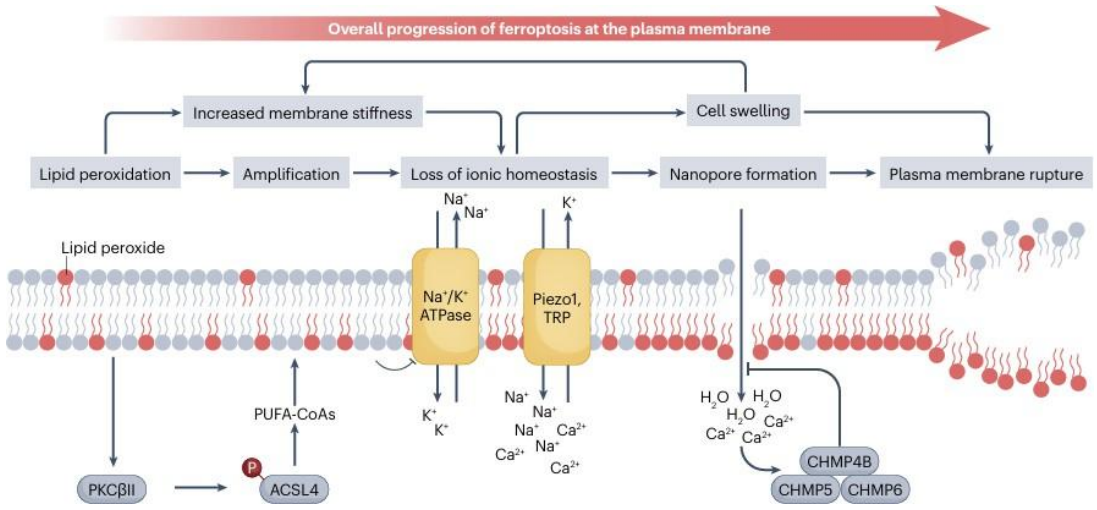

Figure 14. The general mechanism of ferroptosis. [taken from (242)]

6.1 The execution and regulation of ferroptosis

The execution of ferroptosis involves the peroxidation of PUFA-containing phospholipids and the formation of lipid hydroperoxides (254). The lipid peroxidation mechanism involves distinct steps of initiation, propagation, and termination. In the initiation step, an allylic hydrogen is removed, generating a carbon-centered lipid radical (L•). During propagation, L• is unstable and reacts rapidly with oxygen, generating a peroxyl radical (LOO•), which then abstracts a hydrogen atom from another PUFA, producing a lipid hydroperoxide (LOOH) and a new lipid radical. The chain reaction is ultimately terminated when LOO• is intercepted by a radical-trapping antioxidant (255). Oxidation of PUFAs can occur through both enzyme-catalyzed pathways and non-enzymatic autoxidation mechanisms within lipid bilayers. The nonenzymatic lipid peroxidation is a process mediated by redox-active metals, especially iron, which reacts with the endogenously produced hydrogen peroxide (H_2O_2) to generate the hydroxyl radical (HO•). These redox reactions mediated by labile iron are known as “Fenton reaction”: $Fe^{2+} + H_2O_2 \rightarrow Fe^{3+} + HO\bullet + OH^-$ (256). Like H_2O_2, LOOH can also undergo the Fenton reaction, a series of reactions where LOOH can be converted to LOO•. If LOOH is not neutralized quickly, it can propagate the peroxidation to neighbor PUFA-PLs, which might further damage the membrane.

Cyclooxygenases (COXs), lipoxygenases (LOXs), and cytochrome p450s (CYPs) are crucial enzymes that promote lipid oxidations. COX-mediated lipid peroxidation produces prostaglandins, which directly link the lipid peroxidation to inflammation and apoptotic processes (257). Oxidoreductases cytochrome p450 (POR), located in the endoplasmic reticulum, is critical for the metabolism and detoxification of many drugs, steroids, and other types of chemicals via oxidation in the endoplasmic reticulum (258). LOXs, especially 12/15-LOX (ALOX15), are a family of iron-dependent enzymes that are critical for several lipid peroxidation pathways (259). However, their involvement remains debated, and non-enzymatic lipid autoxidation is likely the primary driver of ferroptosis (260). Once formed, lipid peroxides interact with iron to generate highly reactive lipid radicals that can then remove hydrogens from neighbouring acyl chains in the lipid membrane to propagate the lipid peroxidation process (261). Hydrogen abstraction preferentially occurs on PUFAs, whose bis-allylic hydrogens have relatively low bond dissociation energies compared with other lipid species. The specific PUFAs that are peroxidized to drive ferroptosis include arachidonyl (C20:4)- and adrenoyl (C22:4)-containing Pes (262). Increasing lipid peroxidation raises membrane tension, which in turn activates Piezo1 and transient receptor potential (TRP) mechano-sensitive ion channels. Channel opening leads to Ca2+ and Na+ influx and K+ efflux. Collectively,

these changes lead to a loss of ionic homeostasis and osmotic cell swelling that result in plasma membrane rupture (249). ACSL4 catalyses the ligation of free PUFAs, such as arachidonic acids and adrenic acids, with CoA to generate PUFA-CoAs (such as arachidonic acid-CoA or adrenic acid-CoA), which are subsequently re-esterified and incorporated into PLs by lysophosphatidylcholine acyltransferase 3 (LPCAT3) to form PUFA- PLs (such as arachidonic acid-PE or adrenic acid-PE) (262, 263).

The lipid composition of a cell, along with the mechanisms by which it imports, synthesizes, stores, and catabolizes different lipids, plays a critical role in determining ferroptosis sensitivity. In particular, the metabolism of PUFAs strongly influences susceptibility to ferroptosis. The key enzymes involved in PUFA metabolism are the very-long-chain ELOVLs and FADS, which convert the essential dietary precursor PUFAs—linoleic acid (18:2n-6) and α-linolenic acid (18:3n-3)—into longer and more unsaturated PUFAs, the primary substrates for lipid peroxidation (264, 265). Recently, ether phospholipids have emerged as important regulators of ferroptosis sensitivity. These lipids, characterized by an ether bond at the sn-1 position of the glycerol backbone, are synthesized through the peroxisomal and endoplasmic reticulum pathways and contribute to membrane structure and redox balance (266). Recent studies show that ether phospholipids enriched with PUFAs can serve as potent substrates for lipid peroxidation, thereby promoting ferroptotic cell death (267). MUFAs are less oxidizable than PUFAs, and therefore their incorporation into membrane phospholipids limits lipid peroxidation and ferroptosis (268). Malonyl-CoA and acetyl-CoA serve as the primary precursors for FA synthesis, catalyzed by FASN, which condenses these substrates to produce saturated fatty acids (SFA) such as palmitate (C16:0) (269). Palmitate can subsequently be desaturated, a process in which SCD1 serves as the key rate-limiting enzyme. SCD1 introduces a double bond at the Δ9 position of both palmitate and stearate, producing palmitoleic acid and oleic acid, respectively (270). Mechanistically, MUFAs appear to displace more oxidizable PUFA species from phospholipids, thereby creating a membrane environment that is less susceptible to lipid peroxidation (271). Before free FAs can be incorporated into more complex lipids such as phospholipids, they must first be “activated” to fatty acyl-CoAs by long-chain fatty acyl-CoA synthetase (ACSL) enzymes. In humans, ACSL isoforms 1 and 3-6 exhibit distinct substrate preferences, with ACSL4 favoring PUFAs and ACSL3 preferring MUFAs. The balance between these two opposing activities, ACSL4-driven PUFA incorporation and ACSL3-mediated MUFA incorporation, may determine the overall susceptibility of cellular membranes to lipid peroxidation (263, 272). The composition of membrane phospholipids can be remodeled through the removal and replacement of specific acyl chains by phospholipases and acyltransferases (273). Reacylation of lyso-

phospholipids, catalyzed by LPCAT3 and potentially other enzymes such as 1-acylglycerol-3-phosphate O-acyltransferase 3 (AGPAT3), can enhance ferroptosis sensitivity by promoting the incorporation of PUFAs into membrane phospholipids(274). As evidenced by its name, ferroptosis execution requires iron, not only for initiating the non-enzymatic Fenton reaction, but also for acting as an essential cofactor for enzymes that participate in lipid peroxidation (such as ALOX and POR) (241, 275). Therefore, iron chelators prevent ferroptosis while loading iron into tumor cells by nanoparticles induces ferroptosis (276). Normally, cellular iron absorption is mainly controlled by the transferrin receptor 1 (TFR1), which carries transferrin-bound iron into cells via receptor-mediated endocytosis and blocking this process prevents ferroptosis induction (277, 278). An imbalanced regulation of iron metabolism can promote or suppress ferroptosis. For example, intracellular iron is stored mostly as inert iron in ferritin, whereas autophagic degradation of ferritin (ferritinophagy) releases iron into the labile iron pool. Consequently, blockade of nuclear receptor coactivator 4 (NCOA4)-mediated ferritinophagy decreases the level of the labile iron pool and confers resistance to ferroptosis (275, 279).

6.2 Ferroptosis defence mechanisms

The cell has several mechanisms that protect against the onset of ferroptosis, involving the activity of coupled enzyme-metabolite systems that prevent the accumulation of membrane lipid peroxides to toxic levels (280) (**Figure 15**). Glutathione peroxidase 4 (GPX4) uses GSH as a co-substrate to reduce potentially toxic lipid hydroperoxides to less dangerous lipid alcohols (245, 281, 282). Genetic deletion or pharmacological inhibition of GPX4 with RSL3 or ML210 leads to uncontrolled lipid peroxidation and robustly induces ferroptosis across a wide range of *in vitro* and *in vivo* settings (245, 283). GPX4 comprises three isoforms with distinct subcellular localizations: cytosolic, mitochondrial, and nuclear GPX4. All three isoforms are encoded by the same GPX4 gene but arise from different transcription initiation sites (284). The cytosolic GPX4 appears to be the most critical isoform for preventing lipid hydroperoxide accumulation in most cells, but mitochondrial GPX4 may also help inhibit ferroptosis in some cases (285, 286). GSH, the cofactor of GPX4, is a thiol-containing tripeptide composed of glycine, glutamate, and cysteine, with cysteine acting as the rate-limiting substrate (287). Intracellular cysteine is primarily supplied through system xc^-–dependent uptake of cystine, the oxidized dimeric form of cysteine, which is then reduced to cysteine in the cytosol. Solute carrier family 7 member 11 (SLC7A11), also known as xCT, is the

transport subunit of system xc^- (288, 289). Eliminating cystine from culture media or pharmacologically inhibiting SLC7A11 using erastin or other ferroptosis-inducing compounds strongly induces ferroptosis in numerous cancer cell lines (290). The SLC7A11–GSH–GPX4 axis is considered the central cellular defense mechanism against ferroptosis. However, certain cancer cell lines remain resistant to ferroptosis even after GPX4 inhibition, suggesting that alternative ferroptosis-protective pathways also exist (291). Recent studies have shown that ferroptosis suppressor protein 1 (FSP1), also known as AIFM2, functions independently of GPX4 to protect cells from ferroptosis (292, 293). FSP1 belongs to the NAD(P)H- dependent oxidoreductase family, and it's capable of reducing ubiquinone (also known as coenzyme Q or CoQ) to ubiquinol ($CoQH_2$) (294). Apart from its well-known function in mitochondrial electron transport, the non-mitochondrial $CoQH_2$ pool generated from FSP1 mainly localizes to LDs and plasma membrane, acting as a radical-trapping antioxidant and scavenging deleterious lipid hydroperoxides (292, 295). A recent study identified a mitochondrial defense pathway in which dihydroorotate dehydrogenase (DHODH) compensates for GPX4 loss by reducing CoQ to $CoQH_2$, thereby limiting mitochondrial lipid peroxidation. Increased DHODH activity protects mitochondria from ferroptosis when GPX4 is inactivated, whereas simultaneous inhibition of GPX4 and DHODH leads to excessive lipid peroxidation and strong induction of ferroptosis (285). Finally, guanosine triphosphate cyclohydrolase 1 (GCH1) was identified as another critical regulator of ferroptosis in a GPX4-independent manner (296, 297). GCH1 is the rate-limiting enzyme for tetrahydrobiopterin (BH_4) synthesis, a cofactor of aromatic amino acid hydroxylases and other enzymes, but capable of trapping lipid peroxyl radicals, functioning as a radical- trapping antioxidant (298). BH_4 requires dihydrofolate reductase (DHFR) for its regeneration. Blockade of DHFR genetically or pharmacologically synergizes with GPX4 inhibition to induce ferroptosis (296). Recent findings highlight that the modulation of FA metabolism contributes to ferroptosis evasion and cancer progression. Calcium-independent phospholipase A2 β (iPLA2 β), a member of the iPLA2 family, is overexpressed in cancers and, by hydrolysing peroxidized PLs, promotes cancer cell escape from ferroptosis (299). Importantly, the lymphatic environment has been observed to promote the escape of melanoma cancer cells from oxidative stress and ferroptosis *in vivo* thanks to ACSL3- mediated MUFA- PL synthesis, which suppresses ferroptosis by displacing PUFAs from PLs (268). Similarly, a recent study has shown that the hypoxic lymphatic niche induces the degradation of GPX4 and reduces GSH levels of lymph node metastatic cells, shifting their reliance on ferroptosis protection on FSP1. This specific dependency renders lymph node metastases selectively sensitive to FSP1 inhibition, while primary tumors remain largely unaffected (300).

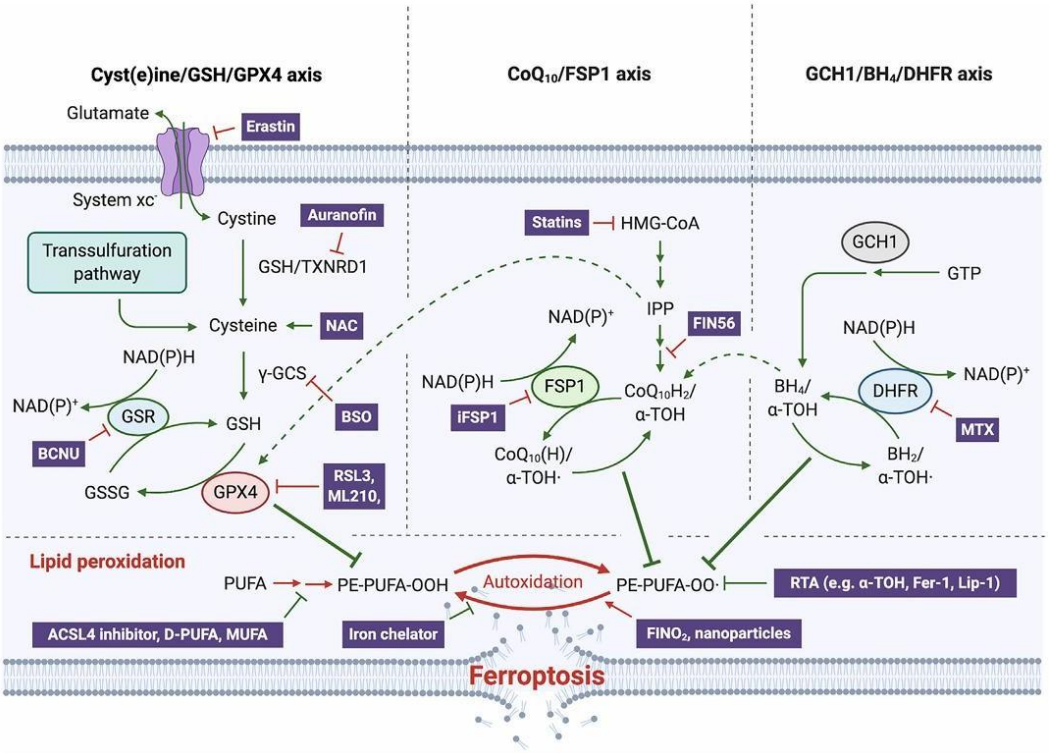

Figure 15. Ferroptosis defence mechanisms. [taken from (280)]

6.3 Ferroptosis vulnerability in cancer

In cancer research, ferroptosis has attracted significant interest, as increasing evidence indicates that its dysregulation intersects with multiple hallmarks of cancer, highlighting its potential as a pleiotropic target (301) (**Figure 16**).

Ferroptosis appears to function as an intrinsic mechanism of tumor suppression, contributing to the anticancer effects of several established tumor suppressor genes, such as p53, BRCA1-associated protein 1 (BAP1), Kelch-like ECH-associated protein 1 (KEAP1), and the epigenetic regulator myeloid/lymphoid or mixed-lineage leukemia 4 (MLL4). For example, the tumor suppressors TP53 and BAP1 exert their ferroptosis-mediated tumor-suppressive activity by inhibiting the cystine transporter SLC7A11 (290, 302). Mutations or deletions of the genes result in the loss of SLC7A11 regulation and, consequently, in the loss of their tumor-suppressive functions (303). Mutations or deficiency of KEAP1 in lung cancer upregulate the expression of FSP1 by stabilizing NRF2 proteins, resulting in ferroptosis resistance (304). Epidermal loss of MLL4 leads to the formation of melanoma precancerous lesions and confers resistance to ferroptosis, through reduced expression of pro-ferroptotic ALOX genes and increased expression of anti-ferroptotic genes (305).

Although ferroptosis functions as a tumor-suppressive mechanism, tumors still develop and progress, indicating that cancer cells possess strategies to evade ferroptosis. Indeed, the stabilization and overexpression of anti-ferroptotic systems are crucial mechanisms evolved by tumor cells to avoid ferroptosis and promote tumor progression. Upregulation of the SLC7A11/GSH/GPX4 axis represents a major ferroptosis evasion strategy adopted by tumor cells. SLC7A11 is overexpressed across multiple cancer types and is among the most extensively characterized mechanisms enabling resistance to ferroptotic cell death (272, 288). Consistently, GSH as well as GPX4 are frequently elevated in tumors, promoting tumor progression and contributing to therapeutic resistance (306, 307). Additionally, NRF2, a master regulator of antioxidant defense, which is upregulated in multiple cancers, regulates components of the ferroptosis cascade, including SLC7A11, GPX4 and FSP1, protecting against ferroptosis and contributing to tumor progression and therapy resistance (308, 309). Numerous oncogenic alterations have been shown to promote ferroptosis resistance in cancer cells by reinforcing antioxidant defense systems and by limiting metabolic processes that drive lipid peroxidation, including the generation of labile iron pools, the biosynthesis of PUFA-containing phospholipids, and the production of ROS. For example, RAS-mutant cancer cells exhibit increased transcription of SLC7A11 and elevated levels of intracellular cysteine and GSH (310). A recent study revealed that enolase 1 (ENO1) possesses a noncanonical function, independent of its traditional role in glycolysis, in suppressing ferroptosis. Specifically, ENO1 inhibits the iron regulatory protein 1–mitoferrin 1 signaling pathway involved in iron metabolism, facilitating the development of liver cancer (311). Another mechanism by which cancer cells evade ferroptosis is the increase in MUFA or MUFA-PLs synthesis. For example, in cancer cells with oncogenic activation of the PI3K-AKT pathway, mTORC1 hyperactivation induces the expression of SREBP1, which subsequently upregulates the expression of SCD1, a crucial enzyme in MUFA biosynthesis (312). Similarly, lung cancers harboring KRAS mutations often display elevated expression of ACSL3, which promotes the synthesis of MUFA-PLs and thereby strengthens resistance to ferroptosis. Multiple studies have demonstrated that cancer cells resistant to therapy exhibit an unexpected vulnerability to ferroptosis (291, 313, 314). For example, cancer cells in a mesenchymal state, typically resistant to apoptosis induced by conventional therapies, exhibit a strong dependence on GPX4, linked to high expression of zinc finger E-box binding homeobox 1 (ZEB1), a key regulator of EMT and a promoter of lipogenesis. Elevated levels of PUFA-containing PLs in these cells increase their reliance on GPX4 to detoxify lipid peroxides, thereby rendering them highly susceptible to ferroptosis (291). Consistently, recurrent breast cancer cells with mesenchymal characteristics show elevated expression of discoidin domain–containing

receptor 2 (DDR2), likely driven by EMT-associated transcription factors. Increased DDR2 enhances ferroptosis sensitivity in these cancer cells via activation of the Hippo signaling pathway (315). Similarly, our laboratory observed that FADS1/2, key enzymes in PUFA biosynthesis, are highly expressed in a subset of TNBC with poorer prognosis, increasing their susceptibility to ferroptosis. Notably, both genetic knockdown and pharmacological inhibition of FADS1/2 render these tumors resistant to ferroptosis, whereas supplementing exogenous PUFAs, which alters the PUFA/MUFA balance, re-sensitizes resistant tumors to ferroptosis induction (264). Moreover, in our laboratory, we have recently demonstrated that breast cancer harbouring ER-activating mutations (common in the ET-resistant setting) are characterized by increased expression of ACSL4 that promotes ferroptosis susceptibility, suggesting ACSL4 as an important biomarker to identify ER+ breast cancers susceptible to ferroptosis induction (316). The data presented in the manuscript, together with the optimization precedures leading to its publication are described in the current thesis (Chapter IV).

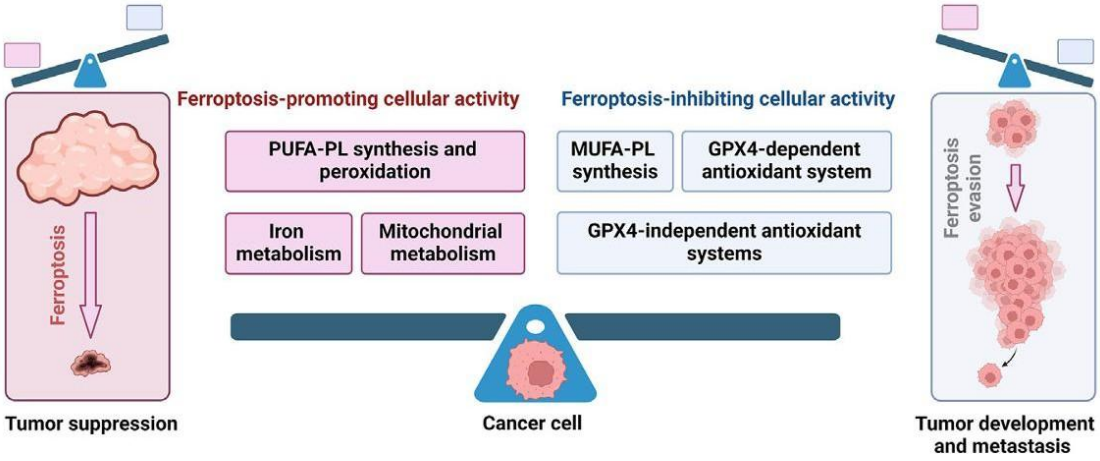

Figure 16. Pro- and anti-ferroptosis activities influence tumor outcomes. [taken from (301)]

6.4 Targeting ferroptosis in cancer therapy

As outlined in the preceding section, ferroptosis represents a vulnerability in certain cancer types, and targeting these vulnerabilities by inducing ferroptosis provides opportunities for cancer treatment (**Figure 17**) (317, 318).

A range of ferroptosis-inducing agents (FINs) has been identified, including some approved clinical drugs such as sulfasalazine and sorafenib, which inhibit SLC7A11 activity. Given the critical role of ferroptosis in tumor suppression, there has been growing interest in exploiting these and other FINs for cancer therapy. Preclinical studies have demonstrated the antitumor efficacy of the SLC7A11 inhibitor imidazole ketone erastin (IKE) and the GPX4 inhibitor JKE-1674 across various animal models (319). In addition, significant progress has been made in developing nanomaterials designed to induce ferroptosis locally or to enhance the effectiveness of existing FINs (320).

Moreover, accumulating evidence indicates that ferroptosis contributes, at least in part, to the tumor-suppressive effects of various conventional cancer therapies, including radiotherapy, chemotherapy, targeted therapy, and immunotherapy, and that FINs may further enhance the effectiveness of these treatments by promoting ferroptosis (252, 253, 317, 321). For example, in hepatocellular carcinoma and advanced renal carcinoma, the overexpression of yes-associated protein /transcriptional coactivator with PDZ-binding motif (YAP/TAZ) or DPP9, respectively, drives SLC7A11 upregulation, which is responsible for resistance to sorafenib, a cornerstone therapy for these cancers. Targeting YAP/TAZ, DPP9, or the downstream effector SLC7A11 overcomes sorafenib resistance in preclinical models of these cancers (308, 322). Beyond sorafenib resistance, induction of ferroptosis has also proven effective in overcoming resistance to other targeted therapies, such as therapies targeting HER2 in breast cancer. Indeed, in HER2+ breast cancer, upregulation of FGFR4 has been shown to suppress ferroptosis and promote resistance to trastuzumab. The FGFR4 inhibitor roblitinib effectively overcomes this resistance by downregulating SLC7A11 and the iron exporter ferroportin 1, thereby restoring both intrinsic and acquired sensitivity to anti-HER2 therapies(323).

Targeting ferroptosis also emerges as a promising strategy to overcome resistance in tumors treated with anti-hormonal therapy. Recent investigations have shown that androgen receptor (AR) antagonists such as enzalutamide induce ferroptosis in cancer cells by diminishing GSH levels through the suppression of SLC7A11, an AR transcriptional target (324). Moreover, recent findings demonstrated that the sex hormone receptors ER and AR drive the expression of membrane-bound glycerophospholipid O-Acyltransferase 1 and 2 (MBOAT1 and MBOAT2), key enzymes in mediating MUFA-PL synthesis, thus rendering the cells resistant to ferroptosis (325).

Enzalutamide and fulvestrant sensitize hormone therapy-resistant cancers to ferroptosis by inhibiting MUFA-PL synthesis. Finally, the combination of IKE with fulvestrant effectively reverses hormone therapy resistance in preclinical models (325). Recent studies have shown that the CDK4/6 inhibitor palbociclib and the ET agent giredestrant prime ER+ breast cancer cells for ferroptosis by promoting lipid peroxide accumulation and disrupting cellular redox homeostasis (274). Under these conditions, GPX4 normally acts as a critical protective mechanism by detoxifying lipid peroxides. Consequently, genetic depletion or pharmacological inhibition of GPX4 markedly enhances the sensitivity of ER+ breast cancer cells to CDK4/6 inhibition and ET (274).

Many studies highlight ferroptosis-inducing strategies as effective approaches to overcome chemoresistance. For instance, CDK1 has been identified as a key mediator of oxaliplatin resistance by promoting the ubiquitin-dependent degradation of ACSL4, thereby suppressing ferroptosis. Accordingly, pharmacological inhibition of CDK1 restores oxaliplatin sensitivity in colorectal cancer through a ferroptosis-dependent mechanism (326). Radiotherapy also induces ferroptosis via multiple mechanisms, including excessive ROS generation, ACSL4 upregulation, and GSH depletion (327). However, tumor cells can develop adaptive resistance to radiotherapy-induced ferroptosis by increasing the expression of key ferroptosis suppressors such as SLC7A11 and GPX4. Targeting these adaptive responses with FINs that inhibit SLC7A11 or GPX4 markedly enhances radiotherapy-induced ferroptosis and improves tumor radiosensitivity (253, 328).

Ultimately, the clinical translation of therapies that exploit ferroptosis vulnerabilities requires the identification and validation of patient populations whose tumors display heightened sensitivity to ferroptotic cell death, informed by insights from preclinical studies. Equally critical is the development of robust and clinically actionable biomarkers. In our study, we observed elevated ACSL4 expression in breast cancers harboring ER–activating mutations, suggesting that ACSL4 may contribute to disease progression and therapeutic response. These findings indicate that ACSL4 expression could serve as a potential biomarker for identifying ER+ breast cancers that are particularly susceptible to ferroptosis-inducing strategies (316). A more detailed discussion of this data will be presented in Chapter IV.

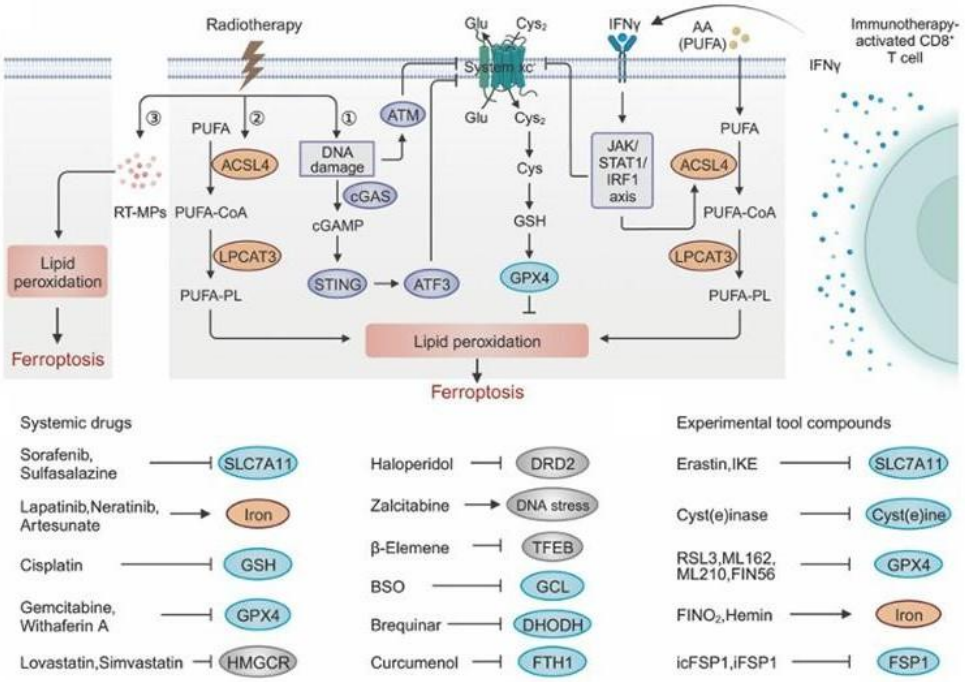

Figure 17. Ferroptosis induction for cancer therapy. [taken from (318)]

Chapter II. Materials and Methods

1. Materials

1.1 Cell lines

Human female breast cancer cells (MCF7 - HTB-22, RRID:CVCL_0031; T47D - HTB-133, RRID: CVCL_0553) were obtained from ATCC and maintained at 37°C/5%CO_2 in phenol red-free RPMI 1640 medium (Gibco #32404014) supplemented with 10% fetal bovine serum (FBS, Euroclone #ECS0180L), 2 mmol/L glutaMAX (Gibco #35050-061), and 1 nmol/L 17β-estradiol (E2, Sigma-Aldrich #E2758). In addition to the parental cell lines, we used: (i) an isogenic *ESR1*-mutant knock-in panel (Y537C, Y537N, Y537S) in MCF7 background, and an *ESR1* Y537C mutant in T47D background, generated as described below in the "Lentivirus infection" sub-section and (ii) long-term E2-deprived (LTED) derivatives either with wild-type *ESR1* ($LTED^{WT}$) or carrying a natural occurring Y537C mutation ($LTED^{Y537C}$), a kind gift of Dr Martin (The Institute of Cancer Research, London) (123). These models allowed us to assess mutation-specific effects, adaptation to estrogen deprivation (in the case of LTED models), and translational relevance as they mimic clinically relevant scenarios. The LTED derivatives were continuously cultured in sterol-depleted, phenol red-free RPMI 1640 medium containing 10% dextran charcoal-stripped FBS (DCC, Hyclone #SH30068.03) and 2 mmol/L glutaMAX (DCC medium) for a minimum of 20 weeks, allowing for the selection of cells with stable endocrine-resistant phenotypes, distinct from parental cells exposed to short-term estrogen deprivation (123, 199, 329, 330). Although charcoal stripping removes not only estrogens but also other steroid hormones, lipids, and growth factors, we have previously shown that the LTED metabolic phenotype results from long-term adaptation rather than transient deprivation (149). To mimic a condition of nutrient deprivation (limited medium), cells were cultured in deprived-DMEM 1X (Gibco #A14430-01), supplemented with 0.1% FBS or DCC, 2 mmol/L glutaMAX, and 0.5 mM glucose (Sigma-Aldrich #G8644). Cells were short tandem repeat tested (BMR Genomics), amplified, stocked, routinely subjected to mycoplasma testing (Lonza, #LT07-318) and, once thawed, were kept in culture for a maximum of 10 passages to minimize passage-related drift.

1.2 PDX-derived 3D models

Ex vivo tumor explants (PDE) and PDX-derived organoids (PDXO) were generated from the PDX models HBCx-239 and HBCx-254, respectively, both established from *ESR1*-mutated metastases of patients progressing on AIs. For the PDX establishment, biopsies of metastatic samples were obtained with patients' informed consent (Institute Curie).

PDX establishment was performed as previously described (331). *In vivo* experimental procedures were approved by the Institutional Animal Care and French Committee (project authorization no. 02163.02) and were performed according to institutional regulations.

The HBCx-239 PDE, generated using the protocol described in (332), was derived from the HBCx-239 PDX model (carrying naturally occurring *ESR1*^{Y537S} mutation), established from a skin metastasis of a patient progressing after treatment with the CDK4/6 inhibitor abemaciclib combined with the AI letrozole and enantone (a luteinising hormone-releasing hormone agonist) in the metastatic setting. Previous lines of treatments for this patient included letrozole and enantone in the adjuvant setting and epirubicin, cyclophosphamide, and docetaxel in the neo-adjuvant setting. The model carries the *ESR1* p.(Tyr537Ser) mutation and mutations in the Tumor Protein P53 (*TP53*) and Phosphatidylinositol-4,5-Bisphosphate 3-Kinase Catalytic Subunit Alpha (*PIK3CA*) genes. In brief, fresh HBCx-239 PDX tissue was finely minced and further dissociated in a digestion medium. This dissociation was enhanced by adding 1 mg/mL Collagenase (Roche #11088793001), 100 U/mL Hyaluronidase (Sigma #H3506), trypsin (GIBCO), Dispase (StemCell Technologies #7913), and DNase (Sigma #D4513). The cells were then resuspended in MEGM (Lonza #CC-3150), and Falcon® 40 µm cell strainers were employed to filter out undigested tissue. The resulting single-cell suspensions were plated in triplicate at $4x10^4$ cells per well in 96-well plates. To assess the impact of RSL3 treatment (120 hours, h), cell viability was measured using the CellTiterGlo assay (Promega #G7571). The experiment was conducted in three biological replicates, and cell viability was normalized to DMSO (vehicle)-treated controls.

The HBCx-254 PDXO model was derived from the HBCx-254 PDX (*ESR1*^{Y537S}) model, as detailed in (333), established from a bone metastasis of a patient progressing after treatment with the cyclin-dependent kinase 4/6 (CDK4/6) inhibitor abemaciclib combined with the AI letrozole in the metastatic setting. Previous lines of treatment for this patient included tamoxifen in the adjuvant setting and epirubicin, cyclophosphamide, and docetaxel in the neo-adjuvant setting. The model carries the *ESR1* p.(Tyr537Ser) mutation and amplification of cyclin D1 (*CCND1*) and fibroblast growth factor receptor 1 (*FGFR1*) genes. Briefly, PDX tumors were dissociated with an enzymatic solution, embedded in 100 µL Matrigel (Corning #354230), and plated in six-well tissue culture plates onto a 70 µL Matrigel base layer. After a 30-minute (min) incubation, organoid medium consisting of advanced DMEM/F12 with 5% FBS, 10 mmol/L HEPES, 1X Glutamax, 1 mg/mL hydrocortisone, 50 mg/mL gentamicin, 10 ng/mL hEGF, 100 ng/mL FGF2, 10 mmol/L Y-27632, and 1 mmol/L N-acetyl cysteine was added. Medium was replenished every 3 to 4 days. Organoids were dissociated using TrypLE Express (Life

Technologies #12605010) for 20 min. Established organoids were treated with RSL3 and elacestrant in quadruplicate combined at different concentrations and cell viability assessed using CellTiter-Glo 3D [Promega #G9682 (v/v)] following 20-min incubation at room temperature.

1.3 Common use solutions

- PBS (Phosphate Buffered Saline): 0.27 g/L di KH2PO4, 0.2 g/L KCl, 8.01 g/L NaCl, 1.78 g/L NaH2PO4 pH 7.4.
- RIPA lysis buffer: 50 mM Tris-HCl pH 7.5, 150 mM NaCl, 1% Nonidet P40, 2 mM EGTA, 100 mM sodium orthovanadate, 100 mM NaF.
- Lysis buffer: Sample Buffer 1X (SB1X).
- SDS−PAGE 4X Sample Buffer: 40% glycerol, 240 mM Tris-HCl pH 6.8, 8% SDS, 0.04% bromophenol blue, 5% β-mercaptoethanol.
- SDS-PAGE 1X running buffer: 25 mM Tris, 192 mM glycine, 0.1% (W/V) SDS, pH 8.3.
- SDS-PAGE 1X blotting buffer: 25 mM Tris, 192 mM glycine, 10% methanol, pH 8.3.
- Blocking solution: non-fat dry milk 2%, tween 0.05% in PBS.
- Washing solution: tween 0.1% in PBS 10X (T-PBS).

1.4 Drugs, compounds, and reagents

TOFA (5(tetradecyloxy)-2-furoic acid, #sc-200653) was purchased from Santa Cruz Biotechnology, dissolved in DMSO, and used at the appropriate concentration as described in Figures and Figure Legends. TVB3166 (4-[1-[5-(4,5-dimethyl-2H-pyrazol-3-yl)-2,4-dimethyl-benzoyl]-azetidin-3-yl] benzonitrile, #SML1694) and rosiglitazione (i.e., ACSL4 inhibitor, ACSL4i, 5-[[4-[2-(Methyl-2 pyridinylamino)ethoxy]phenyl]methyl]-2,4-thiazolidinedione, #R2408), from Sigma-Aldrich were also dissolved in DMSO. RSL3 ((1S,3R) 2-(2-chloroacetyl)-2,3,4,9-tetrahydro-1-[4-(methoxycarbonyl)phenyl]-1H-pyrido[3,4-b]indole-3-carboxylic acid, methyl ester, #HY-100218A) and erastin (2-[1-[4-[2-(4-chlorophenoxy)acetyl]-1piperazinyl]ethyl]-3-(2-ethoxyphenyl)-4(3H)-quinazolinone, #HY15763) were purchased from MedChemExpress, dissolved in DMSO and used at the indicated concentrations as described in Figure and Figure Legends.

1.5 Antibody

Antibody	Application	Dilution	Use	Source	Manifacturer
ACC	WB	1:1000	O/n 4°C	Rabbit	Cell Signaling
pACC	WB	1:1000	O/n 4°C	Rabbit	Cell Signaling
ACLY	WB	1:1000	O/n 4°C	Mouse	Santa Cruz Biotechnologies
ER	WB	1:1000	O/n 4°C	Rabbit	Abcam
ACSL4	WB	1:1000	O/n 4°C	Mouse	Santa Cruz Biotechnologies
HSP90	WB	1:1000	O/n 4°C	Mouse	Santa Cruz Biotechnologies

2. Methods

2.1 General culture conditions

Cell lines were grown under 5% CO2 incubation at 37°C in their corresponding culture medium. For cell passaging, growth medium was removed, and the cells were washed with PBS and incubated with a covering volume of trypsin for 1-2 minutes (min). When cells were detached, medium was added to neutralize trypsin's effect and cells were seeded into a new flask.

2.2 Long-term cell frozen storage

Cells were detached using trypsin, resuspended into their cell culture medium, and pelleted by centrifugation at 1.000 rpm (rotation per minute) for 5 min. Then, pellet was resuspended in 1 mL of cell freezing medium (90% FBS/DCC and 10% DMSO) and cells transferred into specific freezing vials, stored in polystyrene insulated boxes at -80°C for at least 48 h and subsequently in liquid nitrogen for long time. For the thawing procedure, cells were moved into a new flask and resuspended with fresh cell culture medium. The following day, medium was replaced to completely remove DMSO.

2.3 Survival assay

Human breast cancer cells were seeded into 12-well plates at 3–5×10^4 cells/well in either standard conditions (see “Cell cultures and reagents” sub-section) or experimental conditions such as drug administration [e.g., 0.05–10 μM of the GPX4 inhibitor, RSL3, and cystine/glutamate antiporter system X_c^- inhibitor, erastin], as described in Figures and Figure Legends. Cell counts were performed at least in triplicate by three analysts under a 10x objective according to the standard methodology.

2.4 Transient siRNA transfection

MCF7 LTED^{Y537C} cells were seeded into 6-well plates (3×10^5 per well) to achieve 70% confluence the following day, when cells were transfected with 30 nmol/L siRNA targeting *ESR1* (siESR1, GE Healthcare Dharmacon), or the respective negative control (non-targeting small interfering RNA, siCTR, GE Healthcare Dharmacon) using Lipofectamine RNAiMAX Reagent (Thermo Fisher Scientific #13778-150) and Opti-MEM (GIBCO #31985062) accordingly to manufacturer’s instructions. The functional analyses were performed 72 h after transfection as described in Figure Legends.

2.5 Lentivirus infection

HEK293T packaging cells were seeded into 6 cm culture plates (5×10^5 cells per plate) to achieve 50-70% confluence the following day, when cells were transfected using PEI Transfection Reagent (MedChemExpress #HY-K2014) with a mixture of three transfection plasmids used as follows: 1.45 μg of pHAGE_puro (AddGene #118692, RRID:Addgene_118692) or pHAGE-ESR1-Y537C/Y537S/Y537N (AddGene #116372, RRID:Addgene_116372; #116374, RRID:Addgene_116374; #116373, RRID:Addgene_116373; respectively); 1.1 μg of pCMVR8.74 (AddGene #22036, RRID:Addgene_22036); and 0.45 μg of pMD2.G (AddGene #12259, RRID:Addgene_12259). After 48 and 72 h, the supernatants of the media were collected, centrifuged at 550xg for 5 min, and filtered with a 0.45 μm filter. The supernatant containing the virus was stored at 4 °C for cell infection. Breast cancer cells were seeded into 6 cm culture plates (8x10^5 cells per plate), infected the next day with lentivirus for 72 h together with Polybrene (Santa Cruz Biotechnology #sc-134220), and then subjected either to FACS Sorting (for pHAGE-ESR1-Y537C/Y537S/Y537N infected cells) or puromycin (for pHAGE_puro infected cells) for selection of infected cells.

2.6 FACS Sorting

72 h after the infection, breast cancer cells were resuspended in the sorting buffer solution composed of PBS with 1% BSA, $MgCl_2$ (2.5 mM), EDTA (5 mM), HEPES (25 mM), and DNase I (5U/ml) and subsequently subjected to FACS sorting using FACSMelody cell sorter (BD Biosciences) to isolate the fluorescent cells. The sorted cells were then analyzed for the presence of *ESR1* mutation utilizing an external sequencing service provided by BMR Genomics.

2.7 Western blotting

Protein extraction: breast cancer cells were washed with PBS and lysed on ice using 1x Laemmli Sample Buffer (SB) supplemented with protease and phosphatase inhibitors. Protein lysates were collected, kept in ice, and centrifuged at 12.000 rpm for 10 min. After centrifugation, the supernatant was collected, and total proteins were quantified with either BCA (bicinchoninic acid) protein assay.

Protein quantification: The BCA protein assay is based on the notion that proteins can reduce Cu+2 to Cu+1 in an alkaline solution containing BCA resulting in a purple color formation. The absorbance of the BCA/copper complex at 562 nm is directly proportional to the protein concentration. To prepare BCA solution, we combined 50 parts of A solution with 1 part of B solution. In cuvettes for spectrophotometer, we added 45 uL of water (50 uL for the blank), 5 uL of each protein lysate sample, and 950 uL of BCA solution. After 30 min of incubation at 37°C, all the samples and the blank were read by the spectrophotometer at a wavelength of 562 nm. To generate the standard curve, we used Bovine Serum Albumin (BSA), diluting BSA 2 mg/mL concentrated in dH2O to obtain BSA concentrations from 2 µg/mL to 15 µg/mL. Thus, from the values obtained from the standard curve, it is possible to create a curve of the absorbance in function of the concentration; consequently, interpolating absorbance values to the standard curve, it is possible to calculate the final protein concentration of the samples of interest.

SDS-PAGE: it is a technique used for protein separation thanks to their ability to move within an electric current, which is a function of the length of their polypeptide chains or their molecular weight. This is achieved by adding SDS detergent to remove secondary and tertiary protein structures and to maintain the proteins as polypeptide chains. 40–50 µg of cell lysate were boiled for 5 min in SB 4x plus β mercaptoethanol, which leads to disulphuric bond reduction and destabilization of protein tertiary structure, and then loaded in precast SDS-PAGE (sodium dodecyl sulfate-polyacrylamide gel electrophoresis) gels (Biorad). Running was performed at 100-150 V for almost 1 h.

Blotting: After running, protein samples were transferred from the gel to a nitrocellulose membrane (blotting) by Trans-Blot Turbo Transfer Pack (Biorad) to make the proteins accessible for the antibody detection. The proteins embedded into the gel are transferred to the membrane maintaining the organization that they have within the gel. Protein transfer was carried out at 25 V and 2.5 A for either 7 min (for proteins with low molecular weight) or 10 min (for proteins with high molecular weight). After blotting, the membrane was incubated for 1 h in the blocking solution (non-fat dry milk 2%, tween 0.05% in PBS) at room temperature and then overnight in slow agitation at 4°C in a blocking solution with the specific primary antibody. The following day, the membrane was washed three times with a solution of T-PBS and then incubated with the horseradish peroxidase (HRP)-conjugated secondary antibody for 1 h at room temperature and finally washed again for three times with T-PBS. In the chemiluminescence reaction, HRP catalyzes the oxidation of luminol into a reagent which emits light when it decays. Since the HRP is complexed with the secondary antibody specific for the protein of interest on the membrane, amount and location of the emission light are directly correlated with those of the protein of interest. Chemiluminescent protein revelation was carried out with ECL Western Blotting reagents (Biorad) at the Amersham Imager 600.
The antibodies used are described in Chapter II, section 1.5.

2.8 RNA extraction and Quantitative Real-Time PCR (qRT-PCR) analysis

Total RNA was extracted from cultured cells, grown as monolayer, using RNeasy Mini Kit (Qiagen). RNA concentration and quality of the samples were determined by measuring the UV absorbance at 260 nm and 280 nm on Nanodrop 1000 (Thermo Scientific), and 500 ng of total RNA were reverse transcribed to cDNA using the iScript gDNA Clear cDNA Synthesis Kit (Biorad). qRT-PCR analysis was performed using the CFX96 Touch Real-Time PCR Detection System (Biorad) using TaqMan Universal PCR Master Mix (Thermo Fisher Scientific). The following probes were used: PLIN2, ATGL, ESR1, and ACSL4 (Thermo Fisher Scientific). Data were normalized on TBP (TATA-Box Binding Protein) or RNU48 (Thermo Fisher Scientific). The relative quantity was determined using $\Delta\Delta^{Ct}$ by the CFX Maestro software (BioRad).

2.9 Confocal image acquisition and analysis

Breast cancer cells were seeded onto glass coverslips (1-2x10^5 per well of a 6-well plate or 3x10^4 per well of a 12-well plate) to have a 40-50% confluence and subjected to the experimental procedure described in Figures. The day after cells were stained at 37°C

(i) for 15 min with BODIPY$^{493/503}$ (Thermo Fisher Scientific #D3922) to reveal lipid droplet (LD) content, (ii) 30 min with BODIPY-FL-C_{16} (Thermo Fisher Scientific #D3821) for fatty acid uptake or (iii) 1 h with BODIPY$^{581/591}$-C11 to evaluate lipid peroxidation (Thermo Fisher Scientific #D3861) and then fixed with 4% formaldehyde for 10 min. For nuclei staining, fixed cells were incubated with Hoechst 33342 (Thermo Fisher Scientific #H3570) or DAPI (Thermo Fisher Scientific #D3571) for 10 min at room temperature. Sample images were acquired using TCS SP8 microscope (Leica Microsystems) with LAS-AF image acquisition software. The quantification of LDs was performed using CellProfiler software.

2.10 Flow cytometry analysis

Breast cancer cells (3–5×10^4 cells/well) were seeded into 12-well plates and subjected to the experimental procedure described in Figures. The day after, cells were stained at 37°C for (i) 15 min with BODIPY$^{493/503}$ to reveal LD content, (ii) 30 min with BODIPY-FL-C_{16} to reveal FA uptake capacity, or (iii) 1 h with BODIPY$^{581/591}$-C11 to evaluate lipid peroxidation. Live cells resuspended in PBS with 0.1% FBS were subjected to flow cytometry analysis using a FACSCanto II (BD Biosciences). 1×10^4 cells were analyzed for the mean fluorescence intensity (MFI) of the specific probe.

2.11 Reactive oxygen species (ROS) analysis

Sensitive and resistant cells (3–5×10^4 cells/well) were seeded into 12-well plates and subjected to the experimental conditions described in Figures. Cells were stained with 2',7'-dichlorofluorescin diacetate (DCFDA) (Sigma-Aldrich #D6883) to evaluate ROS cytoplasmic content and incubated at 37°C in the dark for 30 min. Then, cells were lysed with RIPA buffer and fluorescence was measured on a microplate reader at 485 nm excitation (Ex) and 520 nm emission (Em).

2.12 Immunohistochemistry (IHC)

Formalin-fixed paraffin-embedded blocks of tumor tissues were from cases of postmenopausal metastatic patients with HR+/HER2- breast cancer enrolled in the ROME Trial (NCT04591431) or from the *Centro di Riferimento Oncologico* (CRO, Aviano, Italy). Breast cancer specimens were fixed in 4% paraformaldehyde and embedded in paraffin for histology and IHC analysis. Sections were stained with the antibody specific

for ACSL4 (abcam #ab155282, RRID:AB_2714020). The specificity of the antibodies was established using a human hepatocellular carcinoma section as positive control. IHC was performed using the Leica BOND-MAX automated system (Leica Microsystems). Slides were developed with 3′3-diaminobenzidine (Bond Polymer Refine Detection, Leica Microsystems) and counterstained with hematoxylin. Images were acquired using a slide scanner (Aperio LV1; Leica Biosystems) and the ACSL4 H-Score was calculated by a breast pathologist (B.C.) using the following formula: 3X + 2Y + Z, where X, Y, and Z are the proportions of tumor cells showing strong (3+), moderate (2+), and weak (1+) cytoplasmic staining intensities, respectively. The maximum H-Score was 300 (strong staining of all tumor cells) and the minimum was 0 (no staining of any tumor cells). Written informed consent was obtained from all patients and the study was conducted in accordance with the Declaration of Helsinki and Good Clinical Practice guidelines as well as authorized by the local Ethics Committee (ROME trial) or by the Institutional Review Board of CRO Aviano (IRB-06-2017).

2.13 *In silico* analysis—analysis of human datasets

ACSL4 (202422_s_at) survival analysis was created using Km-plotter (http:// kmplot.com) by applying the best-performing cut-off to maximize prognostic resolution. The curated dataset of HR+/HER2- (assessed by array data) breast cancers included the post-progression survival data of primary tumor specimens patients, selected independently of any adjuvant or local therapeutic intervention, belonging to the following datasets: GSE1456 (334), GSE16446 (335), GSE20685 (336), GSE20711 (337), GSE3494 (338), GSE42568 (339), GSE45255 (340), GSE65194 (341), GSE69031 (342), GSE7390 (343).

2.14 *In silico* analysis—analysis of RNA sequencing data

MCF7 LTED^{Y537C} and LTED^{WT} RNAseq (GSE100075) and ChIPseq (GSE100074) data were retrieved from (123). Differential gene expression analysis was performed using the “DESeq2” package (version 1.46.0) (344). Raw data were transformed using the regularized log transformation (rlog) function from DESeq2 and subsequently used to generate heatmaps with the “ComplexHeatmap” package (version 2.22.0) (345) in RStudio (R version 4.4.2) (RStudio: Integrated Development Environment for R. Posit Software, PBC, Boston, MA. URL http://www.posit.co/). Gene set enrichment analysis (GSEA) was performed using the “clusterProfiler” R package (346) with genes ranked based on $\log_2$ fold-change from differential expression analysis. Enrichment was

assessed using the gene sets from the Molecular Signatures Database (MSigDB v7.5.1). The HALLMARK FATTY ACID METABOLISM (M5935) and WP FERROPTOSIS (M39768) gene sets were retrieved from the Molecular Signature Database of the Broad (https://www.gsea-msigdb.org/gsea/msigdb/index.jsp) and used to investigate the differential gene expression pattern of LTED^{Y537C} and LTED^{WT} cells.

2.15 Statistics and reproducibility

Statistics were performed using Prism 10 (GraphPad Software). Unless stated otherwise, all numerical data are expressed as the mean ± standard error of the mean (SEM). All experiments were conducted at least 3 times independently, with one or more technical replicates for each experimental condition tested. Unless stated otherwise, comparisons between 2 groups were made using the two-tailed, unpaired Student's t-test. Comparisons between multiple groups were made using one-way or two-way analysis of variance (ANOVA). Bonferroni, Dunnett, Tukey, or Šidák post testing analyses with a confidence interval of 95% were used for individual comparisons as reported in Figure Legends. Multivariate Cox analyses on the cohort of patients analyzed were generated using KM-plotter. Statistical significance was defined when $P < 0.05$. P-values are reported only when biologically relevant, as indicated in Figure Legends. When differences were not statistically significant or the comparison not biologically relevant, no indication was reported in the figures.

2.16 Data availability

The data analyzed in this study were obtained from Gene Expression Omnibus (GEO) at GSE100075 and GSE100074. All other data generated in this study are available upon request from the corresponding author.

Chapter III. *ESR1* activating mutations reveal metabolic vulnerabilities in ER+ breast cancer

1. Results

1.1 ER+ breast cancer cell models resistant to estrogen deprivation show altered lipid metabolism, independently of *ESR1* status

LTED cells are derived from parental cells by culturing in the absence of E2 for 6 to 12 months. This is an established model of acquired AI resistance, which, along with others, we have demonstrated to be clinically relevant for studying ET resistance (149, 224). We have recently shown that lipid metabolic reprogramming is involved in ET resistance. In particular, we found that ER+ MCF7 LTED cells, unlike the parental counterpart MCF7 WT cells, are characterized by increased lipogenesis, lipid uptake, and a concomitant ability to catabolize lipid—a reprogramming orchestrated by LDs, mitochondria, and peroxisomes (149). However, this metabolic reprogramming occurs in LTED cells expressing *ESR1*^{WT}. Given that *ESR1* activating mutations are frequently acquired during the development of resistance and play a critical role in disease progression during ET, we therefore characterized lipid metabolism in an LTED model harboring a spontaneously occurring, clinically relevant *ESR1* mutation (*ESR1*^{Y537C}) (123). To investigate whether alterations in lipid metabolism occur independently of *ESR1* status, we compared parental MCF7 cells to LTED derivatives, either with *ESR1*^{WT} (LTED^{WT}) or with *ESR1* mutation (LTED^{Y537C}). Western blot analysis revealed decreased phosphorylation of the key lipogenic enzyme ACC1, an indicator of enzyme activation, along with increased expression of ACLY in both LTED models compared to parental MCF7 cells (**Figure 18A**). ACLY functions to convert citrate into acetyl-CoA, supplying the central substrate required for FA synthesis, while ACC1 subsequently transforms acetyl-CoA into malonyl-CoA, committing metabolites to lipid synthesis. This biosynthetic cascade predominantly produces palmitate, a 16-carbon saturated FA that contributes to membrane structure and lipid-dependent signaling pathways. In addition to *de novo* synthesis, cells may acquire palmitate from external sources, and increased uptake reflects a greater lipid dependency and metabolic adaptability. Consistent with this, both LTED^{WT} and LTED^{Y537C} cells showed markedly increased incorporation of fluorescently labeled palmitate (BODIPY-FL-C_{16}), as shown by confocal microscopy and flow cytometry

analysis (**Figure 18B,C**). LD accumulation represents a well-recognized hallmark of dysregulated lipid metabolism in multiple cancer types (170). In addition to the upregulation of lipogenesis-related enzymes and FA uptake, analyses by confocal microscopy and flow cytometry using BODIPY$^{493/503}$ revealed a significant increase in LD abundance in both LTED^{WT} and LTED^{Y537C} cells when compared to the parental counterpart (**Figure 18D,E**). Elevated LD content was further supported by increased transcript levels of PLIN2, a key LD-associated structural protein, as measured by qRT-PCR (**Figure 18F**). Together, these data confirm that AI-resistant ER+ breast cancer cells undergo lipid metabolic remodeling and that this metabolic phenotype represents a shared adaptive response to estrogen deprivation independent of ER status.

Figure 18

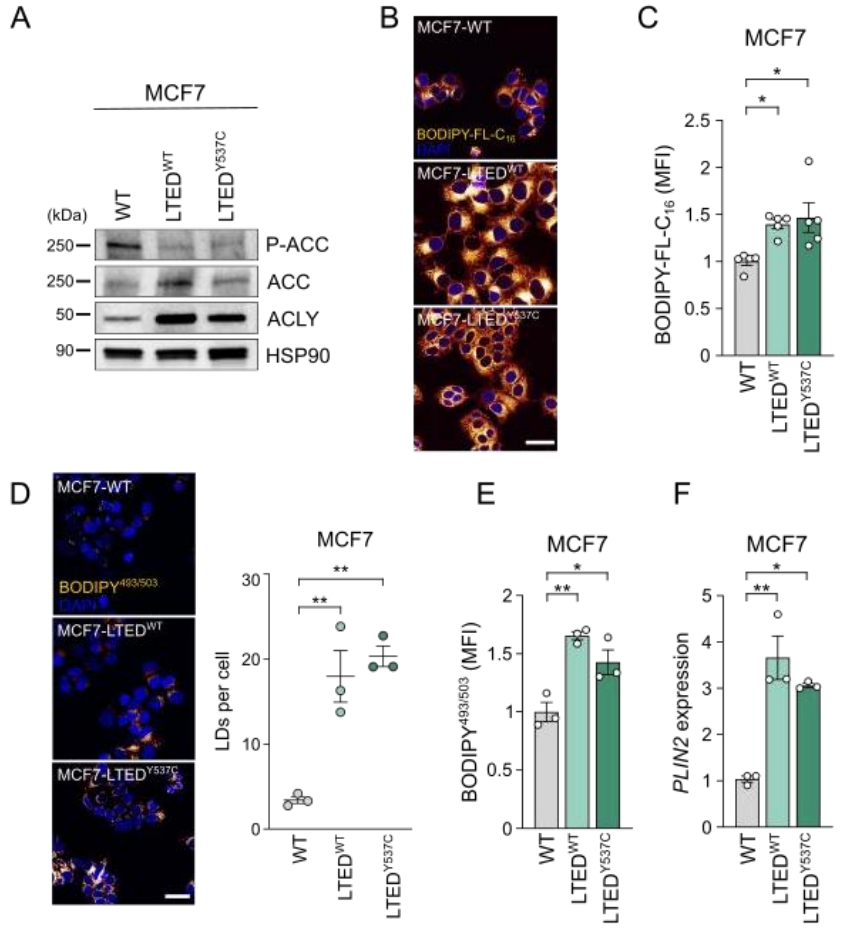

Figure 18. Estrogen deprivation-resistant ER$^+$ breast cancer cells display lipid metabolic reprogramming, independently of *ESR1* status. (**A**) Total protein lysates from MCF7 WT cells and the corresponding LTED^{WT} and LTED^{Y537C} derivatives were subjected to WB analysis with the antibodies indicated. (**B**,**C**) MCF7 WT and LTED cells were incubated with BODIPY-FL-C_{16}, and the uptake was monitored by confocal (B) and quantified by cytofluorimetric analysis (C). *n* = 3 biological replicates in either single or technical duplicate. One-way ANOVA; Tukey-corrected. Representative images of BODIPY-FL-C_{16}

are shown (orange/yellow: BODIPY FL-C_{16}; blue: DAPI, nuclei; scale bar, 10 µm). (**D**,**E**) MCF7 parental and LTED cells were incubated with BODIPY$^{493/503}$ and subjected to confocal (D) and cytofluorimetric analysis (E). *n* = 3 biological replicates. One-way ANOVA; Tukey-corrected. Representative pictures of BODIPY$^{493/503}$ staining and quantification of BODIPY$^{493/503}$ spots per cell are shown (orange/yellow: LDs; blue: DAPI, nuclei; scale bar, 10 µm). (**F**) The RNA derived from MCF7 parental cells and the corresponding LTED^{WT} and LTED^{Y537C} derivatives was analyzed by qRT-PCR analysis using the assay described in the figure. Fold relative enrichment and statistical analysis are shown using parental cells as comparator. *n* = 3 biological replicates. One-way ANOVA; Tukey-corrected. Data are mean ± SEM. * P < 0.05; ** P < 0.01; *** P < 0.001; **** P < 0.0001.

1.2 MCF7 LTED^{Y537C} cells exhibit increased vulnerability under nutritional stress due to impaired LD mobilization

We have previously demonstrated that endocrine-resistant tumor cells *in vitro* and endocrine-resistant breast tumor growth *in vivo* are sensitive to TOFA (5-tetradecyloxy-2-furoic acid) treatment, an allosteric inhibitor of ACC1 (149). Importantly, ACC1 targeting also impairs the survival of LTED^{Y537C} cells in a dose-dependent manner, similar to its effect on LTED^{WT} cells in comparison to parental cells (**Figure 19A**). However, TOFA differentially impacts LD content in the LTED models. Indeed, as shown by confocal microscopy analysis, while TOFA reduced LD content in LTED^{WT} cells, this effect was not observed in LTED^{Y537C} cells (**Figure 19B**), suggesting LDs and lipid metabolism have different dynamics in *ESR1*-mutant cells. Moreover, the FASN inhibitor TVB-3166 selectively impairs the survival of LTED^{Y537C} cells (**Figure 19C**), whereas LTED^{WT} cells and parental counterparts were only marginally affected, consistent with previous reports (149). These findings reflect the well-documented metabolic plasticity of LTED^{WT} cells, which supports their efficient adaptation in conditions of nutritional stress (199, 224). Indeed, LTED^{Y537C} cells, as well as parental MCF7 cells, showed reduced survival when cultured under nutrient-stress conditions, unlike LTED^{WT} cells, highlighting their unique adaptive capacity (**Figure 19D**). Since the metabolic plasticity of LTED^{WT} cells has previously been linked to their capacity to dynamically regulate LDs, we investigated changes in LD abundance under conditions of nutrient deprivation. Upon nutrient restriction, LTED^{WT} cells displayed LD mobilization, resulting in a marked reduction in intracellular LD content, and indicating an active utilization of stored lipids to sustain cellular metabolism during nutrient stress. By contrast, LTED^{Y537C} cells exhibited no comparable LD remodelling when exposed to the same conditions, maintaining LD levels despite limited nutrient availability (**Figure 19E**). These findings suggest that the lack of lipid mobilization from LDs in LTED^{Y537C} cells confers reduced metabolic flexibility and a decreased capacity to sustain metabolic stress. Consistent with this observation, LTED^{Y537C} cells showed significantly lower mRNA expression of ATGL, the key enzyme responsible for the hydrolysis of triacylglycerols within LDs (**Figure 19F**).

Figure 19

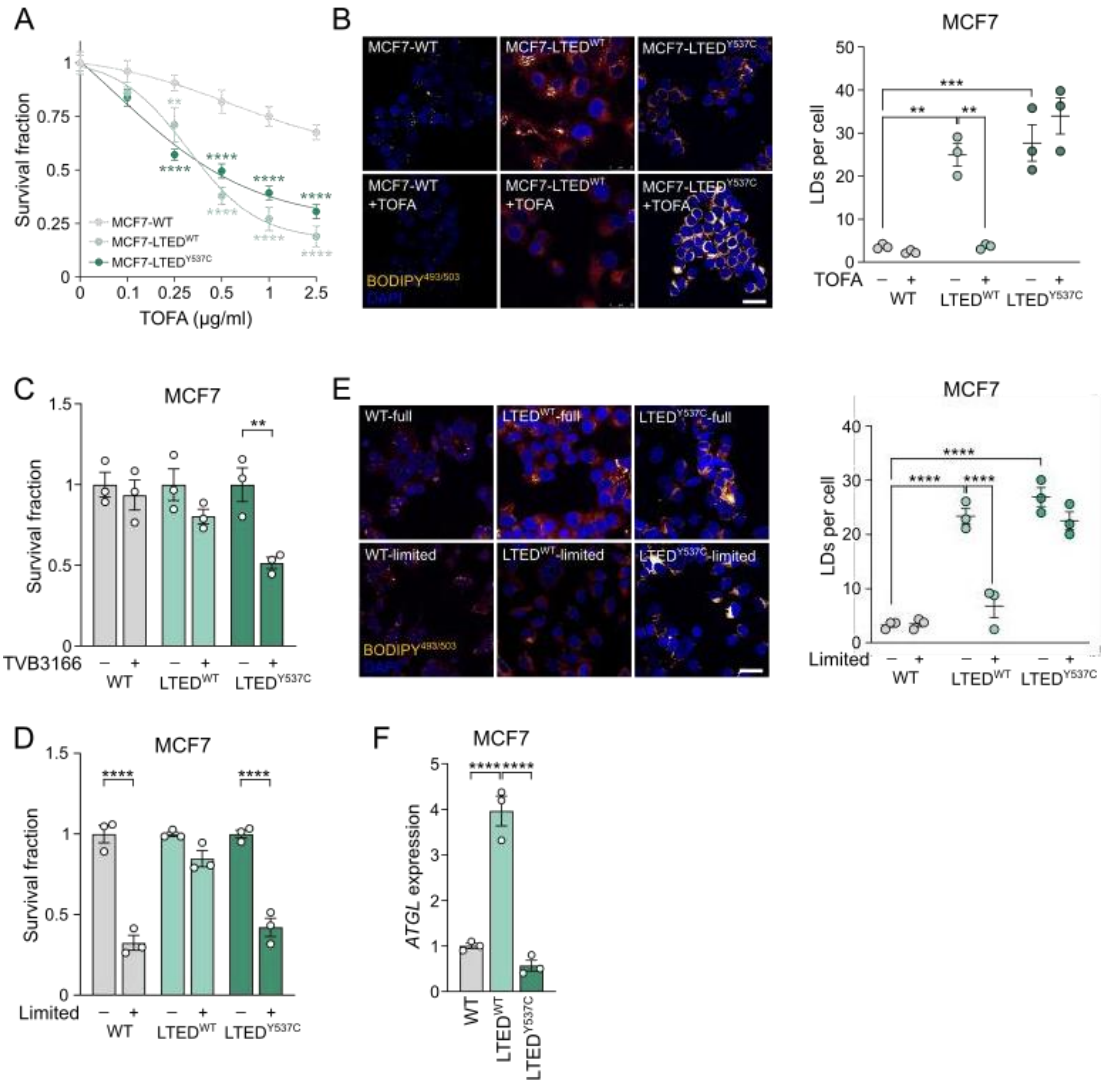

Figure 19. *ESR1*^{Y537C} mutation confers enhanced metabolic vulnerability. (**A**) Three-day TOFA dose-response curves in parental and LTED cells. *n* = 3 biological replicates in technical triplicate. Two-way ANOVA; Tukey-corrected. (**B**) Parental and LTED cells were treated with TOFA (0.5 µg/ml) for 24 h and subjected to confocal analysis. Representative pictures of BODIPY$^{493/503}$ staining and quantification of BODIPY$^{493/503}$ spots per cell are shown (orange/ yellow: LDs; blue: DAPI, nuclei; scale bar, 10 µm). *n* = 3 biological replicates. Two-way ANOVA; Tukey-corrected. (**C**) LTED and parental cells were treated with 200 nM TVB3166 for 72 h and subjected to cell counting. Two-way ANOVA; Sidak-corrected. *n* = 3 biological replicates. (**D**) MCF7 WT and LTED cells were grown either in standard or in limited conditions for 72 h and subjected to cell counting. *n* = 3 biological replicates. Two-way ANOVA; Sidak-corrected. (**E**) LTED derivatives and parental cells were grown in either full or limited conditions for 24 h and subjected to confocal microscopy analysis. Representative pictures of BODIPY$^{493/503}$ staining and the quantification of its intensity are shown (orange/yellow: LDs; blue: DAPI, nuclei; scale bar, 10 µm). *n* = 3 biological replicates. Two-way ANOVA; Tukey-corrected. (**F**) The RNA derived from MCF7 parental cells and the corresponding LTED^{WT} and LTED^{Y537C} derivatives was analyzed by qRT-PCR using the assay described in the figure. Fold relative enrichment and statistical analysis are shown using parental cells as comparator. *n* = 3 biological replicates. One-way ANOVA; Tukey-corrected. Data are mean ± SEM. * P < 0.05; ** P < 0.01; *** P < 0.001; **** P < 0.0001.

1.3 The lipid metabolic phenotype of MCF7 LTED^{Y537C} cells confers ferroptosis sensitivity

To determine how the *ESR1*^{Y537C} mutation reshapes lipid metabolism in the context of resistance to estrogen deprivation, we compared the transcriptomic profiles of LTED^{WT} and LTED^{Y537C} cells. Our investigation focused on the HALLMARK FATTY ACID METABOLISM gene set (M5935), which has been previously linked to the transcriptional landscape of LTED^{Y537C} cells (123). An unsupervised hierarchical clustering of the significantly differentially expressed genes revealed a robust separation between the two LTED models. Notably, in this gene set, ACSL4 emerged as the most strongly upregulated transcript, exhibiting a 3.4-fold increase in LTED^{Y537C} cells compared to LTED^{WT} cells (**Figure 20A, left**). These results led us to hypothesize that ACSL4 upregulation could be directly mediated by an altered transcriptional activity of the mutant ER. Indeed, examining available ChIP-seq data (GSE100074) (123), we identified a specific binding of the mutated form of ER to the ACSL4 promoter in LTED^{Y537C} cells. In contrast, no such interaction was detected in LTED^{WT} cells or in parental MCF7 cells expressing wild-type ER, supporting a neomorphic function of the mutant receptor in directly regulating ACSL4 expression (**Figure 20B**). Because ACSL4 is known to promotes the incorporation of PUFA into membrane phospholipids, thereby promoting lipid peroxidation and susceptibility to ferroptotic cell death (347), we next evaluated differences in the transcriptomic profile of LTED^{WT} and LTED^{Y537C} cells using the WP FERROPTOSIS gene set (M39768), found to be significantly associated with the *ESR1* mutant phenotype [(normalized enrichment score (NES) = -1.56, p-value = 1.18E-02, **Figure 20C**]). Hierarchical clustering demonstrated again a distinct separation between the transcriptomic profiles of the two cell lines, with ACSL4 emerging as the most differentially expressed gene also in this set of analyzed genes (**Figure 20A, right**). Together, these data indicate that LTED^{Y537C} cells are characterized by a distinct lipid metabolic phenotype driven, at least in part, by altered transcriptional activity of the mutant ER. This reprogramming, combined with a reduced metabolic plasticity, suggests the presence of a metabolic vulnerability that may be exploited for therapeutic intervention. To test this, LTED^{WT} and LTED^{Y537C} cells were exposed to the ferroptosis-triggering agent RSL3, a selective inhibitor of GPX4 (245), at different doses and time exposures. Under these conditions, LTED^{Y537C} cells showed a stronger reduction in viability than LTED^{WT} cells (**Figure 20D,E**). This enhanced ferroptosis sensitivity was further observed following treatment with erastin, another ferroptosis inducer that blocks the cystine/glutamate antiporter system Xc^- (241). Erastin significantly impaired the

survival of LTED^{Y537C} cells, whereas LTED^{WT} cells were largely unaffected (**Figure 20F,G**).

Figure 20

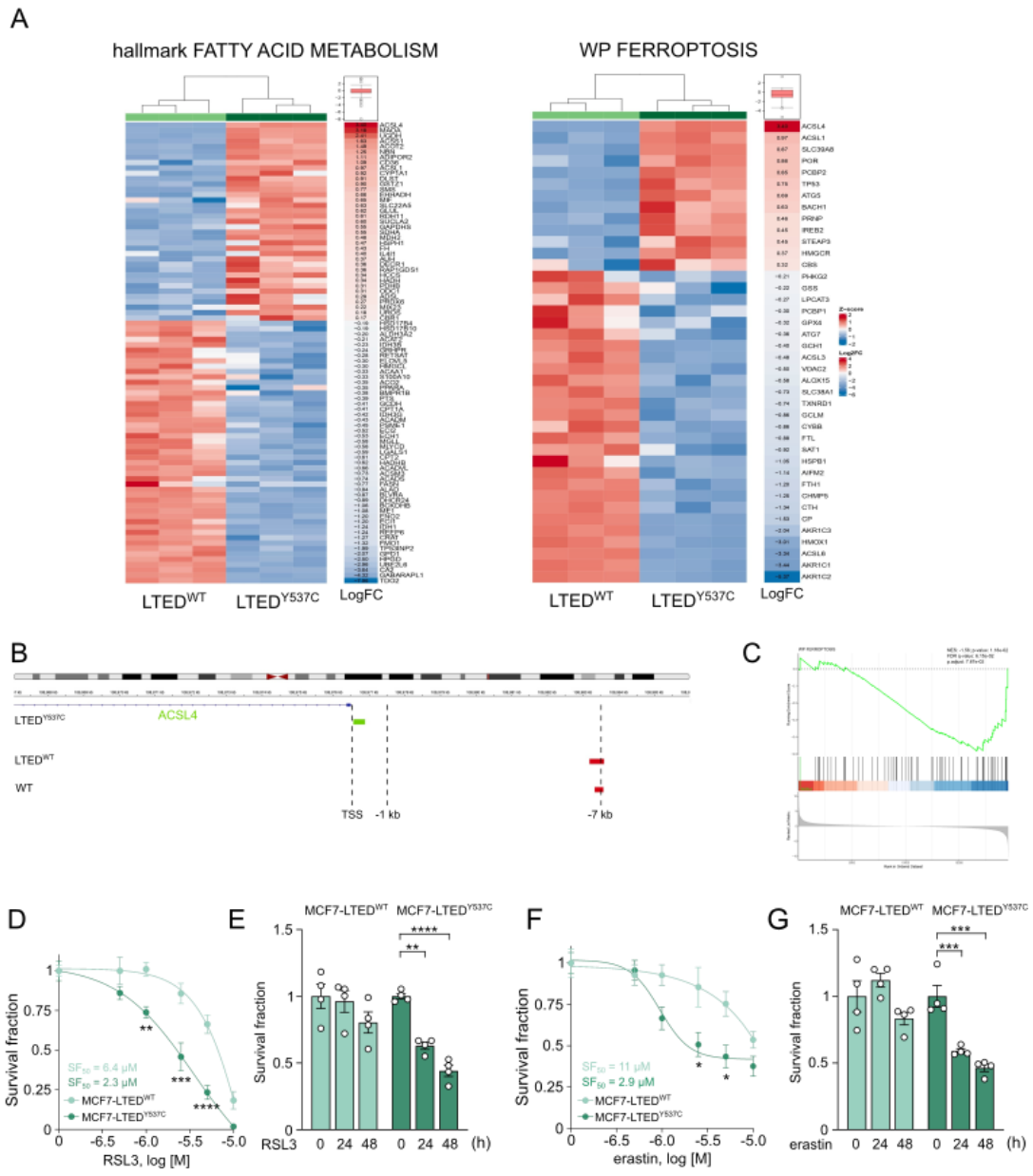

Figure 20. Altered lipid metabolism in MCF7 LTED^{Y537C} cells enhanced ferroptosis vulnerability. (**A**) Heatmap of differentially expressed genes and relative fold enrichment value of LTED^{WT} and LTED^{Y537C} genes included in the hallmark FATTY ACID METABOLISM gene set (left panel) and WP FERROPTOSIS gene set (right panel). (**B**) ChIP-seq data analysis of the ACSL4 promoter region (GSE100074). TSS = transcription start site. (**C**) GSEA on the publicly available transcriptomic data for the WP_FERROPTOSIS gene set (M39768), normalized enrichment score (NES) of -1.56 and a p-value of 1.18E-02. (**D**) 48 h dose-response curve of RSL3 was analysed by cell counting in LTED^{WT} and LTED^{Y537C} cells. *n* =3 biological replicates in either single or technical duplicate. Two-way ANOVA; Sidak-corrected. Survival fraction 50 (SF_{50}) is reported in the figure. (**E**) LTED^{Y537C} and LTED^{WT} cells were treated with 2.5 µM RSL3 and subjected to cell counting after 24 and 48 h. *n* = 3 biological replicates in either single or technical duplicate. Two-way ANOVA; Dunnett-corrected. (**F**) 48 h dose-response curve of erastin was analysed by cell counting in LTED^{WT} and LTED^{Y537C} cells. *n* =3 biological replicates in either single or technical duplicate. Two-way ANOVA; Sidak-corrected. Survival fraction 50

(SF_{50}) is reported in the figure. (**G**) $LTED^{Y537C}$ and $LTED^{WT}$ cells were treated with 5 μM erastin and subjected to cell counting after 24 and 48 h. *n* = 3 biological replicates in either single or technical duplicate. Two-way ANOVA; Dunnett-corrected. Data are mean ± SEM. * P < 0.05; ** P < 0.01; *** P < 0.001; **** P < 0.0001.

1.4 MCF7 $LTED^{Y537C}$ cells exhibit ferroptosis hallmarks following RSL3 treatment

Consistent with increased susceptibility to ferroptotic cell death, exposure of $LTED^{Y537C}$ cells to either RSL3 or erastin resulted in a pronounced accumulation of ROS levels, measured using the DCFDA fluorescent probe (**Figure 21A**), in parallel with a strong increase in lipid oxidative damage, assessed by the oxidation of the lipid-sensitive dye $BODIPY^{581/591}$-C11, reflected by an increased ratio of oxidized to non-oxidized lipids (**Figure 21B**). Lipid peroxidation was further quantified using FACS analysis, which confirmed a significant increase in cells exhibiting oxidized lipids after RSL3 or erastin treatment (**Figure 21C**). In contrast, $LTED^{WT}$ cells displayed minimal or absent increase in ROS levels or lipid peroxidation upon exposure to the same ferroptotic stimuli, as illustrated across multiple panels (**Figure 21D–F**). To functionally confirm that cell death occurred through ferroptosis, $LTED^{Y537C}$ cells were co-treated with RSL3 or erastin together with the known ferroptosis inhibitors ferrostatin-1 (Fer-1), a lipid radical scavenger, or deferoxamine (DFOM), an iron chelator. Both agents efficiently prevented the loss of cell viability induced by RSL3 and erastin (**Figure 21G**), confirming the ferroptotic nature of the observed cell death. Overall, these results indicate that $LTED^{Y537C}$ cells, despite their resistance to estrogen deprivation, display an increased vulnerability to ferroptosis, likely due to their altered lipid metabolic phenotype.

Figure 21

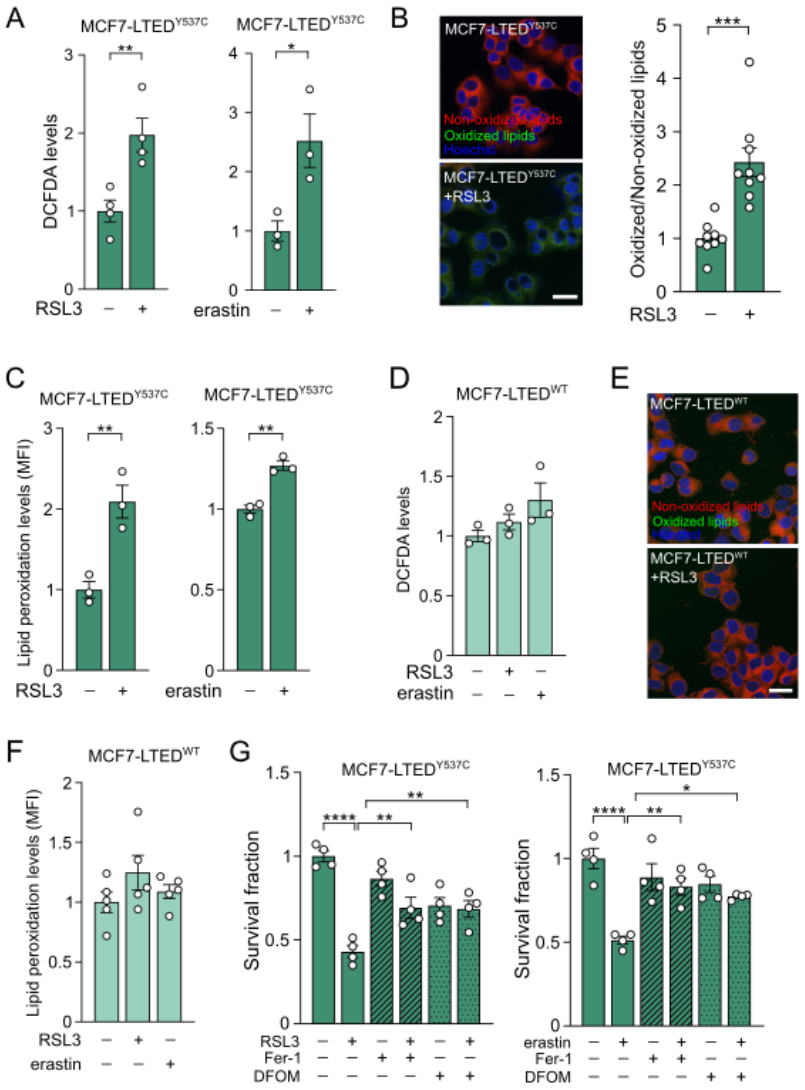

Figure 21. Y537C mutation promotes RSL3- and erastin-increased ROS and lipid peroxidation levels. (**A**) Intracellular ROS levels were measured by DCFDA in LTED^{Y537C} cells treated with 2.5 µM RSL3 or 5 µM erastin for 48 h. *n* = 3 biological replicates in either single or technical duplicate. Student's t-test. (**B**) LTED^{Y537C} cells were treated with 25 µM RSL3 for 2 h and subjected to confocal analysis after incubation with BODIPY$^{581/591}$-C11. Representative pictures of BODIPY$^{581/591}$-C11 staining and quantification of its intensity are shown (green: Oxidized lipids; red: Non-oxidized lipids; blue: Hoechst, nuclei; scale bar, 10 µm). *n* = 3 biological replicates in technical triplicate. Student's t-test. (**C**) LTED^{Y537C} cells were treated with 25 µM RSL3 or 40 µM erastin for 2 h and subjected to cytofluorimetric analysis after incubation with BODIPY$^{581/591}$-C11. *n* = 3 biological replicates. Student's t-test. (**D**) Intracellular ROS levels were measured by DCFDA in LTED^{WT} cells treated with 2.5 µM RSL3 or 5 µM erastin for 48 h. *n* = 3 biological replicates. One-way ANOVA; Dunnett-corrected. (**E**) LTED^{WT} cells were treated with 15 µM RSL3 for 2 h and subjected to confocal analysis to measure lipid peroxidation. Representative pictures of BODIPY$^{581/591}$-C11 staining are shown (green: Oxidized lipids; red: Non-oxidized lipids; blue: Hoechst, nuclei; scale bar, 10 µm). *n* = 3 biological replicates. Student's t-test. (**F**) LTED^{WT} cells were treated with 15 µM RSL3 or 40 µM erastin for 2 h and subjected to cytofluorimetric analysis to measure lipid peroxidation using BODIPY$^{581/591}$-C11. *n* = 3 biological replicates in either single or technical duplicate. One-way ANOVA; Dunnett-corrected. (**G**) LTED^{Y537C} cells were pre-treated with 7.5 µM Fer-1 or 7.5 µM DFOM for 4 h and then exposed for further 48 h to 2.5 µM RSL3 or 5 µM erastin before cell counting. *n* = 3 biological replicates in either single or technical duplicate. One-way ANOVA; Dunnett-corrected. Data are mean ± SEM. * P < 0.05; ** P < 0.01; *** P < 0.001; **** P < 0.0001.

1.5 Ferroptosis sensitivity in MCF7 LTED^{Y537C} cells is driven by ACSL4 expression

High ACSL4 expression has been previously linked to increased susceptibility to ferroptotic stimuli (264). Given that ACSL4 was identified as the most differentially regulated gene between LTED^{WT} and LTED^{Y537C} cells in both the FATTY ACID METABOLISM and FERROPTOSIS gene set analyses (**Figure 20A**), we hypothesized that this enzyme is a key determinant of the increased ferroptosis sensitivity observed in LTED^{Y537C} cells. Western blot analysis confirmed substantially higher ACSL4 protein levels in LTED^{Y537C} cells compared to their LTED^{WT} counterparts (**Figure 22A**). Furthermore, pharmacological inhibition of ACSL4 (ACSL4i) protected LTED^{Y537C} cells from ferroptotic cell death induced by both RSL3 and erastin (**Figure 22B**). This protective effect was accompanied by a marked suppression of ROS accumulation, as measured using the DCFDA fluorescent probe (**Figure 22C**), as well as lipid peroxidation, as demonstrated by both confocal and cytofluorimetric analyses (**Figure 22D,E**). By blocking the accumulation of lipid peroxides and ROS, ACSL4 inhibition effectively suppressed the progression of ferroptosis in LTED^{Y537C} cells.

Although previous studies have described an inverse relationship between ACSL4 and ER expression (348), other reports have shown that estrogen stimulation can upregulate ACSL4 protein levels and promote invasive behavior in breast cancer cells (349). Therefore, to determine whether ACSL4 expression in LTED^{Y537C} cells is regulated by ER signaling, we silenced *ESR1* and observed a pronounced decrease in ACSL4 expression at both protein (**Figure 22F**) and transcript level (**Figure 22G**), indicating that ACSL4 expression in this context is dependent on ER activity.

Figure 22

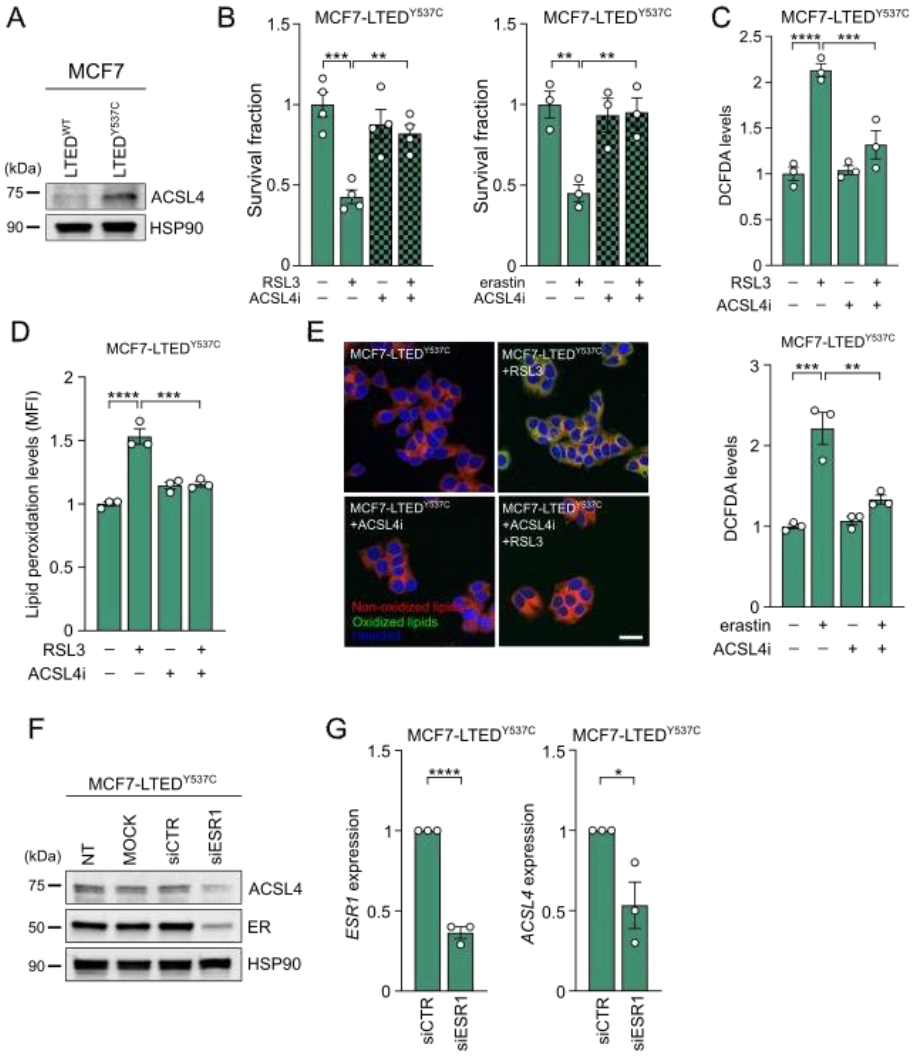

Figure 22. ACSL4 expression drives enhanced ferroptosis sensitivity to MCF7-LTED^{Y537C}. (**A**) Total protein lysates from LTED^{WT} and LTED^{Y537C} cells were subjected to WB analysis with the antibodies indicated. (**B**) LTED^{Y537C} cells were pre-treated with 10 μM ACSL4i for 4 h and then exposed for further 48 h to 2.5 μM RSL3 or 5 μM erastin before cell counting. *n* = 3 biological replicates in either single or technical duplicate One-way ANOVA; Dunnett-corrected. (**C**) LTED^{Y537C} cells were pre-treated with 10 μM ACSL4i for 4 h and then exposed for further 48 h to 2.5 μM RSL3 or 5 μM erastin before measuring intracellular ROS levels. *n* = 3 biological replicate. One-way ANOVA; Dunnett-corrected. (**D**) LTED^{Y537C} cells were pre-treated with 10 μM ACSL4i for 4 h and then exposed for further 24 h to 5 μM RSL3 and subjected to cytofluorimetric analysis after incubation with BODIPY$^{581/591}$-C11. *n* = 3 biological replicates. One-way ANOVA; Dunnett-corrected. (**E**) LTED^{Y537C} cells were pre-treated with 10 μM ACSL4i for 4 h and then exposed for further 24 h to 5 μM RSL3 prior to confocal analysis. Representative pictures of BODIPY$^{581/591}$-C11 staining are shown (green: Oxidized lipids; red: Non-oxidized lipids; blue: Hoechst, nuclei; scale bar, 10 μm). *n* = 3 biological replicates. (**F**,**G**) LTED^{Y537C} cells transfected with non-targeting small interfering RNA (siCTR) or siRNA targeting *ESR1* (siESR1) were subjected to WB analysis with the antibodies indicated (F) or qRT-PCR analysis using the assay described in the figure (G). Fold relative enrichment and statistical analysis are shown using siCTR as comparator. n = 3 biological replicates. Student's t-test. Data are mean ± SEM. * P < 0.05; ** P < 0.01; *** P < 0.001; **** P < 0.0001.

1.6 *ESR1*^{Y537C} mutation drives ferroptosis sensitivity in ER+ breast cancer cells

Since ferroptosis vulnerability in LTED models appeared to be linked to the presence of Y537C mutation, we ectopically introduced *ESR1*^{Y537C} into ER+/HER2− MCF7 and T47D cells, breast cancer models previously characterized by low intrinsic responsiveness to ferroptosis-inducing agents (350). The expression of *ESR1*^{Y537C} resulted in increased ER protein levels, accompanied by concomitant upregulation of ACSL4 in both cell lines compared to their respective control cells transduced with the empty backbone (BB) plasmid (MCF7^{BB} and T47D^{BB}) (**Figure 23A**). Notably, MCF7^{Y537C} and T47D^{Y537C} cells displayed a pronounced sensitivity to the ferroptosis inducers RSL3 and erastin at different doses and time exposures (**Figure 23B–D**). Validation of ACSL4-dependent ferroptosis execution in *ESR1*^{Y537C}-expressing cells after RSL3 and erastin treatment was obtained through different readouts: pronounced increase in oxidative stress, as evidenced by elevated intracellular ROS levels measured by DCFDA (**Figure 23E**), increased lipid peroxidation measured by flow cytometry (**Figure 23F**), and enhanced oxidation of BODIPY$^{581/591}$-C11, as visualized by confocal microscopy and quantified as an increased ratio of oxidized to non-oxidized lipids (**Figure 23G**).

Figure 23

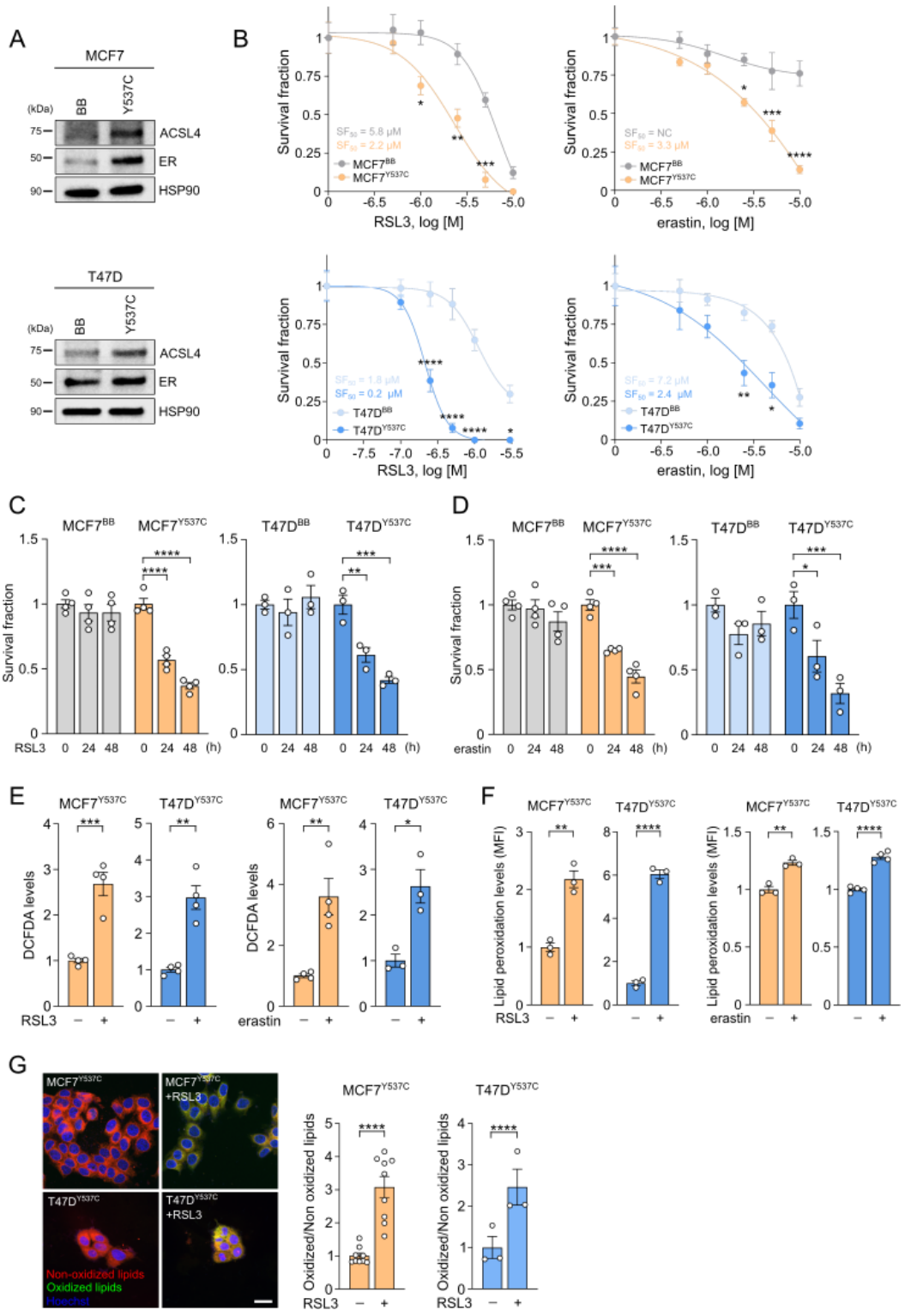

Figure 23. The ectopic expression of *ESR1*^{Y537C} in endocrine sensitive cells confers ferroptosis sensitivity. (**A**) Total protein lysates from MCF7 and T47D cells overexpressing the *ESR1*^{Y537C} mutation (Y537C) or the empty vector backbone (BB) plasmid were subjected to WB analysis with the antibodies indicated. (**B**) 48 h dose response curves of RSL3 and erastin were analyzed by cell counting in MCF7 and T47D cells with Y537C mutation or BB. *n* = 3 biological replicates. Two-way ANOVA; Sidak-corrected. SF_{50} is reported in the figure; NC = not calculable. (**C,D**) MCF7^{BB}, MCF7^{Y537C} and T47D^{BB}, T47D^{Y537C} cells were treated with 2.5 μM and 0.5 μM RSL3 (C), or 5 μM and 2.5 μM erastin (D), respectively, and subjected to

cell counting after 24 and 48 h. *n* = 3 biological replicates in either single or technical duplicate. Two-way ANOVA; Dunnett-corrected. (**E**) Intracellular ROS levels were measured by DCFDA in MCF7^{Y537C} and T47D^{Y537C} cells treated for 48 h with 2.5 µM and 0.5 µM RSL3 or 5 µM and 2.5 µM erastin, respectively. *n* = 3 biological replicates in either single or technical duplicate. Student's t-test. (**F**) MCF7^{Y537C} and T47D^{Y537C} cells were treated with RSL3 (15 µM and 2.5 µM, respectively) or erastin (40 µM and 20 µM, respectively) for 2 h and subjected to cytofluorimetric analysis using BODIPY$^{581/591}$-C11. *n* = 3 biological replicates. Student's t-test. (**G**) MCF7^{Y537C} and T47D^{Y537C} cells were treated with RSL3 (15 µM and 2.5 µM, respectively) for 2 h and subjected to confocal analysis. Representative pictures of BODIPY$^{581/591}$-C11 staining and quantification of BODIPY$^{581/591}$-C11 intensity are shown (green: Oxidized lipids; red: Non-oxidized lipids; blue: Hoechst, nuclei; scale bar, 10 µm). *n* = 3 biological replicates in either single or technical triplicate. Student's t-test. Data are mean ± SEM. * P < 0.05; ** P < 0.01; *** P < 0.001; **** P < 0.0001.

In contrast, ER^{WT} cells transduced with the empty backbone vector (MCF7^{BB} and T47D^{BB}) did not exhibit any of the ferroptosis-related phenotypic alterations observed in *ESR1*^{Y537C}-expressing cells upon treatment with the ferroptosis inducers RSL3 or erastin (**Figure 24A–C**), underscoring the specific role of the *ESR1*^{Y537C} mutation in conferring ferroptosis sensitivity. Importantly, the ferroptotic nature of cell death in *ESR1*^{Y537C}-expressing cells was further confirmed using pharmacological inhibition experiments. The use of the established ferroptosis inhibitors Fer-1 and DFOM, as well as ACSL4i, effectively reversed the cell death induced by both RSL3 and erastin (**Figure 24D,E**). Moreover, inhibition of ACSL4 was sufficient to completely suppress the ferroptotic phenotype triggered by RSL3 and erastin. Specifically, ACSL4i significantly reduces the intracellular ROS accumulation, as assessed by the fluorescent probe DCFDA (**Figure 24F**), and lipid peroxidation, as demonstrated by both quantitative cytofluorimetric analyses (**Figure 24G**) and confocal microscopy imaging (**Figure 24H**). Collectively, these data indicate that ACSL4 plays a central role in mediating ferroptosis in *ESR1*^{Y537C}-expressing cells and further reinforce the conclusion that the ER-activating mutation confers an increased sensitivity to ferroptotic cell death.

Figure 24

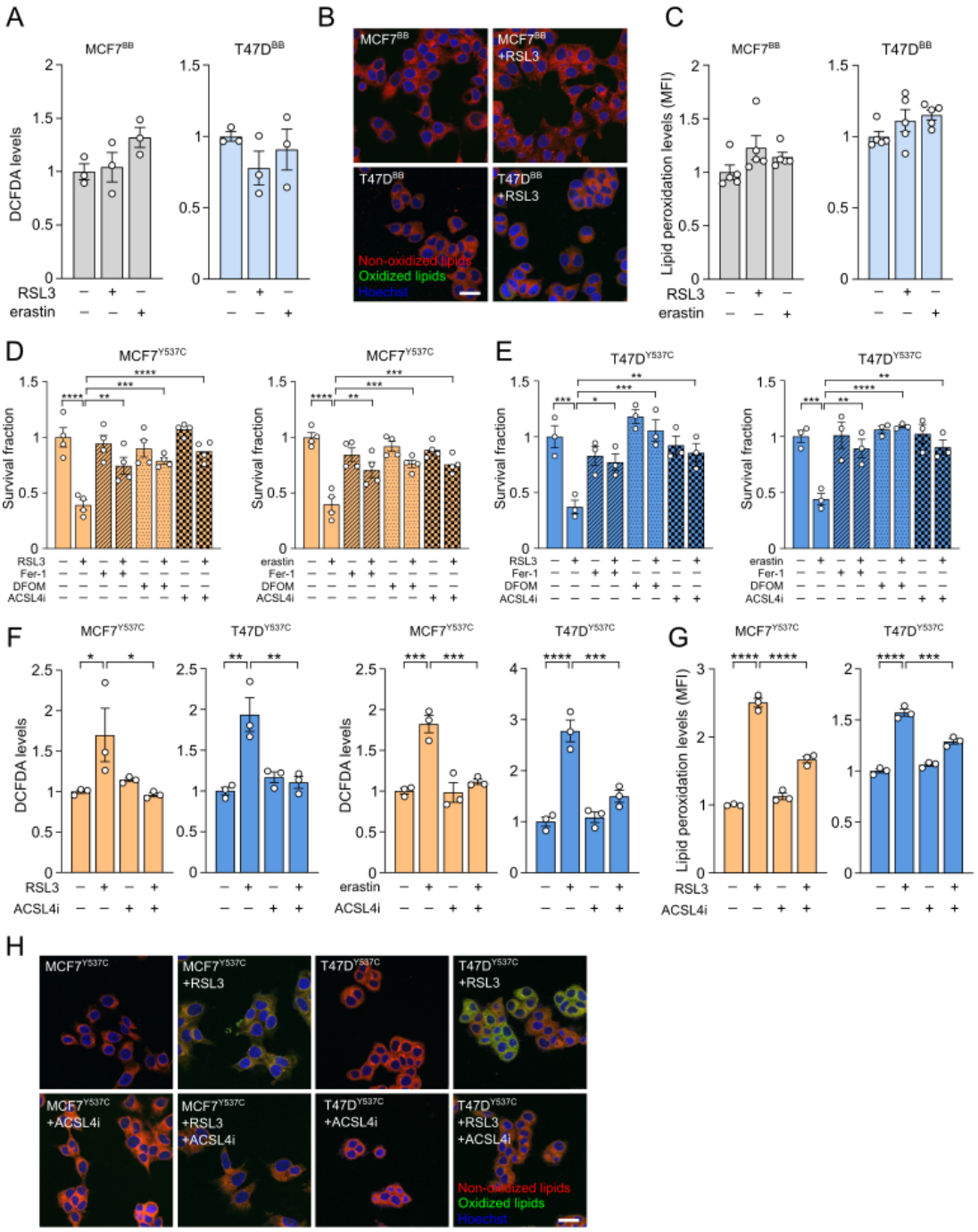

Figure 24. Ferrostatin-1, Deferoxamine, and ACSL4 inhibition prevent RSL3- an erastin- induced ferroptosis in *ESR1*^{Y537C}-expressing cells. (**A**) Intracellular ROS levels were measured by DCFDA in MCF7^{BB} and T47D^{BB} cells treated with 2.5 µM and 0.5 µM RSL3 or 5 µM and 2.5 µM erastin, respectively, for 48 h. *n* = 3 biological replicates. One-way ANOVA; Dunnett-corrected. (**B**) MCF7^{BB} and T47D^{BB} cells were treated with 2.5 µM and 0.5 µM RSL3, respectively, for 2 h and subjected to confocal analysis to measure lipid peroxidation. Representative pictures of BODIPY$^{581/591}$-C11 staining are shown (green: Oxidized lipids; red: Non-oxidized lipids; blue: Hoechst, nuclei; scale bar, 10 µm). *n* = 3 biological replicates. Student's t-test. (**C**) MCF7^{BB} and T47D^{BB} cells were treated with 2.5 µM and 0.5 µM RSL3, respectively, for 2 h and subjected to cytofluorimetric analysis using BODIPY$^{581/591}$-C11. *n* = 3 biological replicates in either single or technical duplicate. One-way ANOVA; Dunnett-corrected. (**D**) MCF7^{Y537C} cells were pre-treated with 7.5 µM Fer-1, 7.5 µM DFOM or 10 µM ACSL4i for 4 h and then exposed for further 48 h to 2.5 µM RSL3 or 5 µM erastin before cell counting. *n* = 3 biological replicates in either single or technical duplicate. One-way ANOVA; Dunnett-corrected. (**E**) T47D^{Y537C} cells were pre-treated with 5 µM Fer-1, 2.5 µM DFOM or 10

µM ACSL4i for 4 h and then exposed for further 48 h to 0.5 µM RSL3 or 2.5 µM erastin before cell counting. *n* = 3 biological replicates in either single or technical duplicate. (**F**) MCF7^{Y537C} and T47D^{Y537C} cells were pre-treated with 10 µM ACSL4i for 4 h and then exposed for further 48 h to 2.5 µM and 0.5 µM RSL3 or 5 µM and 2.5 µM erastin, respectively, before measuring intracellular ROS levels. *n* = 3 biological replicates. One-way ANOVA; Dunnett-corrected. (**G**) MCF7^{Y537C} and T47D^{Y537C} cells were pre-treated with 10 µM ACSL4i for 4 h and then exposed for further 24 h to 5 µM and 1 µM RSL3, respectively, and subjected to cytofluorimetric analysis to measure lipid peroxidation. *n* = 3 biological replicates. One-way ANOVA; Dunnett-corrected. (**H**) MCF7^{Y537C} and T47D^{Y537C} cells were pre-treated with 10 µM ACSL4i for 4 h and then exposed for further 24 h to 5 µM and 1 µM RSL3, respectively, and subjected to confocal analysis. Representative pictures of BODIPY$^{581/591}$-C11 staining are shown (green: Oxidized lipids; red: Non-oxidized lipids; blue: Hoechst, nuclei; scale bar, 10 µm). *n* = 3 biological replicates.

1.7 Clinically relevant ER-activating mutations sensitize ER+ breast cancer cells to ferroptosis

To evaluate whether the observed phenotype was specific to the *ESR1*^{Y537C} mutation, we generated MCF7 cells with additional clinically relevant *ESR1* mutations, specifically Y537S and Y537N. Expression of both mutations led to a pronounced upregulation of ACSL4 protein levels (**Figure 25A**). Consistent with this, MCF7^{Y537S} and MCF7^{Y537N} cells exhibited significantly increased sensitivity to the ferroptosis inducers RSL3 and erastin across multiple doses and exposure times, closely mirroring the response observed in MCF7^{Y537C} cells (**Figure 25B,C**). These findings indicate that enhanced ferroptosis vulnerability represents a shared phenotype of cells harboring clinically relevant ER-activating mutations. To test whether this vulnerability could be recapitulated in clinically relevant settings, we generated *ex vivo* tumor explants (PDE) and organoid (PDXO) from two established ER+/HER2- breast cancer patient-derived xenograft (PDX) models naturally harboring the *ESR1*^{Y537S} mutation (HBCx-239 and HBCx-254). Treatment with RSL3 for 72 hours resulted in a dose-dependent decrease in viability in both models, indicating pronounced sensitivity, with SF_{50} values comparable to those observed for cell lines (**Figure 25D**). Consistent with what was observed in *ESR1*^{Y537C} cells, ferroptosis execution in MCF7^{Y537S} and MCF7^{Y537N} cells was confirmed by (i) a significant increase in ROS species (**Figure 25E**), (ii) elevated lipid peroxidation measured by flow cytometry (**Figure 25F**) and corroborated by confocal imaging showing an increased oxidized-to-non-oxidized lipid ratio (**Figure 25G**).

Figure 25

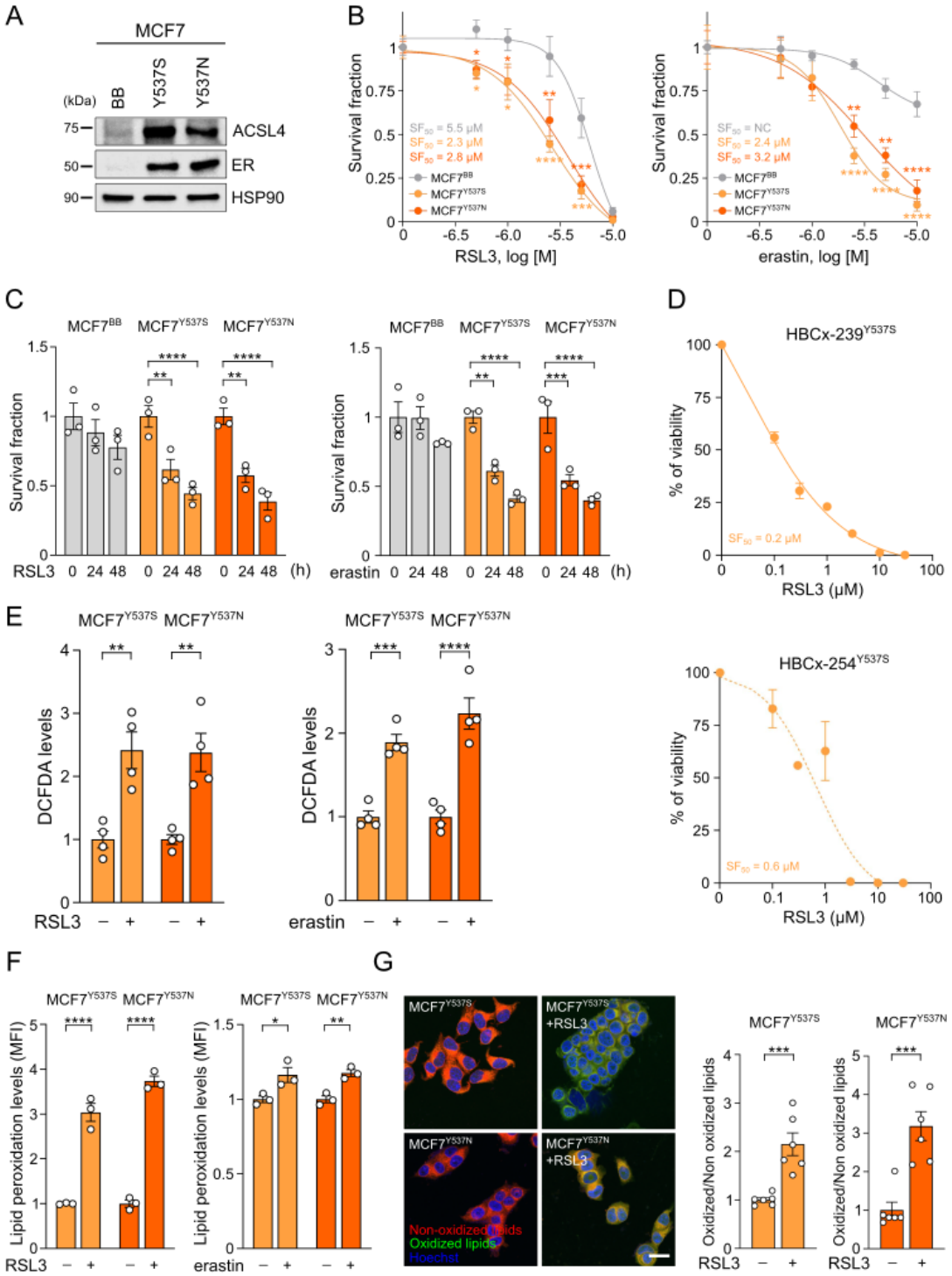

Figure 25. The clinically relevant mutations Y537S and Y537N induce ferroptosis sensitivity in parental cells. (**A**) Total protein lysates from MCF7 cells overexpressing *ESR1*^{Y537S} (Y537S) or *ESR1*^{Y537N} (Y537N) and parental cells with the empty vector backbone (BB) plasmid were subjected to WB analysis with the antibodies indicated. (**B**) 48 h dose response curves of RSL3 and erastin were analyzed by cell counting in MCF7^{BB}, MCF7^{Y537S} and MCF7^{Y537N} cells. *n* = 3 biological replicates. Two-way ANOVA; Dunnett-corrected. SF_{50} is reported in the figure; NC = not calculable. (**C**) MCF7^{Y537S}, MCF7^{Y537N} and MCF7^{BB} cells

were treated with 2.5 µM RSL3 and 5 µM erastin and subjected to cell counting after 24 and 48 h. *n* = 3 biological replicates. Two-way ANOVA; Dunnett-corrected. (**D**) Cell viability of three-dimensional PDE and PDXO derived from the PDX HBCx-239 and HBCx-254 exposed for 72 h to different concentrations of RSL3. *n* = 3 biological replicates. SF_{50} is reported in the figure. (**E**) Intracellular ROS levels were measured by DCFDA in $MCF7^{Y537S}$ and $MCF7^{Y537N}$ cells treated with 2.5 µM RSL3 or 5 µM erastin for 48 h. *n* = 3 biological replicates in either single or technical duplicate. Two-way ANOVA; Sidak-corrected. (**F**) $MCF7^{Y537S}$ and $MCF7^{Y537N}$ cells were treated with 15 µM RSL3 or 40 µM erastin for 2 h and subjected to cytofluorimetric analysis to measure lipid peroxidation using $BODIPY^{581/591}$-C11. *n* = 3 biological replicates. Two-way ANOVA; Sidak-corrected. (**G**) $MCF7^{Y537S}$ and $MCF7^{Y537N}$ cells were treated with 15 µM RSL3 for 2 h and subjected to confocal analysis to measure lipid peroxidation. Representative pictures of $BODIPY^{581/591}$-C11 staining and quantification of its intensity are shown (green: Oxidized lipids; red: Non-oxidized lipids; blue: Hoechst, nuclei; scale bar, 10 µm). *n* = 3 biological replicates. Student's t-test. Data are mean ± SEM. * P < 0.05; ** P < 0.01; *** P < 0.001; **** P < 0.0001.

The involvement of ferroptosis in $MCF7^{Y537S}$ and $MCF7^{Y537N}$ cell death was confirmed through a series of pharmacological rescue experiments. Treatment with the canonical ferroptosis inhibitors Fer-1 and DFOM, and the specific ACSL4i, markedly protected cells from cytotoxicity induced by both RSL3 and erastin (**Figure 26A**). Again, blockade of ACSL4 activity alone was sufficient to induce a pronounced reduction in oxidative stress, as evidenced by decreased intracellular ROS levels measured by DCFDA (**Figure 26B**) and a concomitant suppression of lipid peroxidation, as confirmed by flow cytometric quantification (**Figure 26C**) and confocal microscopy analysis (**Figure 26D**). Collectively, these findings identify ACSL4 as a key effector of ferroptosis in cells harboring clinically-relevant ER-activating mutations, conferring increased susceptibility to ferroptotic cell death.

Figure 26

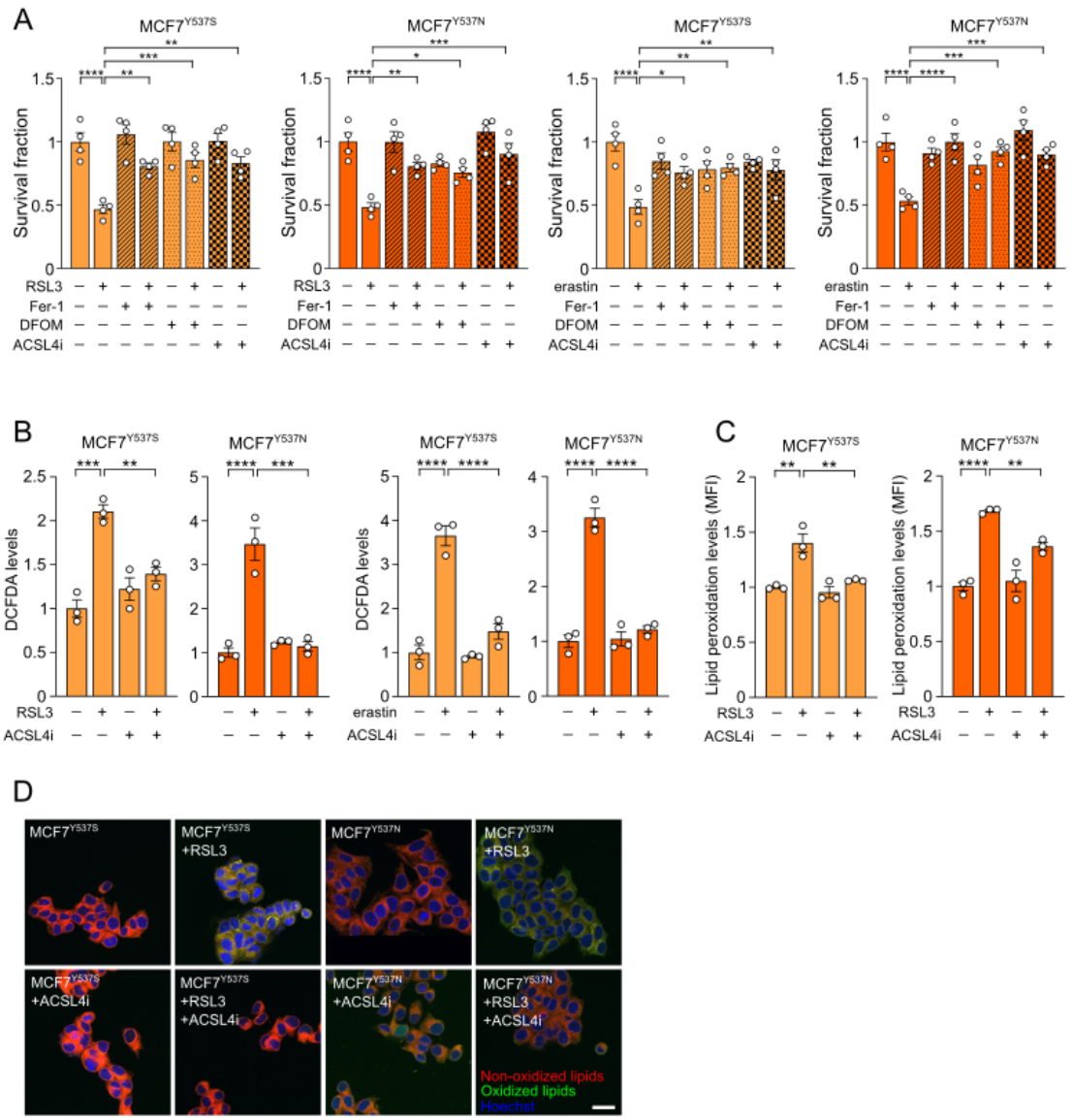

Figure 26. ACSL4 targeting prevents ferroptosis execution in MCF7^{Y537S} and MCF7^{Y537N} cells. (**A**) MCF7^{Y537S} and MCF7^{Y537N} cells were pre-treated with 7.5 μM Fer-1, 7.5 μM DFOM or 10 μM ACSL4i for 4 h and then exposed for further 48 h to 2.5 μM RSL3 or 5 μM erastin before cell counting. *n* = 3 biological replicates in either single or technical duplicate. One-way ANOVA; Dunnett-corrected. (**B**) MCF7^{Y537S} and MCF7^{Y537N} cells were pre-treated with 10 μM ACSL4i for 4 h and then exposed for further 48 h to 2.5 μM RSL3 or 5 μM erastin, before measuring intracellular ROS levels. *n* = 3 biological replicates. One-way ANOVA; Dunnett-corrected. (**C**) MCF7^{Y537S} and MCF7^{Y537N} cells were pre-treated with 10 μM ACSL4i for 4 h and then exposed for further 24 h to 5 μM RSL3 and subjected to cytofluorimetric analysis to measure lipid peroxidation using BODIPY$^{581/591}$-C11. *n* = 3 biological replicates. One-way ANOVA; Dunnett-corrected. (**D**) MCF7^{Y537S} and MCF7^{Y537N} cells were pre-treated with 10 μM ACSL4i for 4 h and then exposed for further 24 h to 5 μM RSL3 and subjected to confocal analysis to measure lipid peroxidation. Representative pictures of BODIPY$^{581/591}$-C11 staining are shown (green: Oxidized lipids; red: Non-oxidized lipids; blue: Hoechst, nuclei; scale bar, 10 μm). *n* = 3 biological replicates. Data are mean ± SEM. * P < 0.05; ** P < 0.01; *** P < 0.001; **** P < 0.0001.

1.8 Ferroptosis induction potentiates fulvestrant and elacestrant treatment in *ESR1*-mutated breast cancer models

The SERD fulvestrant represents the standard therapeutic option for metastatic breast cancers harboring *ESR1* mutations. Recently, the next-generation SERD elacestrant has gained approval for patients with *ESR1*-mutant disease who have progressed on prior ET. Given that *ESR1* mutations confer an increased susceptibility to ferroptotic cell death, we sought to determine whether this vulnerability could be exploited to improve the antitumor activity of SERDs. To this end, LTED^{Y537C} (**Figure 27A**), MCF7^{Y537C} (**Figure 27B**), MCF7^{Y537S} (**Figure 27C**), MCF7^{Y537N} (**Figure 27D**), and T47D^{Y537C} (**Figure 27E**) cells were exposed to increasing concentrations of fulvestrant or elacestrant, either alone or together with the ferroptosis inducers RSL3 or erastin, showing a more pronounced decrease in cell viability with combination treatments. No relevant synergy was observed between either RSL3 or erastin and SERDs treatment in the LTED^{WT} cells (**Figure 27F**). We next evaluated the therapeutic relevance of this combination strategy using the *ESR1*^{Y537S}-mutant HBCx-254 PDXO model (**Figure 25D**). Doses of RSL3 and elacestrant, which individually produced minimal impact on viability after 72 hours, were selected for combination treatment. Notably, concurrent administration of both agents resulted in a pronounced synergistic response, leading to a substantial reduction in the surviving fraction of HBCx-254 PDXO (**Figure 27G**). Overall, these data indicate that activation of ferroptotic pathways *via* RSL3 or erastin enhances the antitumor efficacy of fulvestrant and elacestrant, supporting a role for ferroptosis induction as a strategy to sensitize *ESR1*-mutant breast cancer to SERD treatment.

Figure 27

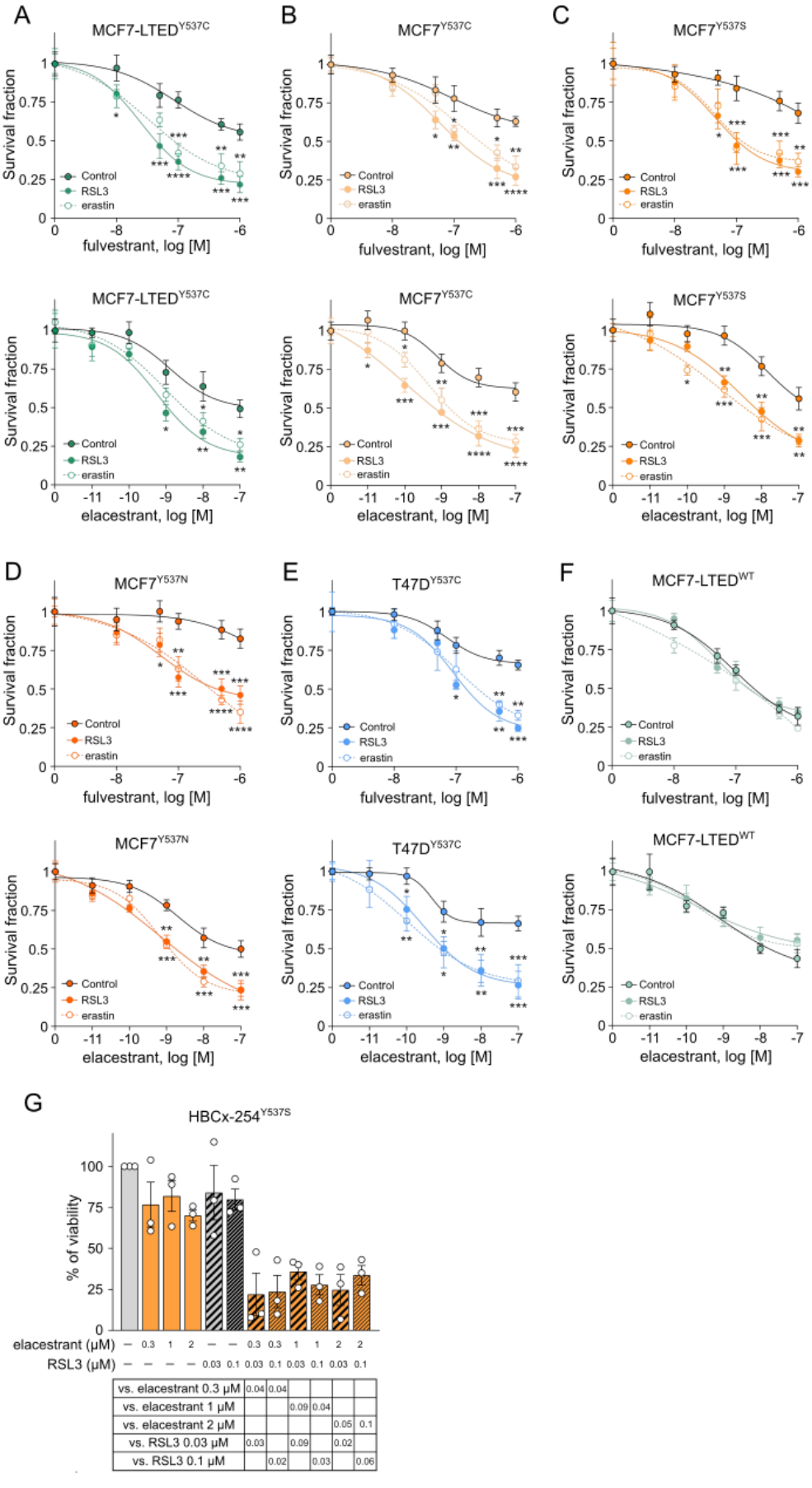
A
MCF7-LTED^Y537C
B
MCF7^Y537C
C
MCF7^Y537S
D
MCF7^Y537N
E
T47D^Y537C
F
MCF7-LTED^WT
Survival fraction
fulvestrant, log [M]
elacestrant, log [M]
Control
RSL3
erastin
G
HBCx-254^Y537S
% of viability
elacestrant (μM)
RSL3 (μM)
vs. elacestrant 0.3 μM
vs. elacestrant 1 μM
vs. elacestrant 2 μM
vs. RSL3 0.03 μM
vs. RSL3 0.1 μM

Figure 27. Ferroptosis induction potentiates fulvestrant and elacestrant treatment. (**A**) MCF7-LTED^{Y537C} cells were treated with increasing doses of fulvestrant and elacestrant together with 0.5 μM RSL3 or 1 μM erastin and subjected to cell counting after 72 h. *n* = 3 biological replicates in either single or technical duplicate. Two-way ANOVA; Dunnett-corrected. (**B**,**C**,**D**) MCF7^{Y537C} (B), MCF7^{Y537S} (C), and MCF7^{Y537N} (D) cells were treated with increasing doses of fulvestrant and elacestrant together with 0.75 μM RSL3 or 1 μM erastin and subjected to cell counting after 72 h. *n* = 3 biological replicates in either single or technical duplicate. Two-way ANOVA; Dunnett-corrected. (**E**) T47D^{Y537C} cells were treated with increasing doses of fulvestrant and elacestrant together with 0.1 μM RSL3 or 0.75 μM erastin and subjected to cell counting after 72 h. *n* = 3 biological replicates in either single or technical duplicate. Two-way ANOVA; Dunnett-corrected. (**F**) MCF7-LTED^{WT} cells were treated with increasing doses of fulvestrant and elacestrant together with 0.5 μM RSL3 or 1 μM erastin and subjected to cell counting after 72 h. *n* = 3 biological replicates in technical triplicate. Two-way ANOVA; Dunnett-corrected. (**G**) Cell viability of three-dimensional explants derived from HBCx-254 exposed for 72 h to different concentrations of RSL3 and elacestrant. *n* = 3 biological replicates. Kruskal-Wallis. The exact *p*-value is reported in the figure as a table. Data are mean ± SEM. * P < 0.05; ** P < 0.01; *** P < 0.001; **** P < 0.0001.

1.9 High ACSL4 expression correlates with poor prognosis in breast cancer

To assess the clinical relevance of ACSL4, we conducted a retrospective evaluation of ER+/HER2- breast cancer patients grouped according to high or low ACSL4 mRNA expression levels. Patients with elevated ACSL4 expression exhibited significantly shorter post-progression survival compared with those with lower expression (hazard ratio [HR] = 1.69, log-rank P = 0.0011; n = 271; **Figure 28A**). However, due to the lack of genomic profiling data for this cohort, it was not possible to establish whether the association between increased ACSL4 expression and poorer clinical outcome was directly attributable to the presence of *ESR1* mutations.

Nonetheless, evidence supporting a more general prognostic role for ACSL4 in breast cancer comes from prior work demonstrating that high ACSL4 levels are linked to reduced recurrence-free survival in TNBC (264), suggesting that diverse biological pathways may drive ACSL4 upregulation across different breast cancer subtypes. To further explore the connection between ACSL4 expression and *ESR1* mutational status, we performed immunohistochemical analyses on a curated collection of ER+ breast cancer biopsies classified as either *ESR1*^{MUT} or *ESR1*^{WT} (**Table 1**). Tumors carrying *ESR1* mutations showed a significantly higher ACSL4 H-score (**Figure 28B**). Considering that *ESR1* mutations commonly arise in the metastatic setting of ER+ breast cancer (124), where fulvestrant has shown improved efficacy compared with other ET (129), these data suggest a potential role for ACSL4 in driving disease progression and influencing therapeutic response in *ESR1*-mutant tumors. Thus, our findings support the potential utility of ACSL4 expression as a biomarker to inform treatment strategies.

Figure 28

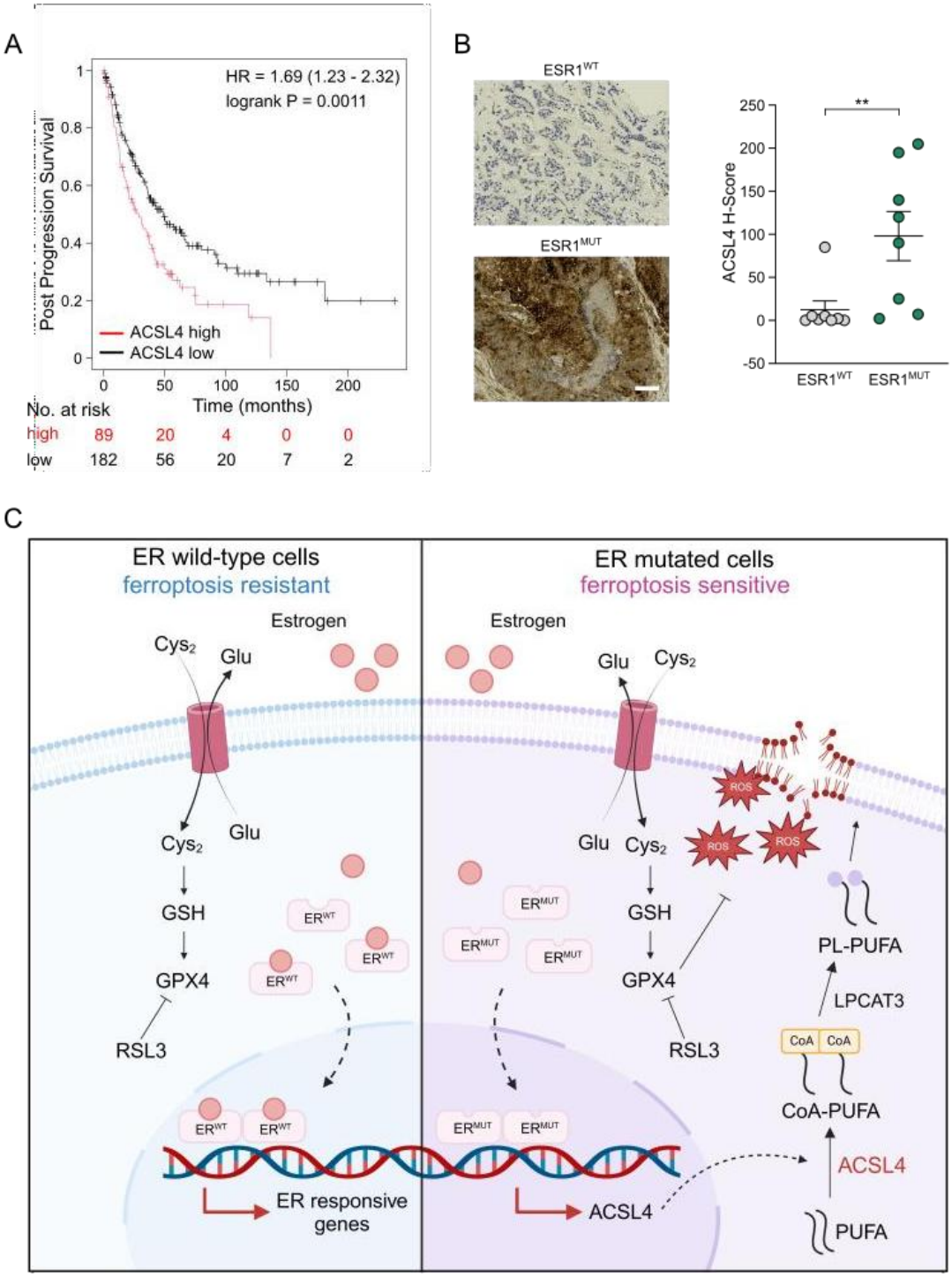

Figure 28. ACSL4 correlates with poor prognosis in ER+ breast cancer. (**A**) Kaplan–Meier analysis of post progression survival of a curated cohort of ER+/HER2- patients divided into high and low ACSL4 expression as described in the Materials and Methods section. HR and log-rank Mantel-Cox P values are shown. (**B**) Representative 10X images of ACSL4 IHC staining and relative quantification (ACSL4 H-score) of three different areas derived from *ESR1*^{WT} and *ESR1*^{MUT} tumor specimens (scale bar, 200 μm). ACSL4 H-Score is calculated as described in Materials and Methods section, each dot is a tumor specimen. Student's t-test. Data are mean ± SEM. ** P < 0.01. (**C**) Schematic representation of the proposed mechanism describing the connection between estrogen, ER/ER^{MUT} signaling pathway, ACSL4, and lipid metabolism during ferroptosis execution in ER+ breast cancer.

Table S1. *ESR1* status of patients analyzed

Patient	*ESR1* status	evaluation of *ESR1* status on	VAF (%) Tissue/Liquid B.	Specimen Source	ACSL4 H-score
1	D538G	Liquid B.	2	Primary	195
2	*ESR1* amplification	Tissue	-	Primary	90
3	D538G, Y537C	Liquid B.	2	Primary	25
4	Y537N, D538G	Tissue/Liquid B.	40/10	Pleural Met	7
5	L536P	Tissue/Liquid B.	58/40	Liver Met	205
6	Y537C	Tissue	69	Local Rec	140
7	E380Q	Tissue	40	LN Met	120
8	D538G	Tissue	11	Local Rec	2
9	WT	Tissue	-	Primary	5
10	WT	Tissue	-	LN Met	85
11	WT	Tissue	-	Pleural Met	0
12	WT	Tissue	-	Liver Met	1
13	WT	Tissue	-	LN Met	5
14	WT	Tissue	-	Primary	5
15	WT	Tissue	-	Primary	2
16	WT	Tissue	-	Primary	0

Liquid B.: liquid biopsy; Local Rec: local recurrence; Met: metastasis; LN: Lymph node; VAF: Variant allele frequency

2. Discussion

Our study focused on elucidating the impact of *ESR1* mutations on the metabolic reprogramming of breast cancer. Consistent with prior studies reporting that lipid metabolic reprogramming can be exploited as a vulnerability in ER+ breast cancer (149, 351) and TNBC subtypes (264, 352), we demonstrated that breast cancers harboring *ESR1*-activating mutations display a distinct lipid metabolic phenotype that creates therapeutic vulnerabilities, rendering these tumors more susceptible to ferroptosis inducers (**Figure 28C**). Ferroptosis is a regulated form of cell death triggered by excessive lipid peroxidation and is closely linked to altered lipid metabolism (242). During tumor progression or in response to therapy, cancer cells frequently undergo lipid metabolic reprogramming, a process that can increase their susceptibility to ferroptosis (353). Accordingly, targeting lipid metabolism to induce ferroptotic cell death offers a promising therapeutic strategy to selectively kill cancer cells while sparing normal tissues. However, the ability to adapt and reprogram lipid metabolism is essential to enable cancer cells to evade ferroptosis. We found that *ESR1*-activating mutations impair efficient LD mobilization, a process we previously identified as crucial for maintaining metabolic plasticity in *ESR1*^{WT} breast cancer cells (149). Additionally, we have demonstrated that metastatic TNBC cells exposed to ferroptosis-inducing agents

respond by rapidly forming protective LDs. Notably, inhibition of LD biogenesis enhances the anticancer activity of ferroptosis inducers (264). SERDs are the current first-line treatment for *ESR1*-mutant breast cancer. Fulvestrant, the most common SERD, is often used for advanced or metastatic ER+ disease, particularly following the development of resistance to AIs. Elacestrant, a newer orally available SERD, has shown clinical benefit in patients with *ESR1*-mutant tumors and is generally used after progression on prior ET (128). Nevertheless, analyses from the PALOMA-3 trial indicate that patients harboring *ESR1* mutations exhibit reduced OS when treated with fulvestrant alone compared with those with *ESR1*^{WT} tumors, although survival is improved with the addition of palbociclib (53, 354). Our findings indicate that activation of ferroptosis potentiates the antitumor activity of both fulvestrant and elacestrant in *ESR1*-mutant breast cancer cells, highlighting ferroptosis induction as a promising approach to overcome therapeutic resistance in this breast cancer subtype. Collectively, our data indicate that *ESR1*-activating mutations alone are sufficient to confer sensitivity to ferroptosis, without the need for additional alterations in other signaling pathways. However, the LTED^{Y537C} model retains heterozygosity for both *ESR1*^{WT} and mutant *ESR1* alleles, complicating the attribution of specific effects to either receptor form. Consistent with this, ectopic overexpression of *ESR1* mutants in parental cell lines may result in competition with endogenous *ESR1*^{WT}, further complicating mechanistic interpretation. Despite these limitations, increased ACSL4 expression emerges as a consistent feature across *ESR1*-mutant models and is further validated in patient samples. ACSL4 promotes the esterification of PUFAs into membrane phospholipids and is enriched in cancer cells that display increased ferroptosis sensitivity (263). Recent evidence demonstrates that ACSL4 supports lipid peroxidation during ferroptosis by boosting PUFA-phospholipid synthesis (355). Importantly, ACSL4 can also be expressed independently of ER signaling and remains clinically relevant, as shown previously (341). Together, these findings support the potential of ACSL4 as a biomarker for identifying tumors likely to respond to ferroptosis-targeting agents.

The metabolic phenotype identified in *ESR1*-mutant cells, which increases their vulnerability to ferroptosis, is consistent with evidence that combining CDK4/6i with ER-targeting therapies further enhances ferroptosis susceptibility in breast cancer cells (274). These observations support the rationale for adding ferroptosis inducers into therapeutic regimens that include CDK4/6i and ER-targeted treatments to enhance clinical efficacy in ER+ breast cancer. Ferroptosis may thus be a new therapeutic strategy to overcome endocrine resistance in *ESR1*-mutant tumors.

Mechanistically, cancer cells regulate ferroptosis through the activation of anti-ferroptotic defense pathways. Previous studies have shown that the system Xc^- subunits SLC7A11

and SLC3A2, which facilitate cystine uptake and are directly inhibited by erastin, are transcriptionally regulated by ER, thereby contributing to the intrinsic ferroptosis resistance observed in ER+ breast cancer (350). In our LTED^{Y537C} model, however, the expression of these genes was not significantly altered in comparison to LTED^{WT} cells, indicating that alternative mechanisms may drive the increased ferroptosis sensitivity of *ESR1*-mutant breast cancer cells. Additionally, this study did not investigate whether *ESR1* mutations affect the intracellular labile iron pool, another key determinant of ferroptosis susceptibility. Recent lipidomic analyses have highlighted that intrinsic ferroptosis resistance in some ER$^+$ breast cancer cell lines may come from specific lipid compositions and metabolic states (274). It is well recognized that elevated levels of PUFAs, particularly in plasma membranes, can sensitize cells to ferroptosis (265). Notably, our previous work demonstrated that the synergistic effect of ET and ferroptosis induction is independent of the desaturases FADS1 and FADS2, which are the main enzymes responsible for PUFA synthesis (264). A detailed characterization of the lipidomic profile in therapy-resistant breast cancer cells, together with analysis of key ferroptosis regulators such as ACSL4, could provide critical insights for developing more effective combination treatments and help identify patient subsets more likely to benefit from ferroptosis-targeting strategies.

Collectively, our study underscores the importance of metabolic reprogramming in *ESR1*-mutant breast cancer and highlights the therapeutic potential of ferroptosis induction. Exploring how lipid metabolism influences ferroptosis in endocrine-resistant breast cancer may lead to the development of new treatment strategies aimed at improving clinical outcomes.

3. Future perspectives

The manipulation of ferroptosis represents a promising yet complex strategy for cancer therapy, particularly in the context of treatment resistance. A growing body of evidence indicates that inducing ferroptosis can effectively eliminate cancer cells that are refractory to conventional therapies, as therapy-resistant cells often retain sensitivity to ferroptotic cell death (356). These findings suggest that integrating ferroptosis inducers into existing treatment regimens may enhance therapeutic efficacy through complementary mechanisms of action and reduce the development of resistance. However, the role of ferroptosis in cancer is highly context-dependent, presenting both therapeutic opportunities and challenges. While ferroptosis induction can suppress tumor growth, it may also promote tumor progression under certain conditions by exacerbating inflammation, impairing antitumor immune responses, or contributing to an

immunosuppressive tumor microenvironment (357, 358). Moreover, systemic ferroptosis induction can cause excessive lipid peroxidation, raising significant safety concerns due to toxicity in normal tissues, particularly in the liver and kidneys, thereby introducing a layer of complexity when translating preclinical findings into more clinical relevant settting, which may narrow the therapeutic window of opportunity of this approach (359). These challenges are worsened by the limited clinical translatability of commonly used experimental ferroptosis inducers, such as erastin and RSL3, which have poor bioavailability, limited tumor specificity, and lack of demonstrated efficacy in human studies. Consequently, the development of clinically viable ferroptosis-targeting agents remains a critical priority, including new small molecules, targeted delivery systems, and emerging approaches like targeted protein degradation using PROTACs or lysosome-targeting chimeras (360, 361). Additionally, shifting therapeutic focus away from master regulators like GPX4 toward downstream ferroptosis modulators may improve safety. Successful clinical implementation will also depend on appropriate patient selection, as ferroptosis sensitivity varies according to tumor type, genetic background, and microenvironmental context; incorporating molecular and genetic profiling into treatment strategies may therefore enhance clinical benefit. Notably, the ongoing evaluation of the FDA-approved drug sulfasalazine as a ferroptosis-inducing adjunct in multiple phase I and II clinical trials (NCT06134388, NCT04205357, NCT05580861, NCT05664464) highlights both the potential of ferroptosis-based therapies and the need for further refinement to ensure safety, efficacy, and context-specific application.

References

1. Kim J, Harper A, McCormack V, Sung H, Houssami N, Morgan E, et al. Global patterns and trends in breast cancer incidence and mortality across 185 countries. Nat Med. 2025;31(4):1154-62.
2. Organization WH. Breast cancer, World Health Organization. 2024.
3. Loibl S, Poortmans P, Morrow M, Denkert C, Curigliano G. Breast cancer. Lancet. 2021;397(10286):1750-69.
4. Harbeck N, Penault-Llorca F, Cortes J, Gnant M, Houssami N, Poortmans P, et al. Breast cancer. Nat Rev Dis Primers. 2019;5(1):66.
5. Perou CM, Sørlie T, Eisen MB, van de Rijn M, Jeffrey SS, Rees CA, et al. Molecular portraits of human breast tumours. Nature. 2000;406(6797):747-52.
6. Mayrovitz HN. Breast Cancer. 2022.
7. Schettini F, Prat A. Dissecting the biological heterogeneity of HER2-positive breast cancer. Breast. 2021;59:339-50.
8. Network CGA. Comprehensive molecular portraits of human breast tumours. Nature. 2012;490(7418):61-70.
9. Sommer S, Fuqua SA. Estrogen receptor and breast cancer. Semin Cancer Biol. 2001;11(5):339-52.
10. Russo J, Ao X, Grill C, Russo IH. Pattern of distribution of cells positive for estrogen receptor alpha and progesterone receptor in relation to proliferating cells in the mammary gland. Breast Cancer Res Treat. 1999;53(3):217-27.
11. Shoker BS, Jarvis C, Clarke RB, Anderson E, Hewlett J, Davies MP, et al. Estrogen receptor-positive proliferating cells in the normal and precancerous breast. Am J Pathol. 1999;155(6):1811-5.
12. Miziak P, Baran M, Błaszczak E, Przybyszewska-Podstawka A, Kałafut J, Smok-Kalwat J, et al. Estrogen Receptor Signaling in Breast Cancer. Cancers (Basel). 2023;15(19).
13. Clemons M, Goss P. Estrogen and the risk of breast cancer. N Engl J Med. 2001;344(4):276-85.
14. De Cicco P, Catani MV, Gasperi V, Sibilano M, Quaglietta M, Savini I. Nutrition and Breast Cancer: A Literature Review on Prevention, Treatment and Recurrence. Nutrients. 2019;11(7).
15. Torres-de la Roche LA, Acevedo-Mesa A, Lizarazo IL, Devassy R, Becker S, Krentel H, et al. Hormonal Contraception and the Risk of Breast Cancer in Women of Reproductive Age: A Meta-Analysis. Cancers (Basel). 2023;15(23).
16. Russo J, Russo IH. The role of estrogen in the initiation of breast cancer. J Steroid Biochem Mol Biol. 2006;102(1-5):89-96.
17. Jia M, Dahlman-Wright K, Gustafsson J. Estrogen receptor alpha and beta in health and disease. Best Pract Res Clin Endocrinol Metab. 2015;29(4):557-68.
18. Kumar R, Zakharov MN, Khan SH, Miki R, Jang H, Toraldo G, et al. The dynamic structure of the estrogen receptor. J Amino Acids. 2011;2011:812540.
19. Fuentes N, Silveyra P. Estrogen receptor signaling mechanisms. Adv Protein Chem Struct Biol. 2019;116:135-70.
20. Grober OM, Mutarelli M, Giurato G, Ravo M, Cicatiello L, De Filippo MR, et al. Global analysis of estrogen receptor beta binding to breast cancer cell genome reveals an extensive interplay with estrogen receptor alpha for target gene regulation. BMC Genomics. 2011;12:36.
21. Björnström L, Sjöberg M. Mechanisms of estrogen receptor signaling: convergence of genomic and nongenomic actions on target genes. Mol Endocrinol. 2005;19(4):833-42.
22. Cui J, Shen Y, Li R. Estrogen synthesis and signaling pathways during aging: from periphery to brain. Trends Mol Med. 2013;19(3):197-209.

23. Klinge CM. Estrogen receptor interaction with estrogen response elements. Nucleic Acids Res. 2001;29(14):2905-19.
24. O'Lone R, Frith MC, Karlsson EK, Hansen U. Genomic targets of nuclear estrogen receptors. Mol Endocrinol. 2004;18(8):1859-75.
25. Kalaitzidis D, Gilmore TD. Transcription factor cross-talk: the estrogen receptor and NF-kappaB. Trends Endocrinol Metab. 2005;16(2):46-52.
26. Gaub MP, Bellard M, Scheuer I, Chambon P, Sassone-Corsi P. Activation of the ovalbumin gene by the estrogen receptor involves the fos-jun complex. Cell. 1990;63(6):1267-76.
27. Carmeci C, Thompson DA, Ring HZ, Francke U, Weigel RJ. Identification of a gene (GPR30) with homology to the G-protein-coupled receptor superfamily associated with estrogen receptor expression in breast cancer. Genomics. 1997;45(3):607-17.
28. Xu S, Yu S, Dong D, Lee LTO. G Protein-Coupled Estrogen Receptor: A Potential Therapeutic Target in Cancer. Front Endocrinol (Lausanne). 2019;10:725.
29. Marino M, Pallottini V, Trentalance A. Estrogens cause rapid activation of IP3-PKC-alpha signal transduction pathway in HEPG2 cells. Biochem Biophys Res Commun. 1998;245(1):254-8.
30. Dos Santos EG, Dieudonne MN, Pecquery R, Le Moal V, Giudicelli Y, Lacasa D. Rapid nongenomic E2 effects on p42/p44 MAPK, activator protein-1, and cAMP response element binding protein in rat white adipocytes. Endocrinology. 2002;143(3):930-40.
31. Marino M, Acconcia F, Trentalance A. Biphasic estradiol-induced AKT phosphorylation is modulated by PTEN via MAP kinase in HepG2 cells. Mol Biol Cell. 2003;14(6):2583-91.
32. Picotto G, Massheimer V, Boland R. Acute stimulation of intestinal cell calcium influx induced by 17 beta-estradiol via the cAMP messenger system. Mol Cell Endocrinol. 1996;119(2):129-34.
33. de Leeuw R, Neeɳes J, Michalides R. A role for estrogen receptor phosphorylation in the resistance to tamoxifen. Int J Breast Cancer. 2011;2011:232435.
34. Song RX, Zhang Z, Chen Y, Bao Y, Santen RJ. Estrogen signaling via a linear pathway involving insulin-like growth factor I receptor, matrix metalloproteinases, and epidermal growth factor receptor to activate mitogen-activated protein kinase in MCF-7 breast cancer cells. Endocrinology. 2007;148(8):4091-101.
35. Wang C, Mayer JA, Mazumdar A, Fertuck K, Kim H, Brown M, et al. Estrogen induces c-myc gene expression via an upstream enhancer activated by the estrogen receptor and the AP-1 transcription factor. Mol Endocrinol. 2011;25(9):1527-38.
36. Musgrove EA, Caldon CE, Barraclough J, Stone A, Sutherland RL. Cyclin D as a therapeutic target in cancer. Nat Rev Cancer. 2011;11(8):558-72.
37. Huppert LA, Gumusay O, Idossa D, Rugo HS. Systemic therapy for hormone receptor-positive/human epidermal growth factor receptor 2-negative early stage and metastatic breast cancer. CA Cancer J Clin. 2023;73(5):480-515.
38. Burstein HJ. Systemic Therapy for Estrogen Receptor-Positive, HER2-Negative Breast Cancer. N Engl J Med. 2020;383(26):2557-70.
39. Xiong X, Zheng LW, Ding Y, Chen YF, Cai YW, Wang LP, et al. Breast cancer: pathogenesis and treatments. Signal Transduct Target Ther. 2025;10(1):49.
40. Gustafsson KL, Movérare-Skrtic S, Farman HH, Engdahl C, Henning P, Nilsson KH, et al. A tissue-specific role of membrane-initiated ERα signaling for the effects of SERMs. J Endocrinol. 2022;253(2):75-84.
41. Maximov PY, Lee TM, Jordan VC. The discovery and development of selective estrogen receptor modulators (SERMs) for clinical practice. Curr Clin Pharmacol. 2013;8(2):135-55.
42. Sweety Das SK, Yogesh Singh, Pradeep Kumar, Suresh Thareja. Selective Estrogen Receptor Modulators (SERMs) for the treatment of ER+ breast cancer: An overview. Journal of Molecular Structure2022.
43. Jordan VC, Collins MM, Rowsby L, Prestwich G. A monohydroxylated metabolite of tamoxifen with potent antioestrogenic activity. J Endocrinol. 1977;75(2):305-16.

44. Hu R, Hilakivi-Clarke L, Clarke R. Molecular mechanisms of tamoxifen-associated endometrial cancer (Review). Oncol Lett. 2015;9(4):1495-501.
45. Shang Y, Brown M. Molecular determinants for the tissue specificity of SERMs. Science. 2002;295(5564):2465-8.
46. Davies C, Godwin J, Gray R, Clarke M, Cutter D, Darby S, et al. Relevance of breast cancer hormone receptors and other factors to the efficacy of adjuvant tamoxifen: patient-level meta-analysis of randomised trials. Lancet. 2011;378(9793):771-84.
47. Mishra A, Srivastava A, Pateriya A, Tomar MS, Mishra AK, Shrivastava A. Metabolic reprograming confers tamoxifen resistance in breast cancer. Chem Biol Interact. 2021;347:109602.
48. Goetz MP, Bagegni NA, Batist G, Brufsky A, Cristofanilli MA, Damodaran S, et al. Lasofoxifene versus fulvestrant for ER+/HER2- metastatic breast cancer with an ESR1 mutation: results from the randomized, phase II ELAINE 1 trial. Ann Oncol. 2023;34(12):1141-51.
49. Damodaran S, O'Sullivan CC, Elkhanany A, Anderson IC, Barve M, Blau S, et al. Open-label, phase II, multicenter study of lasofoxifene plus abemaciclib for treating women with metastatic ER+/HER2- breast cancer and an ESR1 mutation after disease progression on prior therapies: ELAINE 2. Ann Oncol. 2023;34(12):1131-40.
50. Neupane N, Bawek S, Gurusinghe S, Ghaffary EM, Mirmosayyeb O, Thapa S, et al. Oral SERD, a Novel Endocrine Therapy for Estrogen Receptor-Positive Breast Cancer. Cancers (Basel). 2024;16(3).
51. Bhatia N, Hazra S, Thareja S. Selective Estrogen receptor degraders (SERDs) for the treatment of breast cancer: An overview. Eur J Med Chem. 2023;256:115422.
52. Valachis A, Mauri D, Polyzos NP, Mavroudis D, Georgoulias V, Casazza G. Fulvestrant in the treatment of advanced breast cancer: a systematic review and meta-analysis of randomized controlled trials. Crit Rev Oncol Hematol. 2010;73(3):220-7.
53. Cristofanilli M, Rugo HS, Im SA, Slamon DJ, Harbeck N, Bondarenko I, et al. Overall Survival with Palbociclib and Fulvestrant in Women with HR+/HER2- ABC: Updated Exploratory Analyses of PALOMA-3, a Double-blind, Phase III Randomized Study. Clin Cancer Res. 2022;28(16):3433-42.
54. Turner NC, Swift C, Kilburn L, Fribbens C, Beaney M, Garcia-Murillas I, et al. Mutations and Overall Survival on Fulvestrant versus Exemestane in Advanced Hormone Receptor-Positive Breast Cancer: A Combined Analysis of the Phase III SoFEA and EFECT Trials. Clin Cancer Res. 2020;26(19):5172-7.
55. Bardia A, Cortés J, Bidard FC, Neven P, Garcia-Sáenz J, Aftimos P, et al. Elacestrant in ER+, HER2- Metastatic Breast Cancer with ESR1-Mutated Tumors: Subgroup Analyses from the Phase III EMERALD Trial by Prior Duration of Endocrine Therapy plus CDK4/6 Inhibitor and in Clinical Subgroups. Clin Cancer Res. 2024;30(19):4299-309.
56. Hong Y, Yu B, Sherman M, Yuan YC, Zhou D, Chen S. Molecular basis for the aromatization reaction and exemestane-mediated irreversible inhibition of human aromatase. Mol Endocrinol. 2007;21(2):401-14.
57. Secreto G, Sieri S, Agnoli C, Grioni S, Muti P, Zumoff B, et al. A novel approach to breast cancer prevention: reducing excessive ovarian androgen production in elderly women. Breast Cancer Res Treat. 2016;158(3):553-61.
58. Nelson LR, Bulun SE. Estrogen production and action. J Am Acad Dermatol. 2001;45(3 Suppl):S116-24.
59. Molehin D, Rasha F, Rahman RL, Pruitt K. Regulation of aromatase in cancer. Mol Cell Biochem. 2021;476(6):2449-64.
60. Miller WR, Bartlett J, Brodie AM, Brueggemeier RW, di Salle E, Lønning PE, et al. Aromatase inhibitors: are there differences between steroidal and nonsteroidal aromatase inhibitors and do they matter? Oncologist. 2008;13(8):829-37.

61. Bhattacharjee D, Kumari KM, Avin S, Babu VAM. The Evolutionary Tale and Future Directions of Aromatase Inhibitors in Breast Carcinoma. Anticancer Agents Med Chem. 2017;17(11):1487-99.
62. Jänicke F. Are all aromatase inhibitors the same? A review of the current evidence. Breast. 2004;13 Suppl 1:S10-8.
63. Lombardi P. Exemestane, a new steroidal aromatase inhibitor of clinical relevance. Biochim Biophys Acta. 2002;1587(2-3):326-37.
64. Lin NU, Winer EP. Advances in adjuvant endocrine therapy for postmenopausal women. J Clin Oncol. 2008;26(5):798-805.
65. Pan H, Gray R, Braybrooke J, Davies C, Taylor C, McGale P, et al. 20-Year Risks of Breast-Cancer Recurrence after Stopping Endocrine Therapy at 5 Years. N Engl J Med. 2017;377(19):1836-46.
66. Shiino S, Kinoshita T, Yoshida M, Jimbo K, Asaga S, Takayama S, et al. Prognostic Impact of Discordance in Hormone Receptor Status Between Primary and Recurrent Sites in Patients With Recurrent Breast Cancer. Clin Breast Cancer. 2016;16(4):e133-40.
67. Ma CX, Reinert T, Chmielewska I, Ellis MJ. Mechanisms of aromatase inhibitor resistance. Nat Rev Cancer. 2015;15(5):261-75.
68. Yan S, Ji J, Zhang Z, Imam M, Chen H, Zhang D, et al. Targeting the crosstalk between estrogen receptors and membrane growth factor receptors in breast cancer treatment: Advances and opportunities. Biomed Pharmacother. 2024;175:116615.
69. Dowsett M. Overexpression of HER-2 as a resistance mechanism to hormonal therapy for breast cancer. Endocr Relat Cancer. 2001;8(3):191-5.
70. Pernas S, Tolaney SM. HER2-positive breast cancer: new therapeutic frontiers and overcoming resistance. Ther Adv Med Oncol. 2019;11:1758835919833519.
71. Pegram M, Jackisch C, Johnston SRD. Estrogen/HER2 receptor crosstalk in breast cancer: combination therapies to improve outcomes for patients with hormone receptor-positive/HER2-positive breast cancer. NPJ Breast Cancer. 2023;9(1):45.
72. Kaufman B, Mackey JR, Clemens MR, Bapsy PP, Vaid A, Wardley A, et al. Trastuzumab plus anastrozole versus anastrozole alone for the treatment of postmenopausal women with human epidermal growth factor receptor 2-positive, hormone receptor-positive metastatic breast cancer: results from the randomized phase III TAnDEM study. J Clin Oncol. 2009;27(33):5529-37.
73. Johnston S, Pippen J, Pivot X, Lichinitser M, Sadeghi S, Dieras V, et al. Lapatinib combined with letrozole versus letrozole and placebo as first-line therapy for postmenopausal hormone receptor-positive metastatic breast cancer. J Clin Oncol. 2009;27(33):5538-46.
74. Hanker AB, Sudhan DR, Arteaga CL. Overcoming Endocrine Resistance in Breast Cancer. Cancer Cell. 2020;37(4):496-513.
75. Gutteridge E, Agrawal A, Nicholson R, Cheung KL, Robertson J, Gee J. The effects of gefitinib in tamoxifen-resistant and hormone-insensitive breast cancer: a phase II study. Int J Cancer. 2010;126(8):1806-16.
76. Kruger DT, Alexi X, Opdam M, Schuurman K, Voorwerk L, Sanders J, et al. IGF-1R pathway activation as putative biomarker for linsitinib therapy to revert tamoxifen resistance in ER-positive breast cancer. Int J Cancer. 2020;146(8):2348-59.
77. Gradishar WJ, Yardley DA, Layman R, Sparano JA, Chuang E, Northfelt DW, et al. Clinical and Translational Results of a Phase II, Randomized Trial of an Anti-IGF-1R (Cixutumumab) in Women with Breast Cancer That Progressed on Endocrine Therapy. Clin Cancer Res. 2016;22(2):301-9.
78. Robertson JF, Ferrero JM, Bourgeois H, Kennecke H, de Boer RH, Jacot W, et al. Ganitumab with either exemestane or fulvestrant for postmenopausal women with advanced, hormone-receptor-positive breast cancer: a randomised, controlled, double-blind, phase 2 trial. Lancet Oncol. 2013;14(3):228-35.

79. Turner N, Pearson A, Sharpe R, Lambros M, Geyer F, Lopez-Garcia MA, et al. FGFR1 amplification drives endocrine therapy resistance and is a therapeutic target in breast cancer. Cancer Res. 2010;70(5):2085-94.
80. Mao P, Cohen O, Kowalski KJ, Kusiel JG, Buendia-Buendia JE, Cuoco MS, et al. Acquired FGFR and FGF Alterations Confer Resistance to Estrogen Receptor (ER) Targeted Therapy in ER. Clin Cancer Res. 2020;26(22):5974-89.
81. Coombes RC, Badman PD, Lozano-Kuehne JP, Liu X, Macpherson IR, Zubairi I, et al. Results of the phase IIa RADICAL trial of the FGFR inhibitor AZD4547 in endocrine resistant breast cancer. Nat Commun. 2022;13(1):3246.
82. Razavi P, Chang MT, Xu G, Bandlamudi C, Ross DS, Vasan N, et al. The Genomic Landscape of Endocrine-Resistant Advanced Breast Cancers. Cancer Cell. 2018;34(3):427-38.e6.
83. Loi S, Haibe-Kains B, Majjaj S, Lallemand F, Durbecq V, Larsimont D, et al. PIK3CA mutations associated with gene signature of low mTORC1 signaling and better outcomes in estrogen receptor-positive breast cancer. Proc Natl Acad Sci U S A. 2010;107(22):10208-13.
84. Di Cosimo S, Baselga J. Phosphoinositide 3-kinase mutations in breast cancer: a "good" activating mutation? Clin Cancer Res. 2009;15(16):5017-9.
85. Juric D, Janku F, Rodón J, Burris HA, Mayer IA, Schuler M, et al. Alpelisib Plus Fulvestrant in PIK3CA-Altered and PIK3CA-Wild-Type Estrogen Receptor-Positive Advanced Breast Cancer: A Phase 1b Clinical Trial. JAMA Oncol. 2019;5(2):e184475.
86. André F, Ciruelos E, Rubovszky G, Campone M, Loibl S, Rugo HS, et al. Alpelisib for. N Engl J Med. 2019;380(20):1929-40.
87. Angus L, Smid M, Wilting SM, van Riet J, Van Hoeck A, Nguyen L, et al. The genomic landscape of metastatic breast cancer highlights changes in mutation and signature frequencies. Nat Genet. 2019;51(10):1450-8.
88. Riggio M, Polo ML, Blaustein M, Colman-Lerner A, Lüthy I, Lanari C, et al. PI3K/AKT pathway regulates phosphorylation of steroid receptors, hormone independence and tumor differentiation in breast cancer. Carcinogenesis. 2012;33(3):509-18.
89. Faridi J, Wang L, Endemann G, Roth RA. Expression of constitutively active Akt-3 in MCF-7 breast cancer cells reverses the estrogen and tamoxifen responsivity of these cells in vivo. Clin Cancer Res. 2003;9(8):2933-9.
90. Jones RH, Casbard A, Carucci M, Cox C, Butler R, Alchami F, et al. Fulvestrant plus capivasertib versus placebo after relapse or progression on an aromatase inhibitor in metastatic, oestrogen receptor-positive breast cancer (FAKTION): a multicentre, randomised, controlled, phase 2 trial. Lancet Oncol. 2020;21(3):345-57.
91. Turner NC, Oliveira M, Howell SJ, Dalenc F, Cortes J, Gomez Moreno HL, et al. Capivasertib in Hormone Receptor-Positive Advanced Breast Cancer. N Engl J Med. 2023;388(22):2058-70.
92. Baselga J, Campone M, Piccart M, Burris HA, Rugo HS, Sahmoud T, et al. Everolimus in postmenopausal hormone-receptor-positive advanced breast cancer. N Engl J Med. 2012;366(6):520-9.
93. Hortobagyi GN, Chen D, Piccart M, Rugo HS, Burris HA, Pritchard KI, et al. Correlative Analysis of Genetic Alterations and Everolimus Benefit in Hormone Receptor-Positive, Human Epidermal Growth Factor Receptor 2-Negative Advanced Breast Cancer: Results From BOLERO-2. J Clin Oncol. 2016;34(5):419-26.
94. Pearson A, Proszek P, Pascual J, Fribbens C, Shamsher MK, Kingston B, et al. Inactivating. Clin Cancer Res. 2020;26(3):608-22.
95. Bertucci F, Ng CKY, Patsouris A, Droin N, Piscuoglio S, Carbuccia N, et al. Genomic characterization of metastatic breast cancers. Nature. 2019;569(7757):560-4.
96. Lian T, Li C, Wang H. Trametinib in the treatment of multiple malignancies harboring MEK1 mutations. Cancer Treat Rev. 2019;81:101907.
97. Sullivan RJ, Infante JR, Janku F, Wong DJL, Sosman JA, Keedy V, et al. First-in-Class ERK1/2 Inhibitor Ulixertinib (BVD-523) in Patients with MAPK Mutant Advanced Solid Tumors: Results of a Phase I Dose-Escalation and Expansion Study. Cancer Discov. 2018;8(2):184-95.

98. Nair BC, Vadlamudi RK. Regulation of hormonal therapy resistance by cell cycle machinery. Gene Ther Mol Biol. 2008;12:395.
99. Butt AJ, McNeil CM, Musgrove EA, Sutherland RL. Downstream targets of growth factor and oestrogen signalling and endocrine resistance: the potential roles of c-Myc, cyclin D1 and cyclin E. Endocr Relat Cancer. 2005;12 Suppl 1:S47-59.
100. Stendahl M, Kronblad A, Rydén L, Emdin S, Bengtsson NO, Landberg G. Cyclin D1 overexpression is a negative predictive factor for tamoxifen response in postmenopausal breast cancer patients. Br J Cancer. 2004;90(10):1942-8.
101. Mukherjee S, Conrad SE. c-Myc suppresses p21WAF1/CIP1 expression during estrogen signaling and antiestrogen resistance in human breast cancer cells. J Biol Chem. 2005;280(18):17617-25.
102. Finn RS, Martin M, Rugo HS, Jones S, Im SA, Gelmon K, et al. Palbociclib and Letrozole in Advanced Breast Cancer. N Engl J Med. 2016;375(20):1925-36.
103. Turner NC, Slamon DJ, Ro J, Bondarenko I, Im SA, Masuda N, et al. Overall Survival with Palbociclib and Fulvestrant in Advanced Breast Cancer. N Engl J Med. 2018;379(20):1926-36.
104. Finn RS, Dering J, Conklin D, Kalous O, Cohen DJ, Desai AJ, et al. PD 0332991, a selective cyclin D kinase 4/6 inhibitor, preferentially inhibits proliferation of luminal estrogen receptor-positive human breast cancer cell lines in vitro. Breast Cancer Res. 2009;11(5):R77.
105. Miller TW, Balko JM, Fox EM, Ghazoui Z, Dunbier A, Anderson H, et al. ERα-dependent E2F transcription can mediate resistance to estrogen deprivation in human breast cancer. Cancer Discov. 2011;1(4):338-51.
106. Giltnane JM, Hutchinson KE, Stricker TP, Formisano L, Young CD, Estrada MV, et al. Genomic profiling of ER. Sci Transl Med. 2017;9(402).
107. Bardia A, Hurvitz SA, DeMichele A, Clark AS, Zelnak A, Yardley DA, et al. Phase I/II Trial of Exemestane, Ribociclib, and Everolimus in Women with HR. Clin Cancer Res. 2021;27(15):4177-85.
108. Mayer IA, Abramson VG, Formisano L, Balko JM, Estrada MV, Sanders ME, et al. A Phase Ib Study of Alpelisib (BYL719), a PI3Kα-Specific Inhibitor, with Letrozole in ER+/HER2- Metastatic Breast Cancer. Clin Cancer Res. 2017;23(1):26-34.
109. Jeselsohn R, Buchwalter G, De Angelis C, Brown M, Schiff R. ESR1 mutations—a mechanism for acquired endocrine resistance in breast cancer. Nat Rev Clin Oncol. 2015;12(10):573-83.
110. Grinshpun A, Chen V, Sandusky ZM, Fanning SW, Jeselsohn R. ESR1 activating mutations: From structure to clinical application. Biochim Biophys Acta Rev Cancer. 2023;1878(1):188830.
111. Fribbens C, O'Leary B, Kilburn L, Hrebien S, Garcia-Murillas I, Beaney M, et al. Plasma ESR1 Mutations and the Treatment of Estrogen Receptor-Positive Advanced Breast Cancer. J Clin Oncol. 2016;34(25):2961-8.
112. Toy W, Weir H, Razavi P, Lawson M, Goeppert AU, Mazzola AM, et al. Activating. Cancer Discov. 2017;7(3):277-87.
113. Gates LA, Gu G, Chen Y, Rohira AD, Lei JT, Hamilton RA, et al. Proteomic profiling identifies key coactivators utilized by mutant ERα proteins as potential new therapeutic targets. Oncogene. 2018;37(33):4581-98.
114. Li Z, Wu Y, Yates ME, Tasdemir N, Bahreini A, Chen J, et al. Hotspot ESR1 Mutations Are Multimodal and Contextual Modulators of Breast Cancer Metastasis. Cancer Res. 2022;82(7):1321-39.
115. Brett JO, Spring LM, Bardia A, Wander SA. ESR1 mutation as an emerging clinical biomarker in metastatic hormone receptor-positive breast cancer. Breast Cancer Res. 2021;23(1):85.
116. Gelsomino L, Gu G, Rechoum Y, Beyer AR, Pejerrey SM, Tsimelzon A, et al. ESR1 mutations affect anti-proliferative responses to tamoxifen through enhanced cross-talk with IGF signaling. Breast Cancer Res Treat. 2016;157(2):253-65.

117. Zinger L, Merenbakh-Lamin K, Klein A, Elazar A, Journo S, Boldes T, et al. Ligand-binding Domain-activating Mutations of ESR1 Rewire Cellular Metabolism of Breast Cancer Cells. Clin Cancer Res. 2019;25(9):2900-14.
118. Gelsomino L, Panza S, Giordano C, Barone I, Gu G, Spina E, et al. Mutations in the estrogen receptor alpha hormone binding domain promote stem cell phenotype through notch activation in breast cancer cell lines. Cancer Lett. 2018;428:12-20.
119. Gu G, Tian L, Herzog SK, Rechoum Y, Gelsomino L, Gao M, et al. Hormonal modulation of ESR1 mutant metastasis. Oncogene. 2021;40(5):997-1011.
120. Toy W, Shen Y, Won H, Green B, Sakr RA, Will M, et al. ESR1 ligand-binding domain mutations in hormone-resistant breast cancer. Nat Genet. 2013;45(12):1439-45.
121. Katzenellenbogen JA, Mayne CG, Katzenellenbogen BS, Greene GL, Chandarlapaty S. Structural underpinnings of oestrogen receptor mutations in endocrine therapy resistance. Nat Rev Cancer. 2018;18(6):377-88.
122. Jeselsohn R, Bergholz JS, Pun M, Cornwell M, Liu W, Nardone A, et al. Allele-Specific Chromatin Recruitment and Therapeutic Vulnerabilities of ESR1 Activating Mutations. Cancer Cell. 2018;33(2):173-86.e5.
123. Martin LA, Ribas R, Simigdala N, Schuster E, Pancholi S, Tenev T, et al. Discovery of naturally occurring ESR1 mutations in breast cancer cell lines modelling endocrine resistance. Nat Commun. 2017;8(1):1865.
124. Robinson DR, Wu YM, Vats P, Su F, Lonigro RJ, Cao X, et al. Activating ESR1 mutations in hormone-resistant metastatic breast cancer. Nat Genet. 2013;45(12):1446-51.
125. Najim O, Seghers S, Sergoynne L, Van Gaver H, Papadimitriou K, Wouters K, et al. The association between type of endocrine therapy and development of estrogen receptor-1 mutation(s) in patients with hormone-sensitive advanced breast cancer: A systematic review and meta-analysis of randomized and non-randomized trials. Biochim Biophys Acta Rev Cancer. 2019;1872(2):188315.
126. Wander SA. The ELAINE trials and the future of personalized therapy for hormone-receptor positive metastatic breast cancer. Ann Oncol. 2023;34(12):1071-3.
127. Puyang X, Furman C, Zheng GZ, Wu ZJ, Banka D, Aithal K, et al. Discovery of Selective Estrogen Receptor Covalent Antagonists for the Treatment of ERα. Cancer Discov. 2018;8(9):1176-93.
128. Bidard FC, Kaklamani VG, Neven P, Streich G, Montero AJ, Forget F, et al. Elacestrant (oral selective estrogen receptor degrader) Versus Standard Endocrine Therapy for Estrogen Receptor-Positive, Human Epidermal Growth Factor Receptor 2-Negative Advanced Breast Cancer: Results From the Randomized Phase III EMERALD Trial. J Clin Oncol. 2022;40(28):3246-56.
129. Bidard FC, Hardy-Bessard AC, Dalenc F, Bachelot T, Pierga JY, de la Motte Rouge T, et al. Switch to fulvestrant and palbociclib versus no switch in advanced breast cancer with rising ESR1 mutation during aromatase inhibitor and palbociclib therapy (PADA-1): a randomised, open-label, multicentre, phase 3 trial. Lancet Oncol. 2022;23(11):1367-77.
130. Turner N, Huang-Bartlett C, Kalinsky K, Cristofanilli M, Bianchini G, Chia S, et al. Design of SERENA-6, a phase III switching trial of camizestrant in. Future Oncol. 2023;19(8):559-73.
131. Hanahan D, Weinberg RA. Hallmarks of cancer: the next generation. Cell. 2011;144(5):646-74.
132. Pavlova NN, Thompson CB. The Emerging Hallmarks of Cancer Metabolism. Cell Metab. 2016;23(1):27-47.
133. WARBURG O. On the origin of cancer cells. Science. 1956;123(3191):309-14.
134. WARBURG O. On respiratory impairment in cancer cells. Science. 1956;124(3215):269-70.
135. Xiao Y, Yu TJ, Xu Y, Ding R, Wang YP, Jiang YZ, et al. Emerging therapies in cancer metabolism. Cell Metab. 2023;35(8):1283-303.
136. Broadfield LA, Pane AA, Talebi A, Swinnen JV, Fendt SM. Lipid metabolism in cancer: New perspectives and emerging mechanisms. Dev Cell. 2021;56(10):1363-93.

137. Snaebjornsson MT, Janaki-Raman S, Schulze A. Greasing the Wheels of the Cancer Machine: The Role of Lipid Metabolism in Cancer. Cell Metab. 2020;31(1):62-76.
138. Röhrig F, Schulze A. The multifaceted roles of fatty acid synthesis in cancer. Nat Rev Cancer. 2016;16(11):732-49.
139. Kopecka J, Trouillas P, Gašparović A, Gazzano E, Assaraf YG, Riganti C. Phospholipids and cholesterol: Inducers of cancer multidrug resistance and therapeutic targets. Drug Resist Updat. 2020;49:100670.
140. Pietrocola F, Galluzzi L, Bravo-San Pedro JM, Madeo F, Kroemer G. Acetyl coenzyme A: a central metabolite and second messenger. Cell Metab. 2015;21(6):805-21.
141. Mallick R, Bhowmik P, Duttaroy AK. Targeting fatty acid uptake and metabolism in cancer cells: A promising strategy for cancer treatment. Biomed Pharmacother. 2023;167:115591.
142. Porstmann T, Santos CR, Griffiths B, Cully M, Wu M, Leevers S, et al. SREBP activity is regulated by mTORC1 and contributes to Akt-dependent cell growth. Cell Metab. 2008;8(3):224-36.
143. Zaidi N, Swinnen JV, Smans K. ATP-citrate lyase: a key player in cancer metabolism. Cancer Res. 2012;72(15):3709-14.
144. Migita T, Narita T, Nomura K, Miyagi E, Inazuka F, Matsuura M, et al. ATP citrate lyase: activation and therapeutic implications in non-small cell lung cancer. Cancer Res. 2008;68(20):8547-54.
145. Schug ZT, Vande Voorde J, Gottlieb E. The metabolic fate of acetate in cancer. Nat Rev Cancer. 2016;16(11):708-17.
146. Schug ZT, Peck B, Jones DT, Zhang Q, Grosskurth S, Alam IS, et al. Acetyl-CoA synthetase 2 promotes acetate utilization and maintains cancer cell growth under metabolic stress. Cancer Cell. 2015;27(1):57-71.
147. Mashimo T, Pichumani K, Vemireddy V, Hatanpaa KJ, Singh DK, Sirasanagandla S, et al. Acetate is a bioenergetic substrate for human glioblastoma and brain metastases. Cell. 2014;159(7):1603-14.
148. Bian X, Liu R, Meng Y, Xing D, Xu D, Lu Z. Lipid metabolism and cancer. J Exp Med. 2021;218(1).
149. Bacci M, Lorito N, Smiriglia A, Subbiani A, Bonechi F, Comito G, et al. Acetyl-CoA carboxylase 1 controls a lipid droplet-peroxisome axis and is a vulnerability of endocrine-resistant ER. Sci Transl Med. 2024;16(736):eadf9874.
150. Menendez JA, Lupu R. Fatty acid synthase and the lipogenic phenotype in cancer pathogenesis. Nat Rev Cancer. 2007;7(10):763-77.
151. Vanauberg D, Schulz C, Lefebvre T. Involvement of the pro-oncogenic enzyme fatty acid synthase in the hallmarks of cancer: a promising target in anti-cancer therapies. Oncogenesis. 2023;12(1):16.
152. Fu Y, Zou T, Shen X, Nelson PJ, Li J, Wu C, et al. Lipid metabolism in cancer progression and therapeutic strategies. MedComm (2020). 2021;2(1):27-59.
153. Presler M, Wojtczyk-Miaskowska A, Schlichtholz B, Kaluzny A, Matuszewski M, Mika A, et al. Increased expression of the gene encoding stearoyl-CoA desaturase 1 in human bladder cancer. Mol Cell Biochem. 2018;447(1-2):217-24.
154. Wang M, Han J, Xing H, Zhang H, Li Z, Liang L, et al. Dysregulated fatty acid metabolism in hepatocellular carcinoma. Hepat Oncol. 2016;3(4):241-51.
155. Holder AM, Gonzalez-Angulo AM, Chen H, Akcakanat A, Do KA, Fraser Symmans W, et al. High stearoyl-CoA desaturase 1 expression is associated with shorter survival in breast cancer patients. Breast Cancer Res Treat. 2013;137(1):319-27.
156. Griffiths B, Lewis CA, Bensaad K, Ros S, Zhang Q, Ferber EC, et al. Sterol regulatory element binding protein-dependent regulation of lipid synthesis supports cell survival and tumor growth. Cancer Metab. 2013;1(1):3.

157. Williams KJ, Argus JP, Zhu Y, Wilks MQ, Marbois BN, York AG, et al. An essential requirement for the SCAP/SREBP signaling axis to protect cancer cells from lipotoxicity. Cancer Res. 2013;73(9):2850-62.
158. Rudalska R, Zender L, Dauch D. Exploiting lipotoxicity for the treatment of liver cancer. Br J Cancer. 2021;125(11):1459-61.
159. Mullen PJ, Yu R, Longo J, Archer MC, Penn LZ. The interplay between cell signalling and the mevalonate pathway in cancer. Nat Rev Cancer. 2016;16(11):718-31.
160. Luo X, Cheng C, Tan Z, Li N, Tang M, Yang L, et al. Emerging roles of lipid metabolism in cancer metastasis. Mol Cancer. 2017;16(1):76.
161. Ehmsen S, Pedersen MH, Wang G, Terp MG, Arslanagic A, Hood BL, et al. Increased Cholesterol Biosynthesis Is a Key Characteristic of Breast Cancer Stem Cells Influencing Patient Outcome. Cell Rep. 2019;27(13):3927-38.e6.
162. Clendening JW, Pandyra A, Boutros PC, El Ghamrasni S, Khosravi F, Trentin GA, et al. Dysregulation of the mevalonate pathway promotes transformation. Proc Natl Acad Sci U S A. 2010;107(34):15051-6.
163. Pascual G, Avgustinova A, Mejetta S, Martín M, Castellanos A, Attolini CS, et al. Targeting metastasis-initiating cells through the fatty acid receptor CD36. Nature. 2017;541(7635):41-5.
164. Ladanyi A, Mukherjee A, Kenny HA, Johnson A, Mitra AK, Sundaresan S, et al. Adipocyte-induced CD36 expression drives ovarian cancer progression and metastasis. Oncogene. 2018;37(17):2285-301.
165. Watt MJ, Clark AK, Selth LA, Haynes VR, Lister N, Rebello R, et al. Suppressing fatty acid uptake has therapeutic effects in preclinical models of prostate cancer. Sci Transl Med. 2019;11(478).
166. Onal G, Kutlu O, Gozuacik D, Dokmeci Emre S. Lipid Droplets in Health and Disease. Lipids Health Dis. 2017;16(1):128.
167. Petan T, Jarc E, Jusović M. Lipid Droplets in Cancer: Guardians of Fat in a Stressful World. Molecules. 2018;23(8).
168. Olzmann JA, Carvalho P. Dynamics and functions of lipid droplets. Nat Rev Mol Cell Biol. 2019;20(3):137-55.
169. Kimmel AR, Sztalryd C. The Perilipins: Major Cytosolic Lipid Droplet-Associated Proteins and Their Roles in Cellular Lipid Storage, Mobilization, and Systemic Homeostasis. Annu Rev Nutr. 2016;36:471-509.
170. Petan T. Lipid Droplets in Cancer. Rev Physiol Biochem Pharmacol. 2023;185:53-86.
171. Salo VT, Ikonen E. Moving out but keeping in touch: contacts between endoplasmic reticulum and lipid droplets. Curr Opin Cell Biol. 2019;57:64-70.
172. Walther TC, Chung J, Farese RV. Lipid Droplet Biogenesis. Annu Rev Cell Dev Biol. 2017;33:491-510.
173. Jin Y, Tan Y, Wu J, Ren Z. Lipid droplets: a cellular organelle vital in cancer cells. Cell Death Discov. 2023;9(1):254.
174. Jarc E, Petan T. Lipid Droplets and the Management of Cellular Stress. Yale J Biol Med. 2019;92(3):435-52.
175. Cruz ALS, Barreto EA, Fazolini NPB, Viola JPB, Bozza PT. Lipid droplets: platforms with multiple functions in cancer hallmarks. Cell Death Dis. 2020;11(2):105.
176. Cheng X, Geng F, Pan M, Wu X, Zhong Y, Wang C, et al. Targeting DGAT1 Ameliorates Glioblastoma by Increasing Fat Catabolism and Oxidative Stress. Cell Metab. 2020;32(2):229-42.e8.
177. Wilcock DJ, Badrock AP, Wong CW, Owen R, Guerin M, Southam AD, et al. Oxidative stress from DGAT1 oncoprotein inhibition in melanoma suppresses tumor growth when ROS defenses are also breached. Cell Rep. 2022;39(12):110995.
178. Nardi F, Franco OE, Fitchev P, Morales A, Vickman RE, Hayward SW, et al. DGAT1 Inhibitor Suppresses Prostate Tumor Growth and Migration by Regulating Intracellular Lipids and Non-Centrosomal MTOC Protein GM130. Sci Rep. 2019;9(1):3035.

179. Ou J, Miao H, Ma Y, Guo F, Deng J, Wei X, et al. Loss of abhd5 promotes colorectal tumor development and progression by inducing aerobic glycolysis and epithelial-mesenchymal transition. Cell Rep. 2014;9(5):1798-811.
180. Zagani R, El-Assaad W, Gamache I, Teodoro JG. Inhibition of adipose triglyceride lipase (ATGL) by the putative tumor suppressor G0S2 or a small molecule inhibitor attenuates the growth of cancer cells. Oncotarget. 2015;6(29):28282-95.
181. Wang YY, Attané C, Milhas D, Dirat B, Dauvillier S, Guerard A, et al. Mammary adipocytes stimulate breast cancer invasion through metabolic remodeling of tumor cells. JCI Insight. 2017;2(4):e87489.
182. Grace SA, Meeks MW, Chen Y, Cornwell M, Ding X, Hou P, et al. Adipose Triglyceride Lipase (ATGL) Expression Is Associated with Adiposity and Tumor Stromal Proliferation in Patients with Pancreatic Ductal Adenocarcinoma. Anticancer Res. 2017;37(2):699-703.
183. Al-Zoughbi W, Pichler M, Gorkiewicz G, Guertl-Lackner B, Haybaeck J, Jahn SW, et al. Loss of adipose triglyceride lipase is associated with human cancer and induces mouse pulmonary neoplasia. Oncotarget. 2016;7(23):33832-40.
184. Nomura DK, Long JZ, Niessen S, Hoover HS, Ng SW, Cravatt BF. Monoacylglycerol lipase regulates a fatty acid network that promotes cancer pathogenesis. Cell. 2010;140(1):49-61.
185. Ye L, Zhang B, Seviour EG, Tao KX, Liu XH, Ling Y, et al. Monoacylglycerol lipase (MAGL) knockdown inhibits tumor cells growth in colorectal cancer. Cancer Lett. 2011;307(1):6-17.
186. Zhu W, Zhao Y, Zhou J, Wang X, Pan Q, Zhang N, et al. Monoacylglycerol lipase promotes progression of hepatocellular carcinoma via NF-κB-mediated epithelial-mesenchymal transition. J Hematol Oncol. 2016;9(1):127.
187. Yue S, Li J, Lee SY, Lee HJ, Shao T, Song B, et al. Cholesteryl ester accumulation induced by PTEN loss and PI3K/AKT activation underlies human prostate cancer aggressiveness. Cell Metab. 2014;19(3):393-406.
188. Li J, Gu D, Lee SS, Song B, Bandyopadhyay S, Chen S, et al. Abrogating cholesterol esterification suppresses growth and metastasis of pancreatic cancer. Oncogene. 2016;35(50):6378-88.
189. de Gonzalo-Calvo D, López-Vilaró L, Nasarre L, Perez-Olabarria M, Vázquez T, Escuin D, et al. Intratumor cholesteryl ester accumulation is associated with human breast cancer proliferation and aggressive potential: a molecular and clinicopathological study. BMC Cancer. 2015;15:460.
190. Geng F, Cheng X, Wu X, Yoo JY, Cheng C, Guo JY, et al. Inhibition of SOAT1 Suppresses Glioblastoma Growth via Blocking SREBP-1-Mediated Lipogenesis. Clin Cancer Res. 2016;22(21):5337-48.
191. Wang Z, Wang Y, Li Z, Xue W, Hu S, Kong X. Lipid metabolism as a target for cancer drug resistance: progress and prospects. Front Pharmacol. 2023;14:1274335.
192. Cotte AK, Aires V, Fredon M, Limagne E, Derangère V, Thibaudin M, et al. Lysophosphatidylcholine acyltransferase 2-mediated lipid droplet production supports colorectal cancer chemoresistance. Nat Commun. 2018;9(1):322.
193. Schlaepfer IR, Hitz CA, Gijón MA, Bergman BC, Eckel RH, Jacobsen BM. Progestin modulates the lipid profile and sensitivity of breast cancer cells to docetaxel. Mol Cell Endocrinol. 2012;363(1-2):111-21.
194. Therese Sørlie RBC. A Guide to Breast Cancer Research. From Cellular Heterogeneity and Molecular Mechanisms to Therapy. Springer Nature Link2025.
195. Zuo Q, Kang Y. Metabolic Reprogramming and Adaption in Breast Cancer Progression and Metastasis. Adv Exp Med Biol. 2025;1464:347-70.
196. Nakahara R, Maeda K, Aki S, Osawa T. Metabolic adaptations of cancer in extreme tumor microenvironments. Cancer Sci. 2023;114(4):1200-7.
197. Dias AS, Almeida CR, Helguero LA, Duarte IF. Metabolic crosstalk in the breast cancer microenvironment. Eur J Cancer. 2019;121:154-71.

198. Patra KC, Wang Q, Bhaskar PT, Miller L, Wang Z, Wheaton W, et al. Hexokinase 2 is required for tumor initiation and maintenance and its systemic deletion is therapeutic in mouse models of cancer. Cancer Cell. 2013;24(2):213-28.
199. Bacci M, Giannoni E, Fearns A, Ribas R, Gao Q, Taddei ML, et al. miR-155 Drives Metabolic Reprogramming of ER+ Breast Cancer Cells Following Long-Term Estrogen Deprivation and Predicts Clinical Response to Aromatase Inhibitors. Cancer Res. 2016;76(6):1615-26.
200. Liu X, Miao W, Huang M, Li L, Dai X, Wang Y. Elevated Hexokinase II Expression Confers Acquired Resistance to 4-Hydroxytamoxifen in Breast Cancer Cells. Mol Cell Proteomics. 2019;18(11):2273-84.
201. Yang T, Ren C, Qiao P, Han X, Wang L, Lv S, et al. PIM2-mediated phosphorylation of hexokinase 2 is critical for tumor growth and paclitaxel resistance in breast cancer. Oncogene. 2018;37(45):5997-6009.
202. Bartrons R, Rodríguez-García A, Simon-Molas H, Castaño E, Manzano A, Navarro-Sabaté À. The potential utility of PFKFB3 as a therapeutic target. Expert Opin Ther Targets. 2018;22(8):659-74.
203. Jia W, Wu Q, Shen M, Yu X, An S, Zhao L, et al. PFKFB3 regulates breast cancer tumorigenesis and Fulvestrant sensitivity by affecting ERα stability. Cell Signal. 2024;119:111184.
204. Ruprecht B, Zaal EA, Zecha J, Wu W, Berkers CR, Kuster B, et al. Lapatinib Resistance in Breast Cancer Cells Is Accompanied by Phosphorylation-Mediated Reprogramming of Glycolysis. Cancer Res. 2017;77(8):1842-53.
205. Ros S, Wright AJ, D'Santos P, Hu DE, Hesketh RL, Lubling Y, et al. Metabolic Imaging Detects Resistance to PI3Kα Inhibition Mediated by Persistent FOXM1 Expression in ER. Cancer Cell. 2020;38(4):516-33.e9.
206. Lorito N, Bacci M, Smiriglia A, Mannelli M, Parri M, Comito G, et al. Glucose Metabolic Reprogramming of ER Breast Cancer in Acquired Resistance to the CDK4/6 Inhibitor Palbociclib. Cells. 2020;9(3).
207. Khwairakpam AD, Shyamananda MS, Sailo BL, Rathnakaram SR, Padmavathi G, Kotoky J, et al. ATP citrate lyase (ACLY): a promising target for cancer prevention and treatment. Curr Drug Targets. 2015;16(2):156-63.
208. Ismail A, Mokhlis HA, Sharaky M, Sobhy MH, Hassanein SS, Doghish AS, et al. Hydroxycitric acid reverses tamoxifen resistance through inhibition of ATP citrate lyase. Pathol Res Pract. 2022;240:154211.
209. Velez BC, Petrella CP, DiSalvo KH, Cheng K, Kravtsov R, Krasniqi D, et al. Combined inhibition of ACLY and CDK4/6 reduces cancer cell growth and invasion. Oncol Rep. 2023;49(2).
210. Gruslova A, McClellan B, Balinda HU, Viswanadhapalli S, Alers V, Sareddy GR, et al. FASN inhibition as a potential treatment for endocrine-resistant breast cancer. Breast Cancer Res Treat. 2021;187(2):375-86.
211. Rios Garcia M, Steinbauer B, Srivastava K, Singhal M, Mattijssen F, Maida A, et al. Acetyl-CoA Carboxylase 1-Dependent Protein Acetylation Controls Breast Cancer Metastasis and Recurrence. Cell Metab. 2017;26(6):842-55.e5.
212. Feng WW, Wilkins O, Bang S, Ung M, Li J, An J, et al. CD36-Mediated Metabolic Rewiring of Breast Cancer Cells Promotes Resistance to HER2-Targeted Therapies. Cell Rep. 2019;29(11):3405-20.e5.
213. Ruppert PMM, Kersten S. Mechanisms of hepatic fatty acid oxidation and ketogenesis during fasting. Trends Endocrinol Metab. 2024;35(2):107-24.
214. Jiang C, Zhu Y, Chen H, Lin J, Xie R, Li W, et al. Targeting c-Jun inhibits fatty acid oxidation to overcome tamoxifen resistance in estrogen receptor-positive breast cancer. Cell Death Dis. 2023;14(10):653.
215. Wang T, Fahrmann JF, Lee H, Li YJ, Tripathi SC, Yue C, et al. JAK/STAT3-Regulated Fatty Acid β-Oxidation Is Critical for Breast Cancer Stem Cell Self-Renewal and Chemoresistance. Cell Metab. 2018;27(6):1357.

216. Sirois I, Aguilar-Mahecha A, Lafleur J, Fowler E, Vu V, Scriver M, et al. A Unique Morphological Phenotype in Chemoresistant Triple-Negative Breast Cancer Reveals Metabolic Reprogramming and PLIN4 Expression as a Molecular Vulnerability. Mol Cancer Res. 2019;17(12):2492-507.
217. Hultsch S, Kankainen M, Paavolainen L, Kovanen RM, Ikonen E, Kangaspeska S, et al. Association of tamoxifen resistance and lipid reprogramming in breast cancer. BMC Cancer. 2018;18(1):850.
218. Locasale JW. Serine, glycine and one-carbon units: cancer metabolism in full circle. Nat Rev Cancer. 2013;13(8):572-83.
219. Tombari C, Zannini A, Bertolio R, Pedretti S, Audano M, Triboli L, et al. Mutant p53 sustains serine-glycine synthesis and essential amino acids intake promoting breast cancer growth. Nat Commun. 2023;14(1):6777.
220. Perland E, Fredriksson R. Classification Systems of Secondary Active Transporters. Trends Pharmacol Sci. 2017;38(3):305-15.
221. Chen Z, Wang Y, Warden C, Chen S. Cross-talk between ER and HER2 regulates c-MYC-mediated glutamine metabolism in aromatase inhibitor resistant breast cancer cells. J Steroid Biochem Mol Biol. 2015;149:118-27.
222. Saito Y, Matsuda S, Ohnishi N, Endo K, Ashitani S, Ohishi M, et al. Polarity protein SCRIB interacts with SLC3A2 to regulate proliferation and tamoxifen resistance in ER+ breast cancer. Commun Biol. 2022;5(1):403.
223. Saito Y, Li L, Coyaud E, Luna A, Sander C, Raught B, et al. LLGL2 rescues nutrient stress by promoting leucine uptake in ER. Nature. 2019;569(7755):275-9.
224. Bacci M, Lorito N, Ippolito L, Ramazzotti M, Luti S, Romagnoli S, et al. Reprogramming of Amino Acid Transporters to Support Aspartate and Glutamate Dependency Sustains Endocrine Resistance in Breast Cancer. Cell Rep. 2019;28(1):104-18.e8.
225. Possemato R, Marks KM, Shaul YD, Pacold ME, Kim D, Birsoy K, et al. Functional genomics reveal that the serine synthesis pathway is essential in breast cancer. Nature. 2011;476(7360):346-50.
226. Morandi A, Chiarugi P. Metabolic implication of tumor:stroma crosstalk in breast cancer. J Mol Med (Berl). 2014;92(2):117-26.
227. Siebeneicher H, Cleve A, Rehwinkel H, Neuhaus R, Heisler I, Müller T, et al. Identification and Optimization of the First Highly Selective GLUT1 Inhibitor BAY-876. ChemMedChem. 2016;11(20):2261-71.
228. Zhao Y, Liu H, Liu Z, Ding Y, Ledoux SP, Wilson GL, et al. Overcoming trastuzumab resistance in breast cancer by targeting dysregulated glucose metabolism. Cancer Res. 2011;71(13):4585-97.
229. Li L, Fath MA, Scarbrough PM, Watson WH, Spitz DR. Combined inhibition of glycolysis, the pentose cycle, and thioredoxin metabolism selectively increases cytotoxicity and oxidative stress in human breast and prostate cancer. Redox Biol. 2015;4:127-35.
230. Raez LE, Papadopoulos K, Ricart AD, Chiorean EG, Dipaola RS, Stein MN, et al. A phase I dose-escalation trial of 2-deoxy-D-glucose alone or combined with docetaxel in patients with advanced solid tumors. Cancer Chemother Pharmacol. 2013;71(2):523-30.
231. Jin Q, Yuan LX, Boulbes D, Baek JM, Wang YN, Gomez-Cabello D, et al. Fatty acid synthase phosphorylation: a novel therapeutic target in HER2-overexpressing breast cancer cells. Breast Cancer Res. 2010;12(6):R96.
232. Wang T, Fahrmann JF, Lee H, Li YJ, Tripathi SC, Yue C, et al. JAK/STAT3-Regulated Fatty Acid β-Oxidation Is Critical for Breast Cancer Stem Cell Self-Renewal and Chemoresistance. Cell Metab. 2018;27(1):136-50.e5.
233. van Geldermalsen M, Quek LE, Turner N, Freidman N, Pang A, Guan YF, et al. Benzylserine inhibits breast cancer cell growth by disrupting intracellular amino acid homeostasis and triggering amino acid response pathways. BMC Cancer. 2018;18(1):689.

234. Maris M, Salles G, Kim WS, Kim TM, Lyons RM, Arellano M, et al. ASCT2-Targeting Antibody-Drug Conjugate MEDI7247 in Adult Patients with Relapsed/Refractory Hematological Malignancies: A First-in-Human, Phase 1 Study. Target Oncol. 2024;19(3):321-32.
235. Jhaveri K, Modi S. Ganetespib: research and clinical development. Onco Targets Ther. 2015;8:1849-58.
236. Gross MI, Demo SD, Dennison JB, Chen L, Chernov-Rogan T, Goyal B, et al. Antitumor activity of the glutaminase inhibitor CB-839 in triple-negative breast cancer. Mol Cancer Ther. 2014;13(4):890-901.
237. Gouda MA, Voss MH, Tawbi H, Gordon M, Tykodi SS, Lam ET, et al. A phase I/II study of the safety and efficacy of telaglenastat (CB-839) in combination with nivolumab in patients with metastatic melanoma, renal cell carcinoma, and non-small-cell lung cancer. ESMO Open. 2025;10(5):104536.
238. Tajan M, Vousden KH. Dietary Approaches to Cancer Therapy. Cancer Cell. 2020;37(6):767-85.
239. de Groot S, Lugtenberg RT, Cohen D, Welters MJP, Ehsan I, Vreeswijk MPG, et al. Fasting mimicking diet as an adjunct to neoadjuvant chemotherapy for breast cancer in the multicentre randomized phase 2 DIRECT trial. Nat Commun. 2020;11(1):3083.
240. · FLGFAVFIRLCFAB. 248P Targeting triple-negative breast cancer metabolism with neoadjuvant chemotherapy plus fasting-mimicking diet plus/minus metformin: The BREAKFAST trial. Annals of Oncology2023.
241. Dixon SJ, Lemberg KM, Lamprecht MR, Skouta R, Zaitsev EM, Gleason CE, et al. Ferroptosis: an iron-dependent form of nonapoptotic cell death. Cell. 2012;149(5):1060-72.
242. Dixon SJ, Olzmann JA. The cell biology of ferroptosis. Nat Rev Mol Cell Biol. 2024;25(6):424-42.
243. Conrad M, Pratt DA. The chemical basis of ferroptosis. Nat Chem Biol. 2019;15(12):1137-47.
244. Ursini F, Maiorino M. Lipid peroxidation and ferroptosis: The role of GSH and GPx4. Free Radic Biol Med. 2020;152:175-85.
245. Yang WS, SriRamaratnam R, Welsch ME, Shimada K, Skouta R, Viswanathan VS, et al. Regulation of ferroptotic cancer cell death by GPX4. Cell. 2014;156(1-2):317-31.
246. Galluzzi L, Vitale I, Aaronson SA, Abrams JM, Adam D, Agostinis P, et al. Molecular mechanisms of cell death: recommendations of the Nomenclature Committee on Cell Death 2018. Cell Death Differ. 2018;25(3):486-541.
247. Green DR. The Coming Decade of Cell Death Research: Five Riddles. Cell. 2019;177(5):1094-107.
248. Wiernicki B, Dubois H, Tyurina YY, Hassannia B, Bayir H, Kagan VE, et al. Excessive phospholipid peroxidation distinguishes ferroptosis from other cell death modes including pyroptosis. Cell Death Dis. 2020;11(10):922.
249. Hirata Y, Cai R, Volchuk A, Steinberg BE, Saito Y, Matsuzawa A, et al. Lipid peroxidation increases membrane tension, Piezo1 gating, and cation permeability to execute ferroptosis. Curr Biol. 2023;33(7):1282-94.e5.
250. Dixon SJ, Pratt DA. Ferroptosis: A flexible constellation of related biochemical mechanisms. Mol Cell. 2023;83(7):1030-42.
251. Li J, Cao F, Yin HL, Huang ZJ, Lin ZT, Mao N, et al. Ferroptosis: past, present and future. Cell Death Dis. 2020;11(2):88.
252. Wang W, Green M, Choi JE, Gijón M, Kennedy PD, Johnson JK, et al. CD8. Nature. 2019;569(7755):270-4.
253. Lei G, Zhang Y, Koppula P, Liu X, Zhang J, Lin SH, et al. The role of ferroptosis in ionizing radiation-induced cell death and tumor suppression. Cell Res. 2020;30(2):146-62.
254. Pope LE, Dixon SJ. Regulation of ferroptosis by lipid metabolism. Trends Cell Biol. 2023;33(12):1077-87.

255. Porter NA. A perspective on free radical autoxidation: the physical organic chemistry of polyunsaturated fatty acid and sterol peroxidation. J Org Chem. 2013;78(8):3511-24.
256. Lai CS, Piette LH. Spin-trapping studies of hydroxyl radical production involved in lipid peroxidation. Arch Biochem Biophys. 1978;190(1):27-38.
257. Xu Y, Qi J, Yang X, Wu E, Qian SY. Free radical derivatives formed from cyclooxygenase-catalyzed dihomo-γ-linolenic acid peroxidation can attenuate colon cancer cell growth and enhance 5-fluorouracil's cytotoxicity. Redox Biol. 2014;2:610-8.
258. Guengerich FP, Waterman MR, Egli M. Recent Structural Insights into Cytochrome P450 Function. Trends Pharmacol Sci. 2016;37(8):625-40.
259. Yang WS, Kim KJ, Gaschler MM, Patel M, Shchepinov MS, Stockwell BR. Peroxidation of polyunsaturated fatty acids by lipoxygenases drives ferroptosis. Proc Natl Acad Sci U S A. 2016;113(34):E4966-75.
260. Shah R, Shchepinov MS, Pratt DA. Resolving the Role of Lipoxygenases in the Initiation and Execution of Ferroptosis. ACS Cent Sci. 2018;4(3):387-96.
261. Forcina GC, Dixon SJ. GPX4 at the Crossroads of Lipid Homeostasis and Ferroptosis. Proteomics. 2019;19(18):e1800311.
262. Kagan VE, Mao G, Qu F, Angeli JP, Doll S, Croix CS, et al. Oxidized arachidonic and adrenic PEs navigate cells to ferroptosis. Nat Chem Biol. 2017;13(1):81-90.
263. Doll S, Proneth B, Tyurina YY, Panzilius E, Kobayashi S, Ingold I, et al. ACSL4 dictates ferroptosis sensitivity by shaping cellular lipid composition. Nat Chem Biol. 2017;13(1):91-8.
264. Lorito N, Subbiani A, Smiriglia A, Bacci M, Bonechi F, Tronci L, et al. FADS1/2 control lipid metabolism and ferroptosis susceptibility in triple-negative breast cancer. EMBO Mol Med. 2024;16(7):1533-59.
265. Lee JY, Nam M, Son HY, Hyun K, Jang SY, Kim JW, et al. Polyunsaturated fatty acid biosynthesis pathway determines ferroptosis sensitivity in gastric cancer. Proc Natl Acad Sci U S A. 2020;117(51):32433-42.
266. Perez MA, Clostio AJ, Houston IR, Ruiz J, Magtanong L, Dixon SJ, et al. Ether lipid deficiency disrupts lipid homeostasis leading to ferroptosis sensitivity. PLoS Genet. 2022;18(9):e1010436.
267. Zou Y, Henry WS, Ricq EL, Graham ET, Phadnis VV, Maretich P, et al. Plasticity of ether lipids promotes ferroptosis susceptibility and evasion. Nature. 2020;585(7826):603-8.
268. Ubellacker JM, Tasdogan A, Ramesh V, Shen B, Mitchell EC, Martin-Sandoval MS, et al. Lymph protects metastasizing melanoma cells from ferroptosis. Nature. 2020;585(7823):113-8.
269. Harayama T, Riezman H. Understanding the diversity of membrane lipid composition. Nat Rev Mol Cell Biol. 2018;19(5):281-96.
270. Nagao K, Murakami A, Umeda M. Structure and Function of Δ9-Fatty Acid Desaturase. Chem Pharm Bull (Tokyo). 2019;67(4):327-32.
271. Magtanong L, Ko PJ, To M, Cao JY, Forcina GC, Tarangelo A, et al. Exogenous Monounsaturated Fatty Acids Promote a Ferroptosis-Resistant Cell State. Cell Chem Biol. 2019;26(3):420-32.e9.
272. Badgley MA, Kremer DM, Maurer HC, DelGiorno KE, Lee HJ, Purohit V, et al. Cysteine depletion induces pancreatic tumor ferroptosis in mice. Science. 2020;368(6486):85-9.
273. Valentine WJ, Yanagida K, Kawana H, Kono N, Noda NN, Aoki J, et al. Update and nomenclature proposal for mammalian lysophospholipid acyltransferases, which create membrane phospholipid diversity. J Biol Chem. 2022;298(1):101470.
274. Herrera-Abreu MT, Guan J, Khalid U, Ning J, Costa MR, Chan J, et al. Inhibition of GPX4 enhances CDK4/6 inhibitor and endocrine therapy activity in breast cancer. Nat Commun. 2024;15(1):9550.
275. Gaschler MM, Stockwell BR. Lipid peroxidation in cell death. Biochem Biophys Res Commun. 2017;482(3):419-25.

276. Kim SE, Zhang L, Ma K, Riegman M, Chen F, Ingold I, et al. Ultrasmall nanoparticles induce ferroptosis in nutrient-deprived cancer cells and suppress tumour growth. Nat Nanotechnol. 2016;11(11):977-85.
277. Anderson GJ, Vulpe CD. Mammalian iron transport. Cell Mol Life Sci. 2009;66(20):3241-61.
278. Gao M, Monian P, Quadri N, Ramasamy R, Jiang X. Glutaminolysis and Transferrin Regulate Ferroptosis. Mol Cell. 2015;59(2):298-308.
279. Hou W, Xie Y, Song X, Sun X, Lotze MT, Zeh HJ, et al. Autophagy promotes ferroptosis by degradation of ferritin. Autophagy. 2016;12(8):1425-8.
280. Zheng J, Conrad M. The Metabolic Underpinnings of Ferroptosis. Cell Metab. 2020;32(6):920-37.
281. Seiler A, Schneider M, Förster H, Roth S, Wirth EK, Culmsee C, et al. Glutathione peroxidase 4 senses and translates oxidative stress into 12/15-lipoxygenase dependent- and AIF-mediated cell death. Cell Metab. 2008;8(3):237-48.
282. Ingold I, Berndt C, Schmitt S, Doll S, Poschmann G, Buday K, et al. Selenium Utilization by GPX4 Is Required to Prevent Hydroperoxide-Induced Ferroptosis. Cell. 2018;172(3):409-22.e21.
283. Friedmann Angeli JP, Schneider M, Proneth B, Tyurina YY, Tyurin VA, Hammond VJ, et al. Inactivation of the ferroptosis regulator Gpx4 triggers acute renal failure in mice. Nat Cell Biol. 2014;16(12):1180-91.
284. Maiorino M, Scapin M, Ursini F, Biasolo M, Bosello V, Flohé L. Distinct promoters determine alternative transcription of gpx-4 into phospholipid-hydroperoxide glutathione peroxidase variants. J Biol Chem. 2003;278(36):34286-90.
285. Mao C, Liu X, Zhang Y, Lei G, Yan Y, Lee H, et al. DHODH-mediated ferroptosis defence is a targetable vulnerability in cancer. Nature. 2021;593(7860):586-90.
286. Mishima E, Nakamura T, Zheng J, Zhang W, Mourão ASD, Sennhenn P, et al. DHODH inhibitors sensitize to ferroptosis by FSP1 inhibition. Nature. 2023;619(7968):E9-E18.
287. Forman HJ, Zhang H, Rinna A. Glutathione: overview of its protective roles, measurement, and biosynthesis. Mol Aspects Med. 2009;30(1-2):1-12.
288. Koppula P, Zhang Y, Zhuang L, Gan B. Amino acid transporter SLC7A11/xCT at the crossroads of regulating redox homeostasis and nutrient dependency of cancer. Cancer Commun (Lond). 2018;38(1):12.
289. Koppula P, Zhuang L, Gan B. Cystine transporter SLC7A11/xCT in cancer: ferroptosis, nutrient dependency, and cancer therapy. Protein Cell. 2021;12(8):599-620.
290. Jiang L, Kon N, Li T, Wang SJ, Su T, Hibshoosh H, et al. Ferroptosis as a p53-mediated activity during tumour suppression. Nature. 2015;520(7545):57-62.
291. Viswanathan VS, Ryan MJ, Dhruv HD, Gill S, Eichhoff OM, Seashore-Ludlow B, et al. Dependency of a therapy-resistant state of cancer cells on a lipid peroxidase pathway. Nature. 2017;547(7664):453-7.
292. Bersuker K, Hendricks JM, Li Z, Magtanong L, Ford B, Tang PH, et al. The CoQ oxidoreductase FSP1 acts parallel to GPX4 to inhibit ferroptosis. Nature. 2019;575(7784):688-92.
293. Doll S, Freitas FP, Shah R, Aldrovandi M, da Silva MC, Ingold I, et al. FSP1 is a glutathione-independent ferroptosis suppressor. Nature. 2019;575(7784):693-8.
294. Stefely JA, Pagliarini DJ. Biochemistry of Mitochondrial Coenzyme Q Biosynthesis. Trends Biochem Sci. 2017;42(10):824-43.
295. Morré DJ, Morré DM. Non-mitochondrial coenzyme Q. Biofactors. 2011;37(5):355-60.
296. Soula M, Weber RA, Zilka O, Alwaseem H, La K, Yen F, et al. Metabolic determinants of cancer cell sensitivity to canonical ferroptosis inducers. Nat Chem Biol. 2020;16(12):1351-60.
297. Kraft VAN, Bezjian CT, Pfeiffer S, Ringelstetter L, Müller C, Zandkarimi F, et al. GTP Cyclohydrolase 1/Tetrahydrobiopterin Counteract Ferroptosis through Lipid Remodeling. ACS Cent Sci. 2020;6(1):41-53.
298. Thöny B, Auerbach G, Blau N. Tetrahydrobiopterin biosynthesis, regeneration and functions. Biochem J. 2000;347 Pt 1(Pt 1):1-16.

299. Chen D, Chu B, Yang X, Liu Z, Jin Y, Kon N, et al. iPLA2β-mediated lipid detoxification controls p53-driven ferroptosis independent of GPX4. Nat Commun. 2021;12(1):3644.
300. Palma M, Chaufan M, Breuer CB, Müller S, Sabatier M, Fraser CS, et al. Lymph node environment drives FSP1 targetability in metastasizing melanoma. Nature. 2026;649(8096):477-86.
301. Lei G, Zhuang L, Gan B. The roles of ferroptosis in cancer: Tumor suppression, tumor microenvironment, and therapeutic interventions. Cancer Cell. 2024;42(4):513-34.
302. Zhang Y, Shi J, Liu X, Feng L, Gong Z, Koppula P, et al. BAP1 links metabolic regulation of ferroptosis to tumour suppression. Nat Cell Biol. 2018;20(10):1181-92.
303. Wang SJ, Li D, Ou Y, Jiang L, Chen Y, Zhao Y, et al. Acetylation Is Crucial for p53-Mediated Ferroptosis and Tumor Suppression. Cell Rep. 2016;17(2):366-73.
304. Koppula P, Lei G, Zhang Y, Yan Y, Mao C, Kondiparthi L, et al. A targetable CoQ-FSP1 axis drives ferroptosis- and radiation-resistance in KEAP1 inactive lung cancers. Nat Commun. 2022;13(1):2206.
305. Egolf S, Zou J, Anderson A, Simpson CL, Aubert Y, Prouty S, et al. MLL4 mediates differentiation and tumor suppression through ferroptosis. Sci Adv. 2021;7(50):eabj9141.
306. Harris IS, Treloar AE, Inoue S, Sasaki M, Gorrini C, Lee KC, et al. Glutathione and thioredoxin antioxidant pathways synergize to drive cancer initiation and progression. Cancer Cell. 2015;27(2):211-22.
307. Zhang L, Hobeika CS, Khabibullin D, Yu D, Filippakis H, Alchoueiry M, et al. Hypersensitivity to ferroptosis in chromophobe RCC is mediated by a glutathione metabolic dependency and cystine import via solute carrier family 7 member 11. Proc Natl Acad Sci U S A. 2022;119(28):e2122840119.
308. Chang K, Chen Y, Zhang X, Zhang W, Xu N, Zeng B, et al. DPP9 Stabilizes NRF2 to Suppress Ferroptosis and Induce Sorafenib Resistance in Clear Cell Renal Cell Carcinoma. Cancer Res. 2023;83(23):3940-55.
309. Liu S, Zhang HL, Li J, Ye ZP, Du T, Li LC, et al. Tubastatin A potently inhibits GPX4 activity to potentiate cancer radiotherapy through boosting ferroptosis. Redox Biol. 2023;62:102677.
310. Lim JKM, Delaidelli A, Minaker SW, Zhang HF, Colovic M, Yang H, et al. Cystine/glutamate antiporter xCT (SLC7A11) facilitates oncogenic RAS transformation by preserving intracellular redox balance. Proc Natl Acad Sci U S A. 2019;116(19):9433-42.
311. Zhang T, Sun L, Hao Y, Suo C, Shen S, Wei H, et al. ENO1 suppresses cancer cell ferroptosis by degrading the mRNA of iron regulatory protein 1. Nat Cancer. 2022;3(1):75-89.
312. Yi J, Zhu J, Wu J, Thompson CB, Jiang X. Oncogenic activation of PI3K-AKT-mTOR signaling suppresses ferroptosis via SREBP-mediated lipogenesis. Proc Natl Acad Sci U S A. 2020;117(49):31189-97.
313. Hangauer MJ, Viswanathan VS, Ryan MJ, Bole D, Eaton JK, Matov A, et al. Drug-tolerant persister cancer cells are vulnerable to GPX4 inhibition. Nature. 2017;551(7679):247-50.
314. Tsoi J, Robert L, Paraiso K, Galvan C, Sheu KM, Lay J, et al. Multi-stage Differentiation Defines Melanoma Subtypes with Differential Vulnerability to Drug-Induced Iron-Dependent Oxidative Stress. Cancer Cell. 2018;33(5):890-904.e5.
315. Lin CC, Yang WH, Lin YT, Tang X, Chen PH, Ding CC, et al. DDR2 upregulation confers ferroptosis susceptibility of recurrent breast tumors through the Hippo pathway. Oncogene. 2021;40(11):2018-34.
316. Bonechi F, Bacci M, Lorito N, Smiriglia A, Subbiani A, Pagliantini E, et al. ESR1 Activating Mutations Confer Metabolic Vulnerabilities in ER+ Breast Cancer. Cancer Res. 2025.
317. Lei G, Zhang Y, Hong T, Zhang X, Liu X, Mao C, et al. Ferroptosis as a mechanism to mediate p53 function in tumor radiosensitivity. Oncogene. 2021;40(20):3533-47.
318. Zhou Q, Meng Y, Li D, Yao L, Le J, Liu Y, et al. Ferroptosis in cancer: From molecular mechanisms to therapeutic strategies. Signal Transduct Target Ther. 2024;9(1):55.

319. Zhang Y, Tan H, Daniels JD, Zandkarimi F, Liu H, Brown LM, et al. Imidazole Ketone Erastin Induces Ferroptosis and Slows Tumor Growth in a Mouse Lymphoma Model. Cell Chem Biol. 2019;26(5):623-33.e9.
320. Liang C, Zhang X, Yang M, Dong X. Recent Progress in Ferroptosis Inducers for Cancer Therapy. Adv Mater. 2019;31(51):e1904197.
321. Sun X, Ou Z, Chen R, Niu X, Chen D, Kang R, et al. Activation of the p62-Keap1-NRF2 pathway protects against ferroptosis in hepatocellular carcinoma cells. Hepatology. 2016;63(1):173-84.
322. Gao R, Kalathur RKR, Coto-Llerena M, Ercan C, Buechel D, Shuang S, et al. YAP/TAZ and ATF4 drive resistance to Sorafenib in hepatocellular carcinoma by preventing ferroptosis. EMBO Mol Med. 2021;13(12):e14351.
323. Zou Y, Zheng S, Xie X, Ye F, Hu X, Tian Z, et al. N6-methyladenosine regulated FGFR4 attenuates ferroptotic cell death in recalcitrant HER2-positive breast cancer. Nat Commun. 2022;13(1):2672.
324. Sun R, Yan B, Li H, Ding D, Wang L, Pang J, et al. Androgen Receptor Variants Confer Castration Resistance in Prostate Cancer by Counteracting Antiandrogen-Induced Ferroptosis. Cancer Res. 2023;83(19):3192-204.
325. Liang D, Feng Y, Zandkarimi F, Wang H, Zhang Z, Kim J, et al. Ferroptosis surveillance independent of GPX4 and differentially regulated by sex hormones. Cell. 2023;186(13):2748-64.e22.
326. Zeng K, Li W, Wang Y, Zhang Z, Zhang L, Zhang W, et al. Inhibition of CDK1 Overcomes Oxaliplatin Resistance by Regulating ACSL4-mediated Ferroptosis in Colorectal Cancer. Adv Sci (Weinh). 2023;10(25):e2301088.
327. Lei G, Mao C, Yan Y, Zhuang L, Gan B. Ferroptosis, radiotherapy, and combination therapeutic strategies. Protein Cell. 2021;12(11):836-57.
328. Ye LF, Chaudhary KR, Zandkarimi F, Harken AD, Kinslow CJ, Upadhyayula PS, et al. Radiation-Induced Lipid Peroxidation Triggers Ferroptosis and Synergizes with Ferroptosis Inducers. ACS Chem Biol. 2020;15(2):469-84.
329. Nguyen VT, Barozzi I, Faronato M, Lombardo Y, Steel JH, Patel N, et al. Differential epigenetic reprogramming in response to specific endocrine therapies promotes cholesterol biosynthesis and cellular invasion. Nat Commun. 2015;6:10044.
330. Bhola NE, Jansen VM, Bafna S, Giltnane JM, Balko JM, Estrada MV, et al. Kinome-wide functional screen identifies role of PLK1 in hormone-independent, ER-positive breast cancer. Cancer Res. 2015;75(2):405-14.
331. El-Botty R, Morriset L, Montaudon E, Tariq Z, Schnitzler A, Bacci M, et al. Oxidative phosphorylation is a metabolic vulnerability of endocrine therapy and palbociclib resistant metastatic breast cancers. Nat Commun. 2023;14(1):4221.
332. Bruna A, Rueda OM, Greenwood W, Batra AS, Callari M, Batra RN, et al. A Biobank of Breast Cancer Explants with Preserved Intra-tumor Heterogeneity to Screen Anticancer Compounds. Cell. 2016;167(1):260-74.e22.
333. Soosainathan A, Iravani M, El-Botty R, Alexander J, Sourd L, Morisset L, et al. Targeting Transcriptional Regulation with a CDK9 Inhibitor Suppresses Growth of Endocrine- and Palbociclib-Resistant ER+ Breast Cancers. Cancer Res. 2024;84(1):17-25.
334. Pawitan Y, Bjöhle J, Amler L, Borg AL, Egyhazi S, Hall P, et al. Gene expression profiling spares early breast cancer patients from adjuvant therapy: derived and validated in two population-based cohorts. Breast Cancer Res. 2005;7(6):R953-64.
335. Desmedt C, Di Leo A, de Azambuja E, Larsimont D, Haibe-Kains B, Selleslags J, et al. Multifactorial approach to predicting resistance to anthracyclines. J Clin Oncol. 2011;29(12):1578-86.
336. Kao KJ, Chang KM, Hsu HC, Huang AT. Correlation of microarray-based breast cancer molecular subtypes and clinical outcomes: implications for treatment optimization. BMC Cancer. 2011;11:143.

337. Dedeurwaerder S, Desmedt C, Calonne E, Singhal SK, Haibe-Kains B, Defrance M, et al. DNA methylation profiling reveals a predominant immune component in breast cancers. EMBO Mol Med. 2011;3(12):726-41.
338. Miller LD, Smeds J, George J, Vega VB, Vergara L, Ploner A, et al. An expression signature for p53 status in human breast cancer predicts mutation status, transcriptional effects, and patient survival. Proc Natl Acad Sci U S A. 2005;102(38):13550-5.
339. Clarke C, Madden SF, Doolan P, Aherne ST, Joyce H, O'Driscoll L, et al. Correlating transcriptional networks to breast cancer survival: a large-scale coexpression analysis. Carcinogenesis. 2013;34(10):2300-8.
340. Nagalla S, Chou JW, Willingham MC, Ruiz J, Vaughn JP, Dubey P, et al. Interactions between immunity, proliferation and molecular subtype in breast cancer prognosis. Genome Biol. 2013;14(4):R34.
341. Maire V, Némati F, Richardson M, Vincent-Salomon A, Tesson B, Rigaill G, et al. Polo-like kinase 1: a potential therapeutic option in combination with conventional chemotherapy for the management of patients with triple-negative breast cancer. Cancer Res. 2013;73(2):813-23.
342. Chin K, DeVries S, Fridlyand J, Spellman PT, Roydasgupta R, Kuo WL, et al. Genomic and transcriptional aberrations linked to breast cancer pathophysiologies. Cancer Cell. 2006;10(6):529-41.
343. Desmedt C, Piette F, Loi S, Wang Y, Lallemand F, Haibe-Kains B, et al. Strong time dependence of the 76-gene prognostic signature for node-negative breast cancer patients in the TRANSBIG multicenter independent validation series. Clin Cancer Res. 2007;13(11):3207-14.
344. Love MI, Huber W, Anders S. Moderated estimation of fold change and dispersion for RNA-seq data with DESeq2. Genome Biol. 2014;15(12):550.
345. Gu Z, Eils R, Schlesner M. Complex heatmaps reveal patterns and correlations in multidimensional genomic data. Bioinformatics. 2016;32(18):2847-9.
346. Xu S, Hu E, Cai Y, Xie Z, Luo X, Zhan L, et al. Using clusterProfiler to characterize multiomics data. Nat Protoc. 2024;19(11):3292-320.
347. Li D, Li Y. The interaction between ferroptosis and lipid metabolism in cancer. Signal Transduct Target Ther. 2020;5(1):108.
348. Dattilo MA, Benzo Y, Herrera LM, Prada JG, Castillo AF, Orlando UD, et al. Regulatory mechanisms leading to differential Acyl-CoA synthetase 4 expression in breast cancer cells. Sci Rep. 2019;9(1):10324.
349. Belkaid A, Ouellette RJ, Surette ME. 17β-estradiol-induced ACSL4 protein expression promotes an invasive phenotype in estrogen receptor positive mammary carcinoma cells. Carcinogenesis. 2017;38(4):402-10.
350. Cao J, Zhou T, Wu T, Lin R, Huang J, Shi D, et al. Targeting estrogen-regulated system x. Cell Death Dis. 2025;16(1):30.
351. Du T, Sikora MJ, Levine KM, Tasdemir N, Riggins RB, Wendell SG, et al. Key regulators of lipid metabolism drive endocrine resistance in invasive lobular breast cancer. Breast Cancer Res. 2018;20(1):106.
352. Ackermann T, Shokry E, Deshmukh R, Anand J, Galbraith LCA, Mitchell L, et al. Breast cancer secretes anti-ferroptotic MUFAs and depends on selenoprotein synthesis for metastasis. EMBO Mol Med. 2024;16(11):2749-74.
353. Bacci M, Lorito N, Smiriglia A, Morandi A. Fat and Furious: Lipid Metabolism in Antitumoral Therapy Response and Resistance. Trends Cancer. 2021;7(3):198-213.
354. Turner NC, Ro J, André F, Loi S, Verma S, Iwata H, et al. Palbociclib in Hormone-Receptor-Positive Advanced Breast Cancer. N Engl J Med. 2015;373(3):209-19.
355. Zhang HL, Hu BX, Li ZL, Du T, Shan JL, Ye ZP, et al. PKCβII phosphorylates ACSL4 to amplify lipid peroxidation to induce ferroptosis. Nat Cell Biol. 2022;24(1):88-98.
356. Dos Santos AF, Fazeli G, Xavier da Silva TN, Friedmann Angeli JP. Ferroptosis: mechanisms and implications for cancer development and therapy response. Trends Cell Biol. 2023;33(12):1062-76.

357. He F, Zhang P, Liu J, Wang R, Kaufman RJ, Yaden BC, et al. ATF4 suppresses hepatocarcinogenesis by inducing SLC7A11 (xCT) to block stress-related ferroptosis. J Hepatol. 2023;79(2):362-77.
358. Dai E, Han L, Liu J, Xie Y, Zeh HJ, Kang R, et al. Ferroptotic damage promotes pancreatic tumorigenesis through a TMEM173/STING-dependent DNA sensor pathway. Nat Commun. 2020;11(1):6339.
359. Yarmohammadi F, Hayes AW, Karimi G. The role of ferroptosis in organ toxicity. Hum Exp Toxicol. 2021;40(12_suppl):S851-S60.
360. Luo T, Zheng Q, Shao L, Ma T, Mao L, Wang M. Intracellular Delivery of Glutathione Peroxidase Degrader Induces Ferroptosis In Vivo. Angew Chem Int Ed Engl. 2022;61(39):e202206277.
361. Ding Y, Fei Y, Lu B. Emerging New Concepts of Degrader Technologies. Trends Pharmacol Sci. 2020;41(7):464-74.